MONTE CARLO SIMULATION OF LIGHT PROPAGATION IN STRATIFIED WATER

DEWKURUN NARVADA

NATIONAL UNIVERSITY OF SINGAPORE

2005

MONTE CARLO SIMULATION OF LIGHT PROPAGATION IN STRATIFIED WATER

DEWKURUN NARVADA

(B.Sc (HONS), UOM)

A THESIS SUBMITTED

FOR THE DEGREE OF MASTERS OF SCIENCE

DEPARTMENT OF PHYSICS

NATIONAL UNIVERSITY OF SINGAPORE

2005

Acknowledgement

I would like to take this opportunity to express my heartfelt thanks and gratitude to the following people who, in one way or the other, have helped in the completion of this piece of work.

I would like to thank my supervisors Dr Liew Soo Chin and Prof Lim Hock, for their invaluable assistance, patience and advice during the course of this work.

Special thanks are also in order to the following persons from the Centre for Remote Imaging, Sensing and Processing: Heng Wang Cheng Alice, Lim Huei Ni Agnes, Chang Chew Wai and He Jiancheng. They have been of a tremendous support to me during the course of my research and have always done their best to help me in any way they could.

Last but not least, my most sincere thanks would go to my parents and sister. They have left no stone unturned in providing me with everything they could and have always been my emotional anchor. Nobody else showered me with so much care and concern as much as they did.

Contents

Summary

The spectral reflectance of the sea surface contains information about light absorption and scattering properties of water. At present, there are methods that can retrieve the absorption and scattering coefficients of water from above-surface reflectance, and subsequently to obtain the concentrations of water constituents responsible for the absorption and scattering. However, most of the algorithms implicitly assume that the water column is vertically homogeneous while oceanographic observations have shown the existence of vertical inhomogeneity of the sea water constituents. The aim of this thesis is to study the link between the remote sensing reflectance and the vertical structure of the ocean's optical properties.

The tool developed for this purpose is a Monte Carlo code for the simulation of the penetration of light in sea water. The code worked well for the ideal case of homogeneous waters when compared to the results obtained by the Ocean-Colour Algorithms working group of the International Ocean Colour Coordinating Group.

The hypothesis that the reflectance of a stratified water column is the same as that of an equivalent homogeneous ocean, yielding the optical property that is the average of the associated property over the penetration depth was then tested. It was found that this hypothesis works well for both a two-layer ocean and a continuously stratified one, although the agreement is better for a two-layer ocean.

Then the influence of vertical stratification on the reflectance of a water column was studied. Stratifications are included in the water column by using a Gaussian function that describes a depth dependent chlorophyll profile superimposed on a constant background. This Gaussian function describing the vertical chlorophyll profile was then used to simulate a relatively broad range of open ocean conditions characterized by the presence of this chlorophyll maximum at depths greater than or equal to 20m below the water surface. The comparison with a homogeneous ocean (with the background chlorophyll concentration of the stratified case) was carried out and it was seen that the magnitude of the above surface remote sensing reflectance of the stratified cases differed significantly from the reference values of homogeneous oceans, especially in the case of low surface chlorophyll concentrations and shallow pigment maximum.

The analysis of how the depth varying optical constituents contribute to the overall reflectance was then carried out by using a multiband quasi analytical algorithm (QAA) developed for the retrieval of the absorption and backscattering coefficients, as well as the absorption coefficients of phytoplankton pigments and gelbstoff and based on the remote sensing reflectance models derived from the radiative transfer equation. For the case of a homogeneous ocean, the retrieved values compared very well with the actual values found in the water column (the linear error being in the range of 5-8%). This retrieval algorithm was also applied to an inhomogeneous water column. The QAA retrieved absorption and backscattering coefficients were found to have a good correlation with their vertically weighed average values.

It was also analysed whether the reflectance of a stratified ocean is identical to that of a hypothetical homogeneous ocean having a pigment concentration that is the depth weighted average of the actual depth varying pigment concentration. It is seen that the case where both the absorption and scattering coefficients covary with the depth dependent chlorophyll concentration, this hypothesis shows less error than when only the absorption coefficient is made to covary with the chlorophyll concentration.

Field trips were carried out in Singapore waters in June and August 2004 and in situ measurements of reflectance and the depth dependent backscattering coefficient. The data for the backscattering coefficients and the QAA estimated absorption coefficients were used to obtain the reflectance from the Monte Carlo code set up and this reflectance was compared to the measured one for all the 12 locations covered. The QAA retrieved values of the backscattering coefficient were also compared to the measured values.

List of Figures

List of Tables

List of symbols

a	Absorption coefficient of the total,
a_{φ}	Absorption coefficient of phytoplankton pigments m^{-1}
a_g	Absorption coefficient of gelbstoff and detritus m^{-1}
a_w	Absorption coefficient of pure seawater m^{-1}
b	Scattering coefficient
B	Backscattering probability
b_f	Forwardscattering
b_b	Backscattering
b_{bp}	Backscattering coefficient of suspended particles m^{-1}
$b_{bp}(555)$	Backscattering coefficient of suspended particles at 555nm
b_{bw}	Backscattering coefficient of pure seawater m^{-1}
b_b	Backscattering coefficient of the total,
$c(\lambda)$	Total attenuation coefficient
[C]	Pigment concentration mg m^{-3}
Y	Spectral power for particle backscattering coefficient
R_{rs}	Above-surface remote-sensing reflectance sr^{-1}
r_{rs}	Below-surface remote-sensing reflectance sr^{-1}
S	Spectral slope for gelbstoff absorption coefficient nm^{-1}
u	Ratio of backscattering coefficient to the sum of absorption and backscattering coefficients, $\frac{b_b}{a+b_b}$
λ	Wavelength
λ_0	Reference wavelength nm
L	Radiance
Φ	Flux
Ω	Solid angle
E	Irradiance
E_d	Downwelling irradiance
E_u	Upwelling irradiance
$E_{\downarrow}$	Net downward irradiance
E_o	Scalar irradiance
E_{od}	Downwelling scalar irradiance
E_{ou}	Upwelling scalar irradiance
$E_{o\downarrow}$	Net downward scalar irradiance
F	Forwardscattering probability
$\bar{\mu}_d$	Average cosine of a downwelling radiance
$\bar{\mu}_u$	Average cosine of a upwelling radiance
$\bar{\mu}$	Average value of the cosine
$\beta(\theta,\varphi)$	Volume scattering function
$P(\theta)$	Scattering phase function
$K(\lambda, z)$	Irradiance attenuation coefficient

K_d	Attenuation of the downwelling irradiance
K_u	Attenuation of the upwelling irradiance
ω_o	Scattering albedo
$A(\lambda)$	Albedo
θ	Zenith angle
φ	Azimuth angle
α_1-α_5	Random numbers between 0 and 1

Chapter One

Introduction

1.1 Inhomogeneous water columns

The colour of the ocean as measured by the spectral reflectance of the sea surface contains information about light absorption and scattering properties of water. Currently, there are methods that can retrieve the absorption and scattering coefficients of water from above-surface reflectance, and subsequently to obtain the concentrations of water constituents responsible for the absorption and scattering. Most of the algorithms implicitly assume that the water column is vertically homogeneous while oceanographic observations have revealed the existence of vertical inhomogeneity of the sea water constituents. In applications of ocean colour measurements, it is vital to understand the link between the remote sensing reflectance of the ocean and the vertical structure of the ocean's optical properties and seawater constituents. The aim of this thesis is to study the link between the remote sensing reflectance and the vertical structure of the oceans optical properties.

Generally, it can be said that spectral remote sensing reflectance, $R_{rs}(\lambda)$, contains information about the properties of the oceanic surface layer whose thickness depends on the ocean's inherent and apparent optical properties. It was shown by Gordon and McCluney (1975) that in a homogeneous ocean, 90% of water leaving photons backscattered from beneath the sea surface originate from a layer extending down to the penetration depth, z_{90}, at which

the downwelling irradiance falls to 36.8% of its surface value. It has been seen than in natural waters, depth z_{90} can vary in a wide range from ~ 60m to only a few metres (or even less), depending primarily on water clarity and on the wavelength of the light considered. Over the years, oceanographic observations have indicated that the optical properties and optically significant constituents of water often show substantial vertical variation in the upper ocean. This vertical inhomogeneity thus creates a challenge for an understanding of the precise meaning of the values of the ocean properties that are retrieved from remote sensing reflectance.

Gordon and Clark (1978) initially addressed this challenge around more than 20 years ago. Using Monte Carlo radiative transfer simulations, they suggested that the reflectance of an actual ocean with optical properties that are distributed with depth could be related to the reflectance of a homogeneous ocean. The concentration of the optical constituents of such a hypothetical ocean would be equal to the depth weighted average of the actual depth varying constituents' concentrations over the penetration depth. Since the Gordon and Clark weighting function $g(\lambda,z)$ decreases exponentially with depth, z, from a value of 1 at the surface to 0.135 at z_{90} , it means that the contribution of optical properties just below the surface to the depth weighted average optical concentrations is more than sevenfold higher than the contribution coming from the penetration depth.

Gordon (1980) further examined the hypothesis of Gordon and Clark (1978) by using Monte Carlo simulation of radiative transfer for case 1 waters, whose optical properties were described with a refined bio optical model

parameterized by the chlorophyll concentration. The errors in the hypothesis were found to range from a few percent to more than 20% and were smaller when both the particle absorption and the scattering coefficients covaried with the vertical changes in the depth dependent chlorophyll concentration, Chl(z). The Gordon and Clark hypothesis can be considered as a sound theoretical framework for interpreting reflectance of a vertically inhomogeneous ocean in terms of an equivalent homogeneous ocean, but it has its limitations when applied practically.

The reflectance of sea water measured by satellite remote sensing is related to the depth-weighted average chlorophyll concentration but no information is obtained about the concentration profile at each specific depth. Most current algorithms are based on the regression analysis between the in-situ measured reflectances and surface constituents' concentrations determined on discrete water samples taken near the sea surface within the top 7 or 10 m of the water column. An example of such an empirical algorithm would be the Ocean Chlorophyll 4(OC4) algorithm (O'Reilly et al, 1998), which is employed for global processing of data from the Sea viewing Wide Field of view Sensor (SeaWiFS) on-board the Sea Star satellite. This algorithm makes use of regression formulas for calculating the surface chlorophyll concentration from the blue to green ratios of ocean reflectance, based on large data sets obtained from in situ measurements. It should be pointed out however that these algorithms are based on large amount of field data that were collected in various oceanic regions throughout different seasons. It is likely that some of these data were collected in the presence of significant effects of a non

uniform Chl(z) profile on ocean reflectance, and some data were collected in the absence of such effects or under nearly homogeneous conditions in the upper ocean layer.

It was recommended by Gordon and Clark (1980) that when remotely sensed concentrations are compared to surface measurements, the comparison should be made with the weighted average over the penetration depth and thus, this quantity should be measured in all field experiments. Accurate determination of the depth weighted average concentration in the field would require the measurement of the vertical profile with (sufficiently) high resolution in depth as well as optical measurements that would permit the determination of the weighting function $g(\lambda,z)$.

Retrieval of the optical properties from remote sensing is a redoubtable problem that has been addressed by relatively few researchers. Zaneveld (1982) used an analytical approach based on a radiative transfer equation to relate the inherent optical coefficients of backscattering and beam attenuation to remote sensing of a multilayered ocean. An expression from the remotely sensed reflectance just beneath the ocean surface was derived and it was shown that the remotely sensed reflectance at a given depth depends only on the inherent optical properties, the attenuation coefficient for upwelling radiance and two shape factors. However, the relationship derived in that study appears to have limited practical value as they involve the dependence on the ocean's apparent optical properties and volume scattering function (Stramska et al, 2005). More recently, Frette at al (2001) described an approach resolving the vertical structure of oceanic waters that consists of two homogeneous layers with

different chlorophyll concentrations. This approach was based on radiative transfer simulations of the coupled atmosphere-ocean system with various chlorophyll dependent optical properties of the two oceanic layers. In addition to the assumptions of a two layer ocean and its optical properties controlled by chlorophyll alone, their approach can be inadequate for a thick upper layer with relatively low chlorophyll concentration or a thinner upper layer with higher chlorophyll concentration.

Sathyendranath and Platt (1989) suggested that if independent information is available on the shape of the pigment profile (for example, the parameters describing a Gaussian profile), the pigment profile can be retrieved in absolute terms from an ocean colour algorithm. It was also shown that nonuniform pigment profiles can lead to a significant error in the retrieval of water column integrated chlorophyll content. The error was shown to be a function of the parameters of the pigment profile.

It should be noted that conventional retrieval algorithms assume that the water body being examined is of a homogeneous nature. These retrieval algorithms give no indication of the stratification present inside the water column. Hence, despite the significant advances that were made in the current understanding of remote sensing of inhomogeneous ocean, the reality is that the present empirical algorithms for retrieval from ocean colour are affected to an unknown degree by the nonuniformity of the elements' profiles or, more generally, by the nonuniformity of the inherent optical properties (IOPs) of the water column. These algorithms typically relate the surface optical concentration to the blue-to-green band ratio of remote sensing reflectance,

which depends on the vertical structure of water column properties. Thus the vertical structure can affect both the scatter data points and the general trend of such relationships.

1.2 Aim of the thesis

The aim of the thesis is to provide a better understanding of the link between the remote sensing reflectance and the vertical structure of the oceans optical properties, to lead to a better interpretation of its effect on the remote sensing reflectance detected. The focus is on trying to interpret how the depth varying sea water constituents affect the reflectance. In this thesis, the study includes both simulated and in situ data to address the problem stated.

The tool developed for this purpose is a Monte Carlo code to simulate the penetration of light in sea water. This method was employed as it is conceptually simple and is based on a straightforward imitation of nature. It is also very general in the sense that it is applicable to any geometry, incident lighting etc and it highlights the fundamental radiative transfer process of absorption and scattering. As a test for the validity of the code set up, a comparison was drawn with reflectance results obtained by the Ocean-Colour Algorithms working group of the International Ocean Colour Coordinating Group, for the same input conditions.

The hypothesis that the reflectance of a stratified water column is the same as that of an equivalent homogeneous ocean with optical properties equal to the corresponding depth-weighted average properties of the stratified ocean over the penetration depth, was tested. This hypothesis was seen to be

valid for both a two-layer ocean and a continuously stratified ocean, although the agreement is better for the two-layer ocean.

The nonuniform vertical profile of chlorophyll concentration modeled as a Gaussian curve was used as an example for the continuously varying water column. A relatively broad range of open ocean conditions characterized by the presence of this chlorophyll subsurface maximum at depths greater than or equal to 20m was simulated. In this case, the simulations for nonuniform depth dependent chlorophyll concentration profiles, Chl(z), were compared to the simulations of a homogeneous ocean. It was found that for some vertical structures of Chl(z) considered, the wavelength dependent reflectance values of the stratified ocean differed significantly from those of the homogeneous ocean, specially in the case for low surface Chl concentrations and shallow pigment maximum.

It now remains to be seen how the optical constituents located at several specific depths contribute to the overall reflectance, for a continuously stratified water column. For this analysis, a multiband quasi analytical algorithm (QAA) was applied for the retrieval of absorption and backscattering coefficients, as well as the absorption coefficients of phytoplankton pigments and gelbstoff. This algorithm was applied to both homogeneous and inhomogeneous water columns. For the homogeneous case, it was found that the retrieved values of the optical constituents compared well with the actual values found in the water column. For the inhomogeneous case stratification was included by the use of a Gaussian function, characterised by the presence of subsurface chlorophyll maximum at depths greater than or

equal to 20 m. The QAA retrieved values for the absorption coefficients at 440 nm and the backscattering coefficients at 555 nm compared to their vertically weighed average values. The correlation between the two sets of values showed that the least error was found when the depth of the chlorophyll maximum was greater.

Gordon and Clark (1980) suggested that the remotely sensed reflectance of a stratified case 1 ocean is identical to that of a hypothetical homogeneous ocean, with a phytoplankton pigment concentration (<Chl>) that is a depth weighted average of the actual depth varying concentration Chl(z). Here keeping in mind the work done above, the hypothesis is examined with Monte Carlo simulations of the radiative transfer for case 1 waters. Two scenarios are used to relate the inherent optical properties to the pigment profile. Firstly the particle absorption and scattering coefficients were made to vary with Chl(z). In the other scenario, the particle absorption coefficient was permitted to covary with Chl(z) but the scattering coefficient was made independent of depth .

After the analysis of simulations, the focus is on the experimental part. The boat trips taken in June and August 2004 yielded in situ data for Singapore waters. The reflectance at the visible wavelengths together with the particle backscattering coefficients at 470 and 700 nm were measured. Absorption coefficient was not measured during the field trips due to lack of necessary equipment. The QAA was used to estimate the total absorption coefficients from the measured reflectance. The measured backscattering coefficients and estimated absorption coefficients were then used as input to

the Monte Carlo code for the generation of reflectance values, which were then compared to those obtained during the field measurements. For the whole range (400-750 nm), it was found that the Monte Carlo simulated reflectance was slightly higher than the in situ one. This mismatch was attributed to the different surface conditions assumed in the simulations and those present during measurements. A better understanding of the relationship between the constituents of the water column examined and the reflectance measured just above the surface was sought here. Thus the QAA was applied to the in situ reflectance for the retrieval of the backscattering coefficients and these values were then compared to those obtained during the field trips. The root mean square error calculated was less for the data at depths 3m and 5m.

1.3 Thesis content

The work is presented in the following way. Chapter two deals with the concept of radiometry. A brief description of the geometrical radiometry is given to explain the terms often used in optical oceanography. The composition of natural waters is also discussed, together with their effects on absorption and scattering. A definition of the phase function is also given and its effects on oceanic light fields are included. The reflectance and the main methods used to measure the reflectance both above and below the water surface are also discussed.

Chapter three mainly concerns the description of the work that has been carried out in the field of oceanography, concerning the inhomogeneous distribution of optical properties of sea water. Brief literature reviews of the

main papers used and referred to in this study are also given. These papers have been summarized to give the main points concerning the work done on continuously stratified waters and the interpretations derived form the results obtained. This chapter also shows how aerial and satellite images show ocean, estuarine, and lake waters to be quite varied in colour and brightness and that remotely sensed data gives no indication of the stratification present in a water column. The information extracted from this kind of data is mostly representative of that of a homogeneous ocean. But, vertical profiles obtained from diverse regions and environments usually show a subsurface maximum in chlorophyll concentration.

Chapter four deals exclusively with the setting up of a Monte Carlo code, the main tool used in this research. A detailed description of the random number generator, the path length, photon sampling etc is given. The Monte Carlo code is then tested and validated with the results obtained by the Ocean-Colour Algorithms working group of the International Ocean Colour Coordinating group (using the numerical radiative transfer code Hydrolight**).**

In chapter five it will be demonstrated that interpreting the reflectance of a stratified medium in terms of an equivalent homogeneous one yields the average of a combination of the optical property over the penetration depth. Then the effects of a nonuniform vertical profile of the inherent optical properties of the water column associated with the chlorophyll concentration, Chl(z) will be studied. A retrieval algorithm will then be applied to both homogeneous and inhomogeneous (described by the Gaussian profile) oceans to see how the retrieved values of the optical coefficients compare with the

actual values found in the water body. The retrieval algorithm used is the Quasi Analytical Algorithm. Then, it will be seen how the reflectance of a stratified ocean compares with a hypothetical homogeneous one with a pigment concentration (<Chl>) that is the depth weighted average of the actual depth varying concentration Chl(z).

Chapter six mainly concerns the acquisition of in situ data. The data of the boat trips undertaken in June and August 2004 in Singapore waters is analysed. It also shows how algorithms for the retrieval of the absorption coefficients and the chlorophyll coefficients have been applied to the remote sensing reflectance obtained in situ.

Chapter seven mainly gives a summary of the theoretical and experimental work that has been carried out. The chapter also gives an interpretation of all the results obtained.

Chapter 2

Aquatic Optics

2.1 Introduction

This chapter provides a brief description of the concept of radiometry, with special emphasis on the propagation of light in an aquatic medium. The main optical properties of the medium through which the light propagates are also explained. This is followed by a summary of the composition of natural waters and the commonly used models relating the concentrations of water constituents to the light scattering and absorption properties of the medium. This chapter also provides the definition of the remote sensing reflectance and the various ways of retrieval of oceanic constituents from this reflectance are also mentioned.

2.2 Radiance and Irradiance

Radiance and irradiance are the two basic quantities describing the radiation field in a medium.

The radiance $L(\theta, \varphi)$, in a specified direction at a point in the radiation field is defined as the radiant flux (Φ) at that point per unit solid angle (Ω) that passes through a cross sectional area $dA\cos\theta$, where θ is the angle between the direction of radiation and normal to the surface and φ is the azimuth angle measured in the plane containing dA

$$L(\theta,\varphi) = \frac{d^2\Phi}{dA\cos\theta d\Omega} \quad \text{(unit: } \mathrm{Wm^{-2}sr^{-1}}\text{).} \qquad 2.1$$

The term irradiance E refers to the radiant flux impinging upon an infinitesimal surface area dA (containing the point in question) divided by that infinitesimal area

$$E = \frac{d\Phi}{dA} \quad \text{(unit: Wm}^{-2}\text{)}. \tag{2.2}$$

In terms of radiance L, the irradiance E is expressed as

$$E = \int_{\Omega} L(\theta,\varphi) \left|\cos\theta\right| d\Omega \tag{2.3}$$

where the integration is carried out over the half space on either side of the surface. The downwelling irradiance E_d is defined as the irradiance at a point due to the stream of downwelling light and the upwelling irradiance E_u is the irradiance at a point due to the stream of upwelling light. Thus

$$E_d = \int_0^{2\pi}\int_0^{\pi/2} L(\theta,\varphi)\cos\theta\sin\theta\, d\theta\, d\varphi \tag{2.4}$$

$$E_u = -\int_0^{2\pi}\int_{\pi/2}^{\pi} L(\theta,\varphi)\cos\theta\sin\theta\, d\theta\, d\varphi \tag{2.5}$$

The ratio of upwelling irradiance at a point to the downwelling irradiance at that point is termed the irradiance reflectance.

$$R = \frac{E_u}{E_d} \tag{2.6}$$

The average cosine $\bar{\mu}_d$ of the downwelling radiance distribution is expressed as

$$\bar{\mu}_d = \frac{\int_0^{2\pi}\int_0^{\pi/2} L(\theta,\varphi)\cos\theta\sin\theta\, d\theta\, d\varphi}{\int_0^{2\pi}\int_0^{\pi/2} L(\theta,\varphi)\sin\theta\, d\theta\, d\varphi} \tag{2.7}$$

The average cosine $\bar{\mu}_u$ of the upwelling radiance distribution is expressed as

$$\bar{\mu}_u = -\frac{\int_0^{2\pi}\int_{\pi/2}^{\pi} L(\theta,\varphi)\cos\theta\sin\theta\, d\theta\, d\varphi}{\int_0^{2\pi}\int_{\pi/2}^{\pi} L(\theta,\varphi)\sin\theta\, d\theta\, d\varphi} \qquad 2.8$$

2.3 Attenuation of light in an aquatic medium

Photons entering and propagating within a natural water body will undergo scattering or absorption interactions with the materials comprising the natural water body. Both scattering and absorption interactions result in changes to the original subsurface radiance distribution as the photon flux propagates through the aquatic medium and combine to reduce the intensity of the radiance distribution, while the scattering processes also change the directional nature of the radiance distribution.

The absorption coefficient, *a(λ)* is the radiant energy absorbed from a beam as it traverses an infinitesimal distance ∂r and can be expressed in terms of the radiant flux Φ as

$$a(\lambda) = -\frac{[\partial\Phi(r,\lambda)]_{abs}}{\Phi(r,\lambda)\partial r} \quad \text{(unit: m}^{-1}\text{).} \qquad 2.9$$

The subscript abs has been added to indicate the process of absorption.

The radiant flux is also subject to attenuation due to scattering. The scattering coefficient can be defined as the fraction of radiant energy scattered from a beam per unit distance as it traverses an infinitesimal distance ∂r.

$$b(\lambda) = -\frac{[\partial\Phi(r,\lambda)]_{scatt}}{\Phi(r,\lambda)\partial r} \quad \text{(unit: m}^{-1}\text{).} \qquad 2.10$$

The subscript scatt denotes the diminution of radiant energy as it traverses an infinitesimal distance ∂r due to scattering processes.

In a natural medium such as air and water where both absorption and scattering processes are responsible for attenuation, the beam attenuation coefficient, *c(λ)*, is defined as the fraction of radiant energy removed from an incident beam per unit distance as it traverses an infinitesimal distance ∂ r due to the combined processes of absorption and scattering., i.e.

$$c(\lambda) = a(\lambda) + b(\lambda) \quad \text{(unit: m}^{-1}\text{).} \tag{2.11}$$

All three of the optical properties *a(λ)*, *b(λ)* and *c(λ)* qualify as inherent optical properties of the medium as they are independent of the radiation distribution within that medium. The angular distribution of the scattered flux is specified in terms of the volume scattering function, $\beta(\theta,\varphi)$ where θ is the angle of scattering and φ is the azimuthal angle of scattering. Figure 2.1 schematically illustrates an irradiance E_{inc} incident upon an infinitesimal volume *dV* within an attenuating medium. The scattered radiant intensity *dI* is shown as being contained within the cone defined by the solid angle $d\Omega$ at a location defined by the angular coordinates θ and φ. The volume scattering function, $\beta(\theta,\varphi)$ is then defined as the scattered radiant intensity *dI* in a direction (θ,φ) per unit scattering volume *dV* per unit irradiance $E_{inc.}$

$$\beta(\theta,\varphi) = \frac{dI(\theta,\varphi)}{E_{inc}dV} \tag{2.12}$$

Each attenuating medium, is characterized by its own particular $\beta(\theta,\varphi)$ function, and the integral of the volume scattering function coefficient $\beta(\theta)$ over all directions

$$b = 2\pi \int_0^{\pi} \beta(\theta)\sin\theta \, d\theta \tag{2.13}$$

For isotropic scattering, β is a constant, independent of θ and equation 2.13

reduces to

$$b = 2\pi\beta \int_0^{\pi} \sin\theta d\theta = 4\pi\beta \qquad 2.14$$

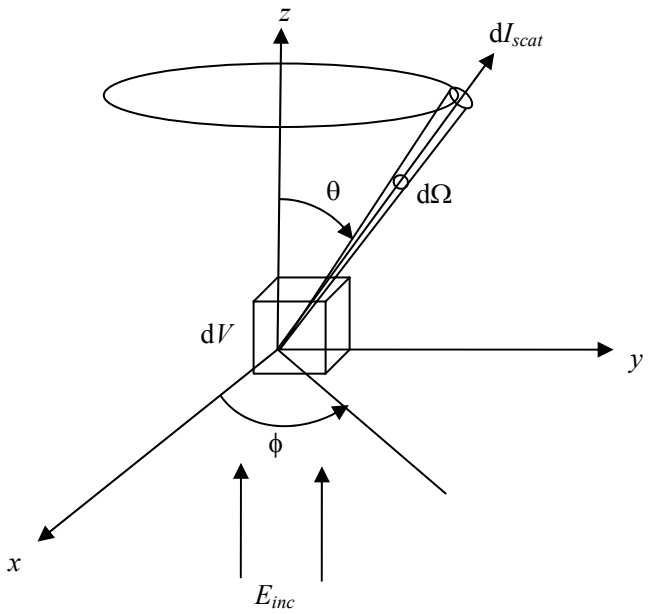

Figure 2.1 Illustration of the volume scattering function β(θ,φ)

When studying photon propagation through an aquatic medium, it is sometimes essential to distinguish among total scattering, directional scattering into the hemisphere trailing the incident flux (backscattering) and directional scattering into the hemisphere ahead the incident flux (forwardscattering)

In other words

$$b = b_f + b_b \qquad 2.15$$

Hence,

$$b_f = 2\pi \int_0^{\pi/2} \beta(\theta)\sin\theta d\theta \qquad 2.16$$

and

$$b_b = 2\pi \int_{\pi/2}^{\pi} \beta(\theta)\sin\theta d\theta . \qquad 2.17$$

The forwardscattering probability, F, is defined as the ratio of the forward scattering coefficient to the total scattering coefficient.

$$F = \frac{b_f}{b} . \qquad 2.18$$

Similarly, the backscattering probability, B, is defined as the ratio of the backscattering coefficient to the total scattering in all directions

$$B = \frac{b_b}{b} . \qquad 2.19$$

Obviously,

$$F+B = 1. \qquad 2.20$$

The irradiance attenuation coefficient, $K(\lambda, z)$, is defined as the logarithmic depth derivative of the spectral irradiance at subsurface depth z

$$K(\lambda,z) = \frac{-1}{E(\lambda,z)}\frac{dE(\lambda,z)}{dz} \qquad \text{(unit: m}^{-1}\text{)} \qquad 2.21$$

Similarly, the values of K_d and K_u may be used to refer to the attenuation of the downwelling E_d and upwelling E_u irradiances at depth z respectively.

$$K_d(\lambda,z) = \frac{-1}{E_d(\lambda,z)}\frac{dE_d(\lambda,z)}{dz} \qquad 2.22$$

and

$$K_u(\lambda,z) = \frac{-1}{E_u(\lambda,z)}\frac{dE_u(\lambda,z)}{dz} \qquad 2.23$$

The value of irradiance attenuation coefficient $K(\lambda,z,\theta_i)$ varies with the value of the solar zenith angle θ_i.

Both c and K represent total subsurface attenuation and consequently define the removal of beam energy due to combined processes of absorption and scattering. Since c is not constrained to a pre-selected direction and is

independent upon the presence of photons in the optical medium, it is an inherent optical property. *K*, being dependent upon the directionality of the radiance distribution comprising the downwelling irradiance, is an apparent optical property of the medium.

The attenuation length l_{att} is the path distance in the attenuating medium that is required to reduce the radiant energy of a light beam by a factor of 1/e. $l_{att}(\lambda,z)$ can therefore be defined as the inverse of the beam attenuation coefficient $c(\lambda,z)$.

$$l_{att}(\lambda,z) = \frac{1}{c(\lambda,z)} \qquad 2.24$$

The penetration depth of the light in the sea is defined for remote sensing purposes as the depth above which 90% of the diffusely reflected irradiance (excluding specular reflectance) originates (Gordon and Mc Cluney, 1975). A more detailed description of the penetration depth of light in sea water is given in Appendix A.

The scattering albedo, ω_o, is defined as the ratio of the scattering coefficient to the attenuation coefficient

$$\omega_o = \frac{b}{c} \qquad 2.25$$

The apparent optical properties of water mass such as the reflectance and irradiation attenuation coefficients are those that are dependent upon the angular distribution of the impinging radiation. Remote sensing, by the very nature of its data gathering devices, its varying viewing positions above the targeted water body, and its atmospheric conditions is not granted the luxury of directly recording the inherent optical properties of the aquatic medium.

The interpretation of data remotely sensed above an aquatic water body must, therefore, rely heavily upon the relationships that link the apparent optical properties of that aquatic body with its inherent optical properties.

2.4 Photon interaction with air-water interface

The photon flux emanating from the volume of the water must interact with the air-water interface on two occasions, namely (a) its downwelling propagation through the atmosphere and (b) its downwelling and upwelling propagation through the aquatic medium. It is then finally recorded on a remote platform. In each instance, part of the impinging radiation will reflect back into the original medium and part of it will refract and transmit into the adjacent medium. The amount of reflection, refraction and transmission for a calm surface are calculable from the indices of refraction of the respective media. The Fresnel reflectance formulae can be used to compute the reflectance from the air-water interface.

2.5 Inherent optical properties of natural water constituents

Natural waters are complex physical, chemical, biological media comprising living, non-living and once living material that may be present in aqueous solution or in aqueous suspension. The various constituents of water are:

1. pure water which is taken to imply water that is free from the optical effects of terrestrially and/or atmospherically derived organic and inorganic matter;

2. dissolved salts and gases that do not contribute significantly to the optical properties at the visible wavelength range;
3. dissolved organic matter which is due to either photosynthetic activity (autochtonic) or direct inputs of terrestrially derived matter (allocthonic);
4. suspended matter which includes mineral particles of terrigenous origin, plankton, detritus (largely residual products of the decomposition of phytoplankton and zooplankton cells as well as macrophytic plants), volcanic ash particles, particulates resulting from in situ chemical reactions, and particles of anthropogenic origin;
5. planktons which are principal living organisms present in water columns, encompassing all vegetable and animal organisms suspended in water (either hovering or floating), unable to resist the current and not rigidly connected to the confining basis.

2.5.1 Absorption by pure sea water

Smith and Baker (1981) determined the absorption coefficient of pure sea water from measured values of the diffuse attenuation coefficients of very clear sea waters. Their tabulated values are widely used. The more recent measurements of water absorption coefficients were carried out by Pope and Fry (1997). The method used is the integrating cavity technique, in which all the light energy removed from the incident light field is measured. The integrating cavity absorption meter (ICAM) allows the measurement of very small optical absorption coefficients (0.001 m^{-1}), virtually independent of

scattering effects in the sample. The sample is isotropically illuminated in a cavity whose walls have a very high diffuse reflectivity (＞99%). The optical energy lost in the cavity is proportional to the absorption coefficient of the sample. The ICAM was used to measure the spectrum of the water in the 380−700 nm wavelength region.

2.5.2 Absorption by dissolved organic matter

Absorption by yellow matter (CDOM or gelbstoff) is quite well described by the model (Bricaud et al, 1981)

$$a_g(\lambda) = a_g(\lambda_0)\exp[-S_g(\lambda - \lambda_0)] \qquad 2.26$$

over the range 350nm ≤ λ ≤450nm, where the reference wavelength λ_o is often chosen to be 440nm. $a_g(\lambda_o)$ is the absorption due to yellow matter at the reference wavelength and the value of $a_g(\lambda)$ is dependent upon the concentration of yellow matter in the water. The exponential constant, S_g, depends on the relative proportion of specific types of yellow matter in the water and some studies have found them to be of values between 0.014 and 0.019 nm^{-1} (Kirk, 1976).

2.5.3 Absorption by phytoplankton

Absorption by chlorophyll, the photosynthetic pigment found in phytoplanktons, is characterized by strong absorption bands in the blue and red (peaking at λ around 440 nm and 675 nm respectively for chlorophyll) (Hemandez et al. 2004) As chlorophyll occurs in all photosynthetic plants, its concentration in milligrams of chlorophyll per cubic meter of water can be

used as the relevant measure of phytoplankton abundance. Chlorophyll concentrations for various waters range from 0.01 mg m^{-3} in the clearest open ocean waters, to 10 mg m^{-3} in productive coastal upwelling regions, to 100 mg m^{-3} in eutrophic estuaries or lakes.

The phytoplankton pigment absorption $a_{ph}(\lambda)$ is expressed as follows

$$a_{ph}(\lambda) = a_{ph}(440) a_{ph}^{*}(\lambda) \qquad 2.27$$

where $a_{ph}^{*}(\lambda)$ is the $a_{ph}(440)$ normalized spectral shape. Absorption by phytoplankton at 440 nm, $a_{ph}(440)$, is often related to the chlorophyll concentration *Chl* (measured in mg/m^3) by an empirical equation of the form (Sathyendranath et al, 1987)

$$a_{ph}(440) = 0.05 Chl^{0.626} \qquad 2.28$$

In oceanic waters, optical properties of phytoplankton and specifically their in vivo absorption coefficient, play a key role in determining both the penetration of the radiant energy within sea water and the use of this radiant energy for photosynthesis. $a_{ph}^{*}(\lambda)$ comes from extensive measurements of Bricaud et al(1995, 1998) and Carder et al (1999).

Figure 2.2 is based on absorption measurements of phytoplanktons for 3 different values of *Chl*, namely 0.7, 1.5 and 3 mgm^{-3}. There are several features of phytoplankton absorption that can be seen:

1. there are distinct absorption peaks at λ=440nm and 675nm;
2. the blue peak is higher than the red one;
3. the absorption between 550 and 650 nm is relatively low.

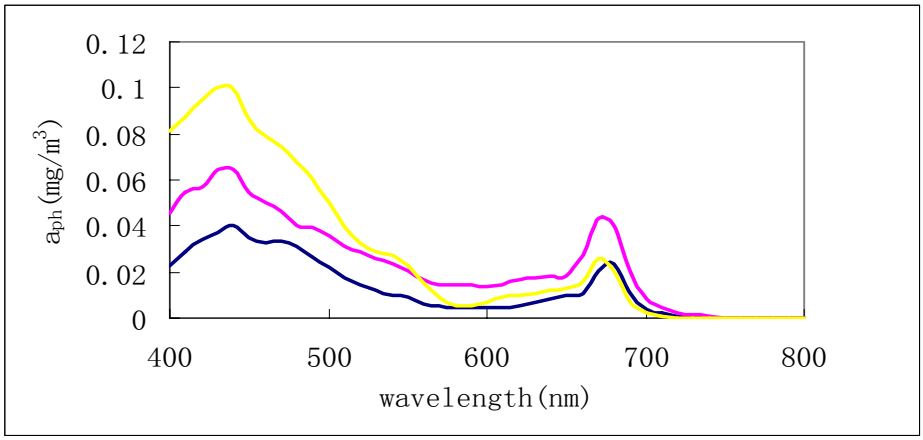

Figure 2.2 Chlorophyll-specific spectral absorption coefficients for 3 values of *Chl.*

For equation 2.28, it should be noted that parameters 0.05 and 0.626 can vary a lot from place to place. These values have been used to merely set the reasonable values and range of $a_{ph}(440)$ for a given chlorophyll concentration. In this thesis, we are concerned mainly with the dependence of reflectance with the absorption and scattering coefficients. As long as $a_{ph}(440)$ values are reasonable, it is not crucial to know how $a_{ph}(440)$ varies with *Chl*.

2.5.4 Absorption by organic detritus

The contributions of living phytoplankton and of non-living detritus to the total particulate absorption cannot be easily separated. Several ways of achieving this separation have yielded the same functional form for absorption by detritus, $a_{det}(\lambda)$

$$a_{\mathrm{det}}(\lambda) = a_{\mathrm{det}}(400)\exp[-S_{\mathrm{det}}(\lambda - 400)] \qquad 2.29$$

where other studies have found the detrital exponent coefficient S_{det} to be of value ranging from 0.006 to 0.011 nm^{-1} (Roesler et al,1989).

2.5.5 Scattering by pure water and pure sea water

In water, random molecular motions give rise to fluctuations in the number of molecules in a given volume ΔV, where ΔV is small compared to the wavelength of light but large compared to atomic scales. The Einstein-Smolouchowski theory of scattering relates these fluctuations in molecule number density to associated fluctuations in the index of refraction, which give rise to scattering. The same basic theory applies to sea water, but random fluctuations in the concentrations of the various ions (Cl^-,Na^+,….) give somewhat greater index of refraction fluctuations and hence greater scattering. Hence for either pure water or pure sea water, the volume scattering function has the following form

$$\beta_w(\varphi,\lambda) = \beta_w(90^0;\lambda^0)\frac{\lambda_0}{\lambda}^{4.32}(1+0.835\cos^2\varphi) \qquad 2.30$$

The wavelength dependence of $\lambda^{-4.32}$ results from the wavelength dependence of the index of refraction. The 0.835 factor is attributable to the anisotropy of the water molecules. The phase function is

$$\tilde{\beta}(\varphi) = 0.06225(1+0.835\cos^2\varphi) \quad (\text{unit:sr}^{-1}) \qquad 2.31$$

and the total scattering coefficient $b_w(\lambda)$ is given by Morel(1974) as

$$b_w(\lambda) = 16.06(\frac{\lambda_0}{\lambda})^{4.32}\beta_w(90,\lambda_0). \qquad 2.32$$

2.5.6 Scattering by particles

The scattering by particles is modeled by the following expression (Morel and Prieur, 1977, Bricaud et al.1981, Bricaud and Morel 1986, Gordon et al.1988)

$$b_{bp} = X(\frac{\lambda_0}{\lambda})^Y \qquad 2.33$$

where λ_o is a reference wavelength often chosen to be around 550 nm in most cases.

2.6 Optical and bio-optical parameters for IOP

It was discussed that once the optical cross section spectra for the indigenous organic and inorganic components were known, the bulk optical properties $a(\lambda)$, $b(\lambda)$ and $b_b(\lambda)$ could be generated for water columns made up of any pre selected combinations of co existing concentrations of those components from the additive equations

$$a(\lambda) = a_w(\lambda) + a_{ph}(\lambda) + a_{\det}(\lambda) + a_g(\lambda)$$
$$b_b(\lambda) = b_{bw}(\lambda) + b_{bp}(\lambda) \qquad 2.34$$

Monte Carlo simulations of the radiative transfer process could then be used to relate the subsurface volume reflectance spectra just beneath the air water interface, $R(0, \lambda)$ to these bulk inherent properties. The ideal bio optical water model incorporates the cross section spectra pertinent to each 'optically active' organic and inorganic aquatic component whether that component is in suspension or solution.

The bio-optical model used throughout this thesis to generate the wavelength dependent inherent optical properties of waters is described as follows

$$a(\lambda) = a_w(\lambda) + a_{\varphi}(\lambda) + a_g(\lambda)$$
$$b_b(\lambda) = b_{bw}(\lambda) + b_{bp}(\lambda) \qquad 2.35$$

The values of $a_w(\lambda)$ and b_{bw} (λ) were taken from Smith and Baker(1981). In equation 2.35, $a_{\det}$ and a_g are lumped together into $a_g(\lambda)$, to represent the absorption due to all the non-chlorophyllous particle components and

dissolved organic matter.

The following bio optical models (Lee et al, 2002) were used to create sets of inherent optical properties that simulate oceanic and coastal waters

$$a_\varphi(440) = (A(Chl)^{-B})(Chl)$$

$$a_g(440) = p_1 a_\varphi(440) \qquad 2.36$$

$$b_{bp}(555) = \{0.002 + 0.02[0.5 - 0.2\log(Chl)\}(Chl)^{0.62}$$

Furthermore

$$a_\varphi(\lambda) = \{a_0(\lambda) + a_1(\lambda)\ln[a_\varphi(440)]\}a_\varphi(440)$$

$$a_g(\lambda) = a_g(400)\exp[-S(\lambda - 400)] \qquad 2.37$$

$$b_{bp} = b_{bp}(555)(\frac{555}{\lambda})^Y$$

where values for $a_o(\lambda)$ and $a_1(\lambda)$ are taken from Lee et al. (1998).

For case 1 waters, $p_1 \approx 0.3$, $Y \approx 1.0\text{-}1.5$ and average A and B values are 0.0403 and 0.332 respectively; so that all optical properties covaries with Chl values and only fixed $r_{rs}(\lambda)$ spectrum is created for a Chl value. It should be pointed out that here Chl is used only as a free parameter for designation for a wide range of absorption and backscattering values.

However, it is found in the field that different $r_{rs}(\lambda)$ spectra exist for the same Chl values. To accommodate such observations, B was kept at 0.332 and the other case 1 parameters were perturbed in the following way

$$A = 0.03 + 0.03\,\alpha_1$$

$$p_1 = 0.3 + (3.7\alpha_2 a_\varphi(440))/(0.02 + a_\varphi(440)) \qquad 2.38$$

$$p_2 = 0.01 + 0.8\alpha_3$$

$$Y = 0.1 + (1.5 + \alpha_4)/(1 + Chl)$$

$$S=0.013 +0.004\alpha_5$$

where α_1, α_2, α_3, α_4, α_5 are random values between 0 and 1. These kinds of perturbation make *A, p_1, p_2, Y* and *S* random values for each Chl value, but fall in a range generally consistent with field observations. In general *A* will range between 0.013 and 0.06, P_1 between 0.3 and 4.0, P_2 between 0.1 and 0.9, *Y* between 0.1 and 2.5 and *S* between 0.013 and 0.017nm^{-1}. Also, to be consistent with field observations, the range for p_1 is narrow for low Chl values (open ocean) and wider for high Chl values (coastal), and *Y* decreases with increasing Chl values, but in a random way for both p_1 and *Y*.

For a range of values of the chlorophyll concentration, Chl, a series of values were generated for the total absorption coefficient at 440nm, *a(440)* and the total backscattering coefficient at 555 nm, $b_b(555)$. As can be seen from Figures 2.3 (a) and (b), most of the *a(440)* values are in the range of 0 - 0.1 m^{-1} and the $b_b(555)$ values are in the range 0 - 0.001 m^{-1}. For each Chl, more than one value of *a(440)*and $b_b(555)$ were generated. The results hence show that the sets of values of *a(440)* generated from the same Chl are not very different , despite the randomness present in the biooptical models. The same can be said for the $b_b(555)$ results.

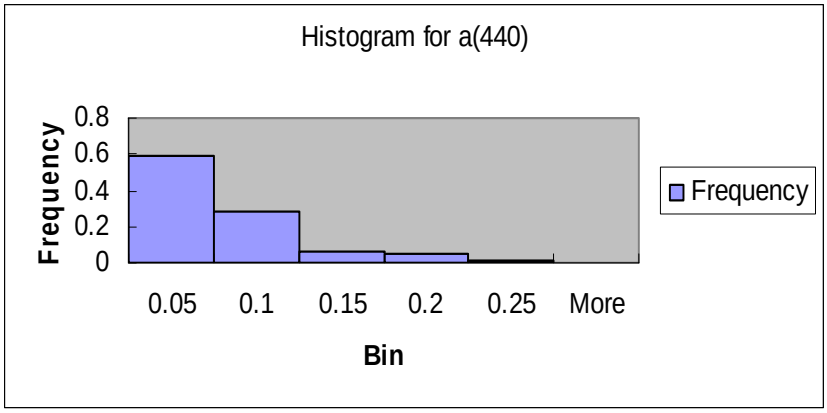

Figure 2.3(a) Histogram for α(440)

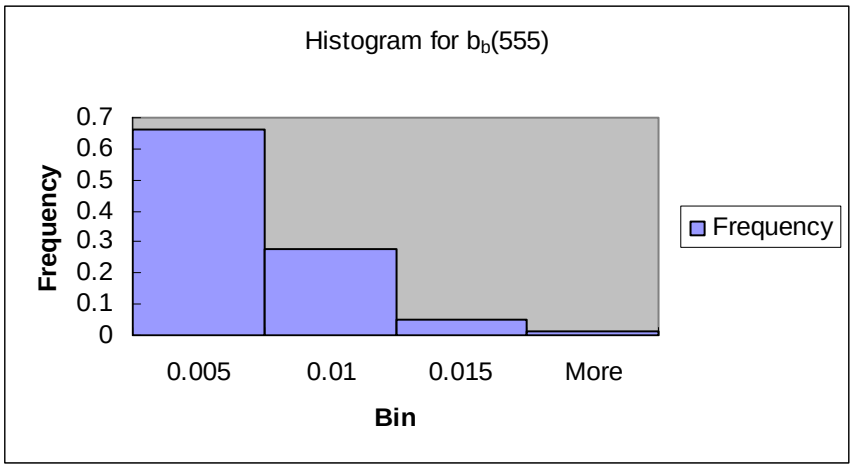

Figure 2.3(b) Histogram for b_b(555)

2.7 Phase function effects on oceanic light fields

The absorption coefficient *a* and the volume scattering function (VSF) β completely determine the inherent optical properties (IOPs) of a medium. Given *a* and β throughout a medium, along with some suitable boundary conditions, the radiative transfer equation can be solved to obtain the radiance distribution within and leaving the medium (Mobley, 2002). Oceanic absorption coefficients have been intensively studied and are routinely measured *in situ* as functions of depth and wavelength with commercially available instruments. However the VSF is rarely measured in the ocean even though β is fundamentally important to understand and predict oceanic radiance distributions and related quantities.

The VSF is a function of the (polar) scattering angle θ which is measured from 0 in the incident (forward) direction. The integral of the VSF over all scattering directions gives the scattering coefficient b, which is a measure of the overall magnitude of scattering without regard to the angular pattern of the scattered light. The VSF is usually factored into b times the

scattering phase function $\tilde{\beta} = \beta / b$ which specifies the angular dependence of the scattering without regard for its magnitude. The unmeasured phase function $\tilde{\beta}$ is usually approximated in one of the three ways.

1. Any of the several simple functional forms for $\tilde{\beta}$ can be used. Although these analytic approximations are mathematically convenient, they often give unrealistic phase functions, especially at small (near forward) or large (near-backward) scattering angles.
2. Mie theory can be used to compute $\tilde{\beta}$ numerically. However, it required as input the complex index of refraction and size distribution of the scattering particles in the water body, and these quantities are seldom measured. Moreover, Mie theory assumes that the particles are homogeneous and spherical, which is seldom the case for oceanic particles.
3. A phase function derived from one of the rare measurements can be employed. The most commonly used VSF data set consists of eight VSFs measured by Petzold in 1971. An average $\tilde{\beta}$ derived from his data is used frequently in numerical radiative transfer studies.

The Petzold average-particle phase function was derived from three measurements of the VSF in San Diego Harbor (Petzold, 1972). When numerically integrated over $90 \leq \varphi \leq 180$ degrees, this phase function gives a particle backscatter fraction of $B = 0.0183$. Because this phase function is based on observations and is so frequently used, it can be considered as a benchmark for defining and evaluating phase functions. This phase function is plotted in Figure 2.4.

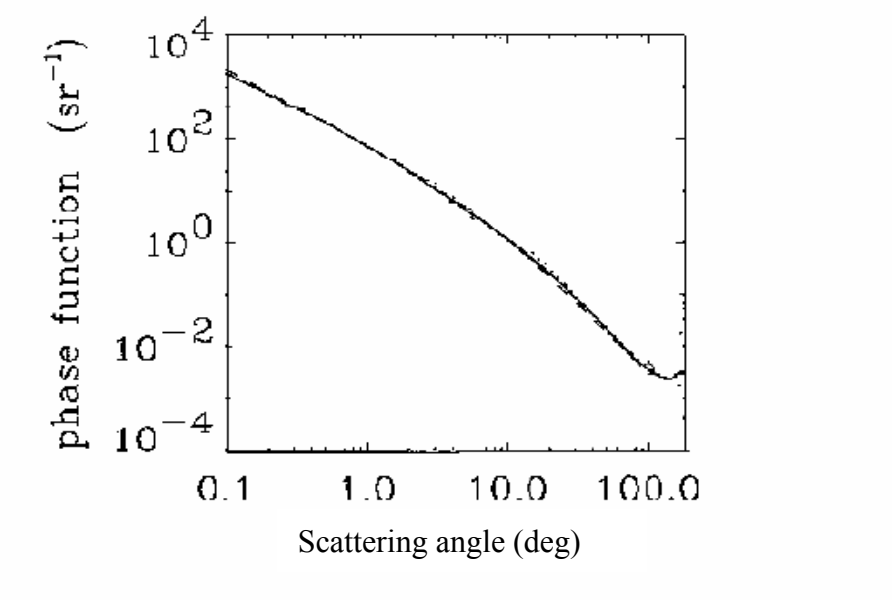

Figure 2.4 Diagrams showing the Petzold phase function. (adapted from Phase function effects on oceanic light field, Mobley (2002))

2.8 Reflectance

The spectral remote sensing reflectance R_{rs} is defined as

$$R_{rs}(\theta,\varphi,\lambda)\frac{L_u(z=z_a,\theta,\varphi,\lambda)}{E_d(z=z_a,\theta,\varphi,\lambda)} \qquad 2.39$$

where depth $z=z_a$ indicates that R_{rs} is evaluated using L and E_d in the air, just above the water surface. L is often called 'the water leaving' radiance. R_{rs} is a measure of how much the downwelling light that is incident into the water surface is eventually returned through the surface in direction (θ,φ), so that it can be detected by a radiometer pointed in the opposite direction.

Spectral remote sensing reflectance $R_{rs}(\lambda)$ contains information about the properties of the oceanic surface layer whose thickness depends on the ocean's inherent and apparent optical properties. Ocean colour remote sensing is an important technique to obtain the optical properties and oceanic constituents in the upper ocean layer. In general, ocean colour remote sensing is one of the passive remote techniques. Experimentally, the sensor, mounted

on a satellite, an aircraft or other remote platform, detects the radiometric flux at several selected wavelengths in the visible and near-infrared domains. The signal received by the sensor is determined by different processes in the water, as well as in the atmosphere. Only the portion of the signal originating from the water body contains information on the water constituents.

From the interaction principle for irradiance,

$$\begin{aligned} E_u(z_a) &= E_u(w)t(w,z_a) + E_d(z_a)r(z_a,w) \\ E_d(w) &= E_u(w)r(w,z_a) + E_d(z_a)t(w,z_a) \end{aligned} \qquad 2.40$$

where z_a indicates that the properties are being evaluated in the air, just above the water surface and w indicated that the properties are being evaluated just beneath the water surface, r and t are the irradiance transfer functions that depend on the nature of the surface and incident radiance distribution and $t=1-r$.

The upwelling radiance just beneath the water surface $L(w;\ \theta,\varphi)$ is related to the water leaving radiance $L_w(a,\theta,\varphi)$ by

$$L_w(z_a;\theta,\varphi) = \frac{t(w,z_a;\theta',\varphi'\to\theta,\varphi)}{{n_w}^2} L(w;\theta',\varphi') \qquad 2.41$$

Substituting Equations 2.40and 2.41 into Equation 2.39 gives

$$R_{rs}(\theta,\varphi) = \frac{t(w,z_a;\theta',\varphi'\to\theta,\varphi)t(z_a,w)}{{n_w}^2} \frac{L(w;\theta',\varphi')}{E_d(w) - E_u(w)r(w,z_a)} \qquad 2.42$$

This equation can be rewritten as

$$R_{rs}(\theta,\phi) = \frac{t(w,z_a;\theta',\varphi'\to\theta,\varphi)t(z_a,w)}{{n_w}^2[1-R(w)r(w,z_a)]} \frac{R(w)}{Q(w,\theta',\varphi')} \qquad 2.43$$

where $R(w) \equiv \dfrac{E_u(w)}{E_d(w)}$ and $Q(w;\theta',\varphi') \equiv \dfrac{E_u(w)}{L(w;\theta',\varphi')}$.

The irradiance reflectance R is almost always less than 0.1 in case 1

waters and Equation 2.43 can be approximated by

$$R_{rs} \approx 0.54 \frac{R}{Q} \qquad 2.44$$

The ratio *R/Q* can be connected with the IOPs of a water body. Gordon et al (1988) showed that for case 1 waters,

$$\frac{R}{Q} \approx 0.095 \frac{b_b}{a + b_b}. \qquad 2.46$$

2.9 Retrieval of oceanic constituents from ocean colour measurements at sea level

There are three major issues in the retrieval of oceanic constituents from ocean colour which is determined by the spectral remote sensing reflectance:

- How to quantify the relationship between optically significant oceanic constituents and inherent optical properties (IOPs) ?
- How do IOPs determine ocean colour ?
- How to obtain oceanic constituents from ocean colour measurements?

The first two issues are the so called 'forward problem', and the last issue is the so called 'inverse problem'.

2.9.1. The forward problem

The forward problem is solved by radiative transfer theory. Radiative transfer theory describes the relationship between the IOPs of the oceanic constituents and the ocean colour. The three main forward modelling techniques are

1. Monte Carlo method
2. semi analytical model

3. Radiative transfer model

2.9.1.1 Monte Carlo Method

Numerical methods that are known as Monte Carlo methods can be loosely described as statistical simulation methods, where statistical simulation is defined in quite general terms to any method that utilizes sequences of random numbers to perform the simulation. Assuming that the evolution of the physical system can be described by probability density functions pdfs, then the Monte Carlo simulation can proceed by sampling from these pdfs, which necessitates a fast and effective way to generate random numbers uniformly distributed on the interval [0, 1]. The outcomes of these random samplings, or trials, must be accumulated or tallied in an appropriate manner to produce the desired result, but the essential characteristic of Monte Carlo is the use of random sampling techniques to arrive at a solution of the physical problem.

Gordon et al (1975) used Monte Carlo simulations to relate the apparent optical properties *K(z), $D_d(z)$* and *R(z)* to the inherent optical properties *c, ω_o, F, B* through the following equations

$$\frac{K(z)}{c\,D_d(z)} = \sum_{n=0}^{N} k_n(z)[\omega_0 F]^n \qquad 2.47$$

and

$$R(z) = \sum_{n=0}^{n=3} r_n(z)[\frac{\omega_0 B}{1-\omega_0 F}]^n \qquad 2.48$$

where ω_o is the scattering albedo, *F* is the forward scattering probability, *B* is the backscattering probability, *K(z)* is the irradiance attenuation coefficient for

downwelling irradiance at depth *z*, *R(z)*is the volume reflectance at depth *z*, $D_d(z)$is the distribution function of downwelling irradiance at depth z (i.e. the inverse of the downwelling average cosine, defined in equation 2.7) and c is the total attenuation coefficient. $k_n(z)$ and $r_n(z)$ are sets of expansion coefficients.

The above equations were inverted to obtain the inherent optical properties from measurements of *K(z), R(z)* and *c*.

$$\omega_0 F = \sum_{n=0}^{N} K'(n) \qquad 2.49$$

$$\frac{\omega_o B}{1-\omega_o F} = \sum_{n=0}^{N} r'_n(z)[R(z)]^n \qquad 2.50$$

Two sets of coefficients $rB'_n(z)$ appropriate for solar angles $\leq\sim 20^o$ (sun case) and appropriate for solar angle $\geq\sim 30^o$ (sky case) have been determined by Gordon et al. The single set of $kB'_n(z)$ coefficient was independent of sun angle.

The distribution function of downwelling irradiance at depth z, $D_d(z)$ was shown to be related to the inherent optical properties as follows

$$D_d(z) - D_{d0}(z) \sum_{n=0}^{N} d_n(z)[\frac{\omega 0 B}{1-\omega 0 F}]^n \qquad 2.51$$

where $d_n(z)$ are expansion coefficients and D_{d0} is the value of the downwelling distribution function at depth z for a water body defined by a scattering albedo ω_o =0.0

Equations 2.48, 2.50 and 2.51 then enabled the apparent optical properties *K(z), R(z)* and the inherent optical property c to be used in the

determination of ω_o and F and hence *a, b* and *B*.

Kirk (1981) also used Monte Carlo simulations of photon propagation to determine relationships between inherent and apparent optical properties. Kirk's simulations concerned turbid inland waters and coastal waters and determined the relationships for $\omega_o \leq 0.968$. The volume scattering function $\beta(\theta)$ obtained in San Diego harbour by Petzold (1972) was used, for which B=0.019.

For the case of vertical incidence, the following relations was obtained by Kirk

$$K_d(z_m) = (a_2 + 0.256ab)^{\frac{1}{2}} \tag{2.52}$$

$$R(0) = 0.328\frac{Bb}{a} \tag{2.53}$$

where z_m is the vertical point of the mid-point of the euphotic zone and *R(0)* is the volume reflectance just beneath the air-water interface. Later, the effect of non vertical incidence was incorporated, leading to the following

$$K_d(z_m) = \frac{1}{\mu_0}[a^2 + (0.473\mu_0 - 0.218)ab]^{\frac{1}{2}}$$
$$R(0) = (0.975 - 0.629\mu_0)Bb/a \tag{2.54}$$

where $\mu_o = cos(\theta_o)$, θ_o being the in water refracted solar angle.

Jerome et al (1988) obtained the following relationships

$$R(0) = \frac{1}{\mu_0}[0.013 + 0.267\frac{Bb}{a}] \tag{2.55}$$

for $0.25 \leq Bb/a \leq 0.50$. At the time of analyses, Jerome et al noted departures from the above relationships at large solar zenith angles, suggestive of a

possible second order relationship between *R(0)* and *Bb/a*, a relationship whose impact increased with increasing θ, indicating that a additional term should perhaps be added to the above equations.

Monte Carlo as a forward simulation method provides a general relationship between the apparent optical properties such as $R_{rs}(\lambda)$) and the inherent optical properties $a(\lambda)$, $b(\lambda)$). It is not directly used for the retrieval of oceanic constituents.

2.9.1.2 Semianalytic model

In the analytic approach, radiative transfer theory provides a relationship between upwelling radiance or irradiance values measured at several wavelengths by inversion of the resultant system of equations. The term 'semi analytical' is invoked as the biooptical pieces of the radiative model are expressed by empirical relationships.

The example of a semi analytic model used by Gordon et al (1988) was developed to predict the upwelled spectral radiance at the sea surface as a function of the phytoplankton pigment concentration for Case 1 waters. Gordon carried out extensive computations of *R/Q* as a function of the optial properties of the water and the solar zenith angle, θ_o, and concluded that for $\theta_o \geq 20^o$, the ratio *R/Q* can be directly related to the inherent optical properties of the water, the absorption coefficient a and the scattering coefficient b_b through

$$\frac{R}{Q} = \sum_{i=1}^{2} l_i \left(\frac{b_b}{a + b_b}\right)^i \qquad 2.56$$

where l_1=0.0949 and l_2=0.0794. The error was less than 10% for a wide range

of realistic scattering phase function.

2.9.1.3 Radiative transfer model

The classical radiative transfer equation is given as (Chandrasekhar 1950)

$$\frac{dL(z,\theta,\varphi)}{dr} = -cL(z,\theta,\varphi) + L^*(z,\theta,\varphi) \qquad 2.57$$

where $L(z,\theta,\varphi)$ is the radiance at depth z of a photon beam propagating in the direction (θ,φ) and $\frac{dL}{dr}$ is the change of radiance along the direction r experienced by this photon beam due to the combined processes of absorption and scattering. The first term on the right hand side of the equation $(-cL(z,\theta,\varphi))$ represents loss due to attenuation and the second term $L^*(z,\theta,\varphi)$ represents gain due to scattering. $L^*(z,\theta,\varphi)$, called the path function, is a consequence of the scattering occurring in every infinitesimal volume of the medium and is generalized in terms of the probability that a photon that is propagating along a direction other than (θ,φ) prior to a scattering event will propagate along the direction (θ,φ) subsequent to the scattering event.

The radiative transfer equation as applicable to oceanographic and limnological remote sensing in the visible region (Bukata et al. 1995) may be written as

$$\cos\theta \frac{dL(z,\theta,\varphi)}{dz} = cL(z,\theta,\varphi) - \beta(\theta,\varphi;\theta_0,\varphi_0)E_i \exp(cz\sec\theta_0) \qquad 2.58$$

$$- \int_{\theta'=0}^{\pi} \int_{\varphi'=0}^{2\pi} \beta(\theta,\varphi;\theta',\varphi')L(z,\theta,\varphi)\sin\theta' d\theta' d\varphi'$$

where

$L(z, \theta, \varphi)$ = radiance of photons at depth z propagating in the direction (θ, φ)

dL/dz= the change in radiance with depth in the water due to scattering and absorption

c=beam attenuation coefficient

E_i= irradiance due to direct sunlight on a plane perpendicular to its propagation direction in the water (which is defined by zenith angle θ_0 and azimuth φ_0, both measured in water)

$\beta(\theta,\varphi;\theta_0,\varphi_0)$ = volume scattering function that defines the probability that the in water direct visible sunlight will scatter from its initial direction (θ_0, φ_0) to the direction (θ,φ)

$\beta(\theta,\varphi;\theta',\varphi')$ = volume scattering function that defines the probability that the in water diffuse visible sunlight will scatter from its initial direction (θ', φ') to the direction (θ,φ).

Equation 2.58 considers the underwater light field as both direct and diffuse. The first term on the right hand side represents the attenuated radiance in the direction of propagation (θ,φ). The second term represents the direct solar irradiance scattered into the observed direction. The third term represents the diffuse radiance outside the propagating direction beam scattered into the propagating direction.

One very highly used model based on radiative transfer is Hydrolight (Sequoia Scentific.Inc) and a brief description of it is given below.

Hydrolight is not a model of the optical properties of the sea, but an algorithm that solves the general radiative transfer equation for unpolarised

and monochromatic light in multilayered plane parallel aquatic media, with constant refraction index, using the mathematically sophisticated invariant imbedding techniques (Mobley, 1994, Chapter 8). Hydrolight solves the radiative transfer equation, in the water body, with boundary conditions at the sea-air interface and at the sea-bottom. Hydrolight models the wind-blown sea surface numerically, via Monte Carlo simulations of the random air-water interface, assumed to have wave slopes with Gaussian probability distribution and variance dependant on wind speed. The bottom is modeled as a flat, opaque, and entirely reflective surface. In our work, all the seabed reflectances are Lambertian. Hydrolight cannot simulate boundary conditions as patchy and sloppy bottoms, asymmetrical seabed Bidirectional Reflectance Distribution Functions (BDRF's), whitecaps, and foam. However, Mobley and Sundman(2003)(proved that Hydrolight simulations have errors smaller than 10% if the bottom is replaced with an area weighted average of the various bottom reflectances and the bottom slopes are equal to less than 20 degrees. The range of wavelengths used in our simulations covers the visible spectrum (400-700 nm at intervals of 10 nm), since the visible region is at the peak of the solar energy radiation and at the minimum of the seawater absorption.

2.9.2 The inverse problem

One example of inverse modeling technique is now discussed, i.e., the quasi analytical algorithm (Lee at al, 2002). This algorithm is based on the relationship between the subsurface remote sensing reflectance r_{rs} and the inherent optical properties of water derived from the radiative transfer

equation.

In general, on the basis of theoretical analyses and numerical simulations of the radiative transfer equation, r_{rs} is a function of the absorption and backscattering coefficients. Specifically, measurement of r_{rs} is a measure of the ratio u of the backscattering and absorption coefficients, with an error of ~2% to 10%.

To illustrate the derivation of u from r_{rs}, the Gordon et al(1988) formula was used

$$r_{rs}(\lambda) = g_0 u(\lambda) + g_1 [u(\lambda)]^2 \qquad 2.59$$

with

$$u = \frac{b_b}{a + b_b} \qquad 2.60$$

b_b is normally expressed as $b_b = b_{bw} + b_{bp}$ (Gordon, 1983 and Morel and Prieur,1977), with b_w is the backscattering coefficients for water molecules. b_{bp} is the backscattering coefficients for non particles, namely suspended particles.

Values of g_o and g_1 (Gordon et al ,1998 and Lee et al , 1999) however, need to be predetermined as in any semianalytical algorithm.

$$u(\lambda) = -\frac{g_0 + [(g_0)^2 + 4g1 r_{rs}(\lambda)]^{\frac{1}{2}}}{2g_1} \qquad 2.61$$

as u is a simple ratio of b_b to $(a + b_b)$, knowing a will lead to

$$b_b = \frac{ua}{(1-u)} \qquad 2.62$$

or knowing b_b will lead to

$$a = \frac{(1-u)b_b}{u} \qquad 2.63$$

for each wavelength, the total absorption coefficient can be expressed as

$$a(\lambda) = a_w(\lambda) + \Delta a(\lambda) \qquad 2.64$$

where $a_w(\lambda)$ is the absorption coefficient of pure water and Δa is the contribution that is due to dissolved and suspended constituents. It is noted that at larger wavelength (> 550 nm), $\Delta a(\lambda)$ is quite small, with $a(\lambda)$ dominated by the values of $a_w(\lambda)$,especially for oligotrophic and mesotrophic waters. As b_b is a simple sum of b_{bw} and b_{bp}, and the value of b_w is already known, then the b_{bp} value at λ_o is calculated.

The wavelength dependence of $b_{bp}(\lambda)$ is normally expressed as (Sathyendranath et al, 2001;Gordon et al, 1980;Smith and Baker, 1981)

$$b_{bp}(\lambda) = b_{bp}(\lambda_0)(\frac{\lambda_0}{\lambda})^Y \qquad 2.65$$

Thus if the power value of Y is known or estimated from remote sensing measurements, then b_{bp} at any wavelength can be calculated. When this calculated $b_{bp}(\lambda)$ value is placed along with the $b_{bw}(\lambda)$ value into equation 2.60, then the total absorption coefficient at that wavelength can be calculated analytically from $r_{rs}(\lambda)$. A detailed explanation of the QAA is given in Appendix B.

Chapter 3

Inhomogeneous distribution of optical properties

3.1 Introduction

It is vital to understand the relationship between the remote sensing reflectance and the vertical structure of the ocean's optical properties and sea water constituents. The spectral remote sensing reflectance $R_{rs}(\lambda)$ provides information about the properties of the oceanic surface layer whose thickness is dependent on the ocean's inherent and apparent optical properties. When interpreting the reflectance data or retrieving the water optical properties and the concentrations of sea water constituents, it is usually assumed that the whole water column is vertically homogeneous. However, oceanographic observations have shown that in the upper ocean, the optical properties and the optically significant constituents of sea water often show substantial vertical variation. Thus it is a challenge to interpret the exact meaning of the values of the ocean properties that are retrieved from remote sensing reflectance, due to this nonuniformity. This chapter gives a summary of the work that has been done by other researchers concerning this problem. The main hypotheses that will be used in Chapter Five are also summarised here.

3.2 Study of inhomogeneous water columns

This challenge of interpreting the effect of the nonuniformity of the optical properties in a water column was initially dealt with by Gordon (1978).

He suggested that interpreting the reflectance of a stratified ocean in terms of an equivalent homogeneous ocean which has the same average value of a particular combination of the water's optical properties over the dimensionless penetration depth τ_{90} (see Appendix A). This result was obtained by performing Monte Carlo simulation of radiative transfer in oceans with various stratifications. Stratification was included in the ocean by taking the single scattering albedo $\omega_o = b/c$ to be a continuous function of the dimensionless depth τ, where

$$\tau = \int_0^z (a+b)dz \qquad 3.1$$

They used the following function

$$\omega_o(\tau) = \omega_\infty[1+\zeta\tau^n \exp(-\varepsilon\tau) \qquad 3.2$$

to model the vertical distribution of ω_0 with n=0 or 1. When n=0, ω_0 decreases (for $\xi > 0$) or increases (for $-1 < \xi < 0$) as one goes deeper in the medium. When n=1, ω_0 has a subsurface minimum ($\xi < 0$) or maximum ($\xi > 0$). They used the scattering phase functions measured by Kullenberg (1968) in the Sargasso Sea with backscattering probability B of 0.0236 (at 655 nm) and 0.0506 (at 460 nm). The average of these two phase functions with B =0.0704 was also used. The phase functions were assumed to be independent of the scattering coefficient.

The computations were carried out for various values of n, ζ, and ε and the diffuse reflectance R was determined for each case. The downwelling irradiance in the ocean was used to determine the dimensionless penetration depth τ_{90} and the mean value of kB over this depth was calculated as

$$\bar{kB} = \frac{1}{\tau_{90}} \int_0^{\tau_{90}} kB d\tau \qquad 3.3$$

where $k = b/a$ and B is the backscattering probability, The relationship between R and $\bar{kB}$ was compared with the R and kB relationship for a homogeneous ocean with kB equal to $\bar{kB}$ of the stratified ocean.

For a homogeneous ocean, Gordon (1975) found that the reflectance is related to kB by an empirical equation of the form,

$$R = 0.00001 + 0.3244u + 0.1425u^2 + 0.1308u^3 \qquad 3.4$$

where

$$u = \frac{kB}{(1+kB)} = \frac{b_b}{a+b_b} \qquad 3.5$$

The results of Gordon (1978) suggested that a similar equation can be used to related the reflectance R of a stratified ocean to the $\bar{kB}$ value. If the reflectance is measured, then $\bar{kB}$ can be obtained by inverting this equation.

Gordon's hypothesis provides a sound theoretical framework for interpreting reflectance of a vertically inhomogeneous ocean in terms of an equivalent homogeneous ocean. This hypothesis will be employed in Chapter 5 (Section 5.2) to study the computations of a diffuse reflectance of a two layer ocean, and a continuously stratified ocean. However, Gordon (1978) realized that this hypothesis has limitations for practical applications since it is difficult to calculate the penetration depth from remote measurements.

From satellite data, the presence of vertical inhomogeneity in the ocean cannot be inferred. Hence, the data obtained from remote measurements are always based on the assumption that the upper ocean column being examined is vertically homogeneous in nature. On this basis, Sathyendranath and Platt

(1989) showed that the assumption of a vertically homogeneous chlorophyll distribution can lead to significant errors in the estimation from satellite data of the pigment profile in the photic depth. The remote sensing of ocean colour, applied to the estimation of chlorophyll biomass, was discussed for the case where the vertical distribution of phytoplankton pigments is non uniform. This was done by the application of a spectral model of reflectance and the consequences of vertical structure were evaluated by sensitivity analysis on a generalized pigment profile. The errors in the estimation of pigment concentration assuming a homogeneous profile were shown to be functions of the parameters of the pigment profile. It was further shown that if the shape of the pigment profile was known, then the entire pigment profile might be recovered from the satellite data.

Gordon and Clark (1980) hypothesised that when remotely sensed concentrations are compared to surface measurements, the comparison should be made with the optical properties averaged over the penetration depth. However, in experimental work, this is problematic because the concentrations calculated from the present remote sensing algorithms do not represent the penetration depth averaged concentrations (Stramska et al, 2005). Until now, there is a lack of any significant field studies that focused on the development of in water algorithms for estimating the penetration depth averaged constituents' concentrations. A vital reason for this apparent lack of interest may be due to the fact that these optical quantities cease to have any biological significance, especially in the presence of vertical inhomogeneity, as shown in the work by Sathyendranath and Platt (1989), discussed above.

Accurate retrieval of nonuniform profiles of optical properties from remote sensing reflectance is a challenging problem that has been addressed by relatively few studies. Zaneveld (1982) used an analytical approach based on radiative transfer to relate the inherent coefficients of backscattering and beam attenuation to remote sensing reflectance of a multilayered ocean. An exact equation for the remotely sensed reflectance (RSR) just beneath the water surface of the ocean was derived from the equation of radiative transfer. It was shown that the RSR at a given depth in the ocean depended only on the inherent optical properties, the attenuation coefficient for downwelling irradiance and two shape factors that depended on the radiance distribution and the volume scattering function. The remotely sensed reflectance (RSR) was defined as

$$RSR(\theta,\varphi,z)=\frac{L(\theta,\varphi,z)}{E_{od}(z)} \qquad 3.6$$

For the purpose of their paper the nadir radiance (0 = π) was used. Furthermore the scalar irradiance E_0 was used rather than the vector irradiance *E*, as the former is much less dependent on solar elevation than the latter. The scalar downwelling irradiance was defined as

$$E_{od}(z)=\int_0^{2\pi}\int_{\pi/2}^{\pi}L(\theta,\varphi,z)\sin\theta d\theta d\varphi \qquad 3.7$$

The definition of the remotely sensed reflectance was thus given by

$$RSR(z)=\frac{L(\pi,z)}{E_{od}(z)} \qquad 3.8$$

where *L(π,z)* was used rather than *L(π,φ,z)* because φ is immaterial for $\theta=\pi$. An exact expression for RSR(z) as a function of inherent and apparent optical properties was then derived from the equation of radiative transfer and was given as

$$RSR(z) = \frac{L(\pi, z)}{E_{od}(z)} = \frac{f_b(z) b_b(z) / 2\pi}{k(\pi, z) + c(z) - b_f(z) f_l(z)} \quad 3.9$$

which was found to be valid at all depths. A large variation of the shape factors f_b and f_l was observed as a function of the shape of the volume scattering function. Nevertheless for the extreme cases analyzed here, f_l was covered by a range from 1.00 to 1.12 and f_b was covered by a range from 0.80 to 1.27.

It can be said that the relationship derived above might have limited practical value because they involve the dependence on the ocean's apparent optical properties and volume scattering function and the depth dependence of these properties cannot be totally accounted for.

A few years ago, Frette et al (2001) discussed a way to resolve the vertical structure of oceanic waters that consists of two homogenous layers with different chlorophyll concentrations. The algorithm developed for this was designed to determine the chlorophyll concentrations of the two layers as well as the thickness of the upper layer. Their technique consisted of using the radiative-transfer computations for a coupled atmosphere-ocean system to simulate the radiances received in various bands of the satellite sensor and to compare these simulated results with measured radiances. The sum of the absolute values of the differences between simulated and measured radiances was minimized by use of an optimization algorithm and the retrieved parameters were those that yielded the minimum sum of the differences between measured and simulated data.

The possible drawback of this model is that in assumption of a two layer

model, the optical properties are driven by chlorophyll alone and this approach might prove to be inadequate for very high or very low chlorophyll concentrations.

3.3 Influence of non uniform pigment profile on diffuse reflectance of a stratified ocean

It was hypothesised by Gordon and Clark (1980) that for a case 1 oceans where the intrinsic optical properties covary with the chlorophyll concentration, the reflectance of a stratified ocean could be related to the reflectance of an equivalent homogeneous ocean for which the pigment concentration has the same value as the weighted average of the actual concentration over the penetration depth of the stratified ocean,

$$< Chl_i >= \frac{\int_0^{z90} g(z) Chl_i(z) dz}{\int_0^{z90} g(z) dz} \qquad 3.10$$

and the weighting function g(z) was expressed as

$$g(z) = \exp[-2\int_0^z K_d(z')dz'] = [\frac{E_d(z)}{E_d(0)}]^2 \qquad 3.11$$

This hypothesis will be tested in Chapter 5 (Section 5.5) using Monte Carlo simulations to relate the inherent optical properties to the pigment profile for two different scenarios. In the first scenario, the particle absorption and scattering coefficients were made to vary with the depth dependent chlorophyll concentration, *Chl(z)* and in the second scenario, the backscattering coefficient was assumed to be independent of depth and only the absorption coefficients vary with depth.

3.4 Oceanographic observation of the presence of inhomogeneity in the water column

Aerial and satellite images show ocean, estuarine, and lake waters to be quite varied in colour and brightness. It is often tempting to interpret this variation in apparent colour as a direct indicator of water depth or water content, but extraction of reliable information of this sort is often questionable since apparent water colour is not uniquely associated with a particular set of optical characteristics. For example, colour which is due to the presence of a particular substance in optically deep homogeneous water may be very similar if not identical, to colour attributable to bottom reflectance in clear optically shallow waters or to a stratified water mass comprised of two or more water types.

Remotely sensed data gives no indication of the stratification present in a water column. The information extracted from this kind of data is mostly representative of that of a homogeneous ocean. Use of remotely sensed water colour data for determining water properties has been most successful in cases where an appropriate set of realistic simplifying assumptions can be applied to reduce or remove any serious ambiguity. For example, given optically deep vertically homogeneous water, it should be possible to discriminate among various substances in the water or to extract estimates of concentration of a dissolved or suspended substance. Such an approach has been particularly useful in mapping chlorophyll and seston and somewhat less successful in mapping pollutants. Any practical attempt to unravel the general ocean colour problem must rely heavily on mathematical models.

The sea-leaving electromagnetic radiation which can be detected by remote optical sensors originates within a surface layer, the 'penetration depth', whose total depth is less than 25% of the thickness of the upper layer where there is enough light for photosynthesis, the photic layer. If the vertical distribution of chlorophyll within the photic layer is homogeneous then the satellite estimation itself provides useful information for primary production studies, but this is seldom the case.

Vertical profiles obtained from diverse regions and environments usually show a subsurface maximum in chlorophyll concentration, commonly referred to as the deep chlorophyll maximum. This subsurface chlorophyll maximum (SCM) usually occurs within the photic zone(the layer of the ocean that is penetrated by sunlight). It may be partially or completely invisible to a remote sensor. The depth, magnitude of the increased concentration with respect to the background, and sharpness of the SCM, all show a wide range of variability, as shown in Figure 3.1, from Cullen and Epley (1981). The physical, chemical and biological processes responsible for the vertical structure of these profiles are diverse as found by Cullen, who compared several vertical profiles of chlorophyll a (Cullen, 1982).

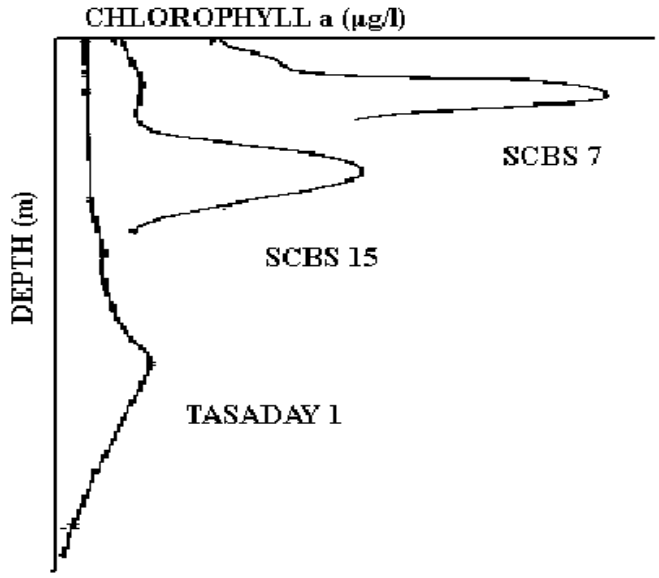

Figure 3.1Chlorophyll profiles from the North pacific Central Gyre (YASADAY 1),Southern California 52km off-shore (SCBS-15) and Southern California 2 km off-shore (SCBS 7)(adapted from remote sensing of vertically structured phytoplankton pigments, Ballestro(1999))

Vertical distribution patterns of chlorophyll concentration vary in different seasons and regions. The chlorophyll concentration maximum is not always found near or at the sea surface but sometimes lies deeper than the bottom of the photic zone (Parsons et al., 1984). In this latter case, ocean color sensors cannot measure the chlorophyll maximum (Gordon and McCluney, 1975).

Platt et al. (1988), after Lewis et al(1983) found that a generalized Gaussian profile performed well at fitting field data from a variety of oceanographic regimes. Ballestro (1999) used this Gaussian representation to numerically calculate the pigment concentration as would be measured by a satellite. In 1998, Kameda and Matsumura (1998) combined the empirical

relations between Gaussian parameters in the model of Matsumura and Shiomoto (1993) and surface chlorophyll concentrations obtained by ocean colour sensors to estimate the chlorophyll biomass integrated in the water column off Sanriku, northwestern Pacific.

This Gaussian function modeling the vertical profile of the depth dependent chlorophyll concentration, *Chl(z)* can be expressed as

$$Chl(z) = Chl_0 + \frac{h}{\sigma(2\pi)^{0.5}} \exp[\frac{-(z - z_{\max})^2}{2\sigma^2}] \qquad 3.12$$

where Chl_0 is the background value of chlorophyll, z_{max} is the depth of the chlorophyll maximum, σ is the standard deviation that controls the thickness of the chlorophyll peak and $\frac{h}{\sigma(2\pi)^{0.5}}$ is the amplitude of the chlorophyll maximum above the value of background Chl_0. The parameter h can be shown to be the depth-integrated value of the Gaussian profile above the background, i.e.

$$h = \int_0^\infty (Chl(z) - Chl_0) dz \qquad 3.13$$

Sathyendranath and Platt (1989) studied the dependence of the ratio of the reflectance in the blue region (440nm) and the green region (550nm) of the spectrum on the parameters, z_{max}, h, σ and C_o, varied one at a time. They found that when h was increased, the total amount of pigment concentration in the whole column in the euphotic zone (the depth at which photosynthetic activity takes place) initially increased and there was an increase in the blue-green ratio of reflectance for the non uniform cases of pigment profile. A change in σ broadened the chlorophyll peak with a consequent increase in the near surface

chlorophyll concentration. As a result, the blue-green ratio for reflectance decreased. As z_{max} was increased, the chlorophyll peak became less prominent and thus the blue-green ratio of reflectance increased. When the background pigment concentration C_0 was increased, there was a consequent decrease in the blue green ratio of the reflectance.

The vertical distribution of chlorophyll concentration is classified into three types (Kameda and Matsumura, 1998) as shown in Fig. 3.2. In Type A, the chlorophyll maximum is in the subsurface layer, in Type B, the chlorophyll maximum is located at or near the sea surface and, in Type C, there is a linear gradient without prominent peaks. Criteria for classification are shown in Table 3.1.

Lalli and Parsons (1993) commented on the relationships between mixing, nutrients and the vertical distribution of phytoplankton in the surface layer. Type C appears in strong mixing in the surface layer. Type B appears when mixing is weakened and primary productivity increases near the surface. Type A is a pattern that appears when nutrients near the surface are exhausted and maximum primary productivity shifts deeper.

Type A	$C_1 \geq (C_0 + z_{\max})$	and	$2\sigma < z_{\max}$
Type B	$C_1 \geq (C_0 + z_{\max})$	and	$2\sigma \geq z_{\max}$
Type C	$C_1 \geq (C_0 + z_{\max})$		

Table 3.1: Classification of vertical distribution of chlorophyll concentration

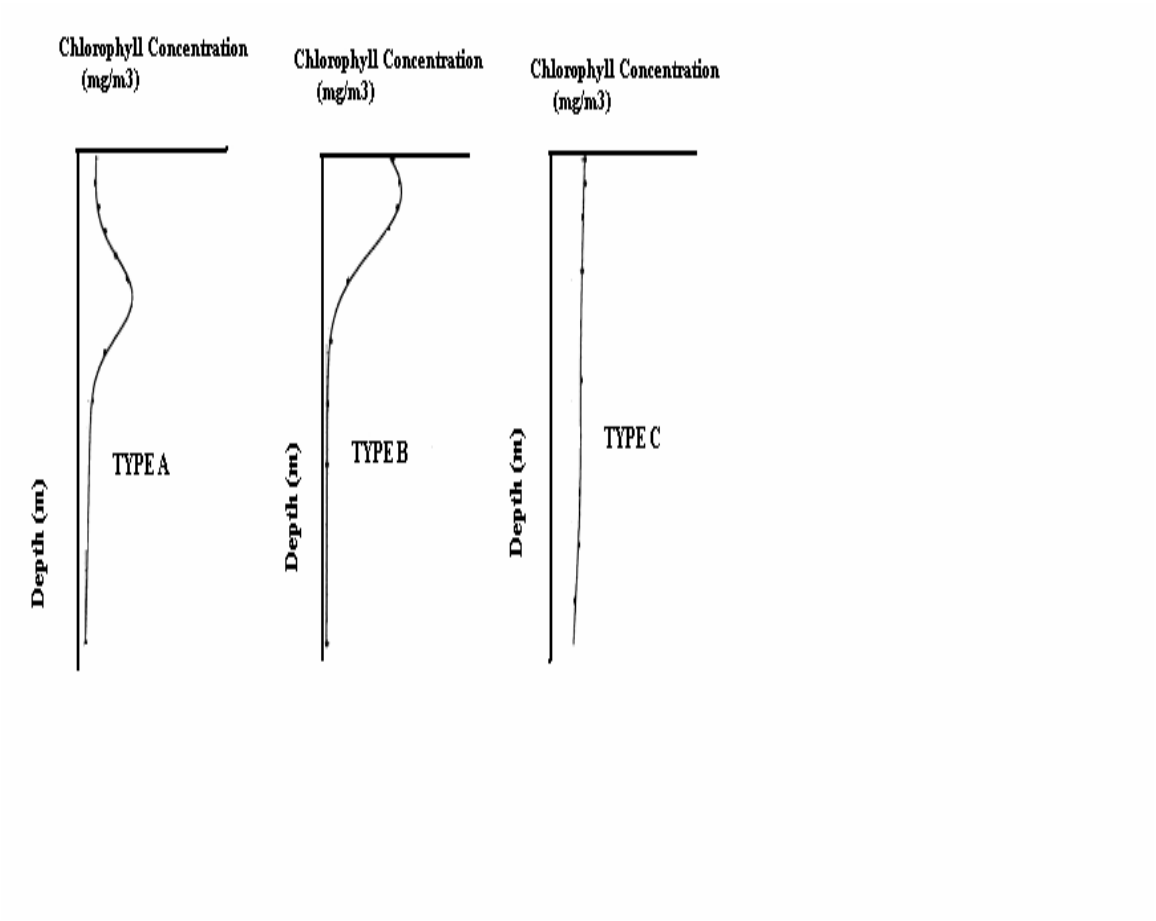

Figure 3.2: Typical patterns of vertical distribution of chlorophyll concentration.(adapted from Kameda and Matsumura, 1998)

In chapter 5, Monte Carlo simulations will be used to examine the effects of a vertically inhomogeneous profile of the inherent optical properties of the water column associated with the vertical profile of the chlorophyll concentration ,*Chl(z),* on the spectral remote sensing reflectance, $R_{rs}(\lambda)$, of the ocean. The *Chl(z)* profile will be described using the Gaussian function (Type A) defined above for the simulation of a broad range of open ocean conditions. Once it has been shown how the reflectance of a stratified medium differs from that of a homogeneous ocean, a retrieval algorithm would be applied to both the homogeneous and inhomogeneous case to see how the

retrieved values compare to the values actually found in the water column.

Chapter 4

Monte Carlo simulation of light propagation in water

4.1 Introduction

In this chapter, it is shown how the forward modeling Monte Carlo technique is implemented to be used as a tool for the theoretical and experimental work. This technique is applicable to solving the three dimensional radiative transfer equation (RTE) in a setting with arbitrary boundary geometry and incident radiance, and with arbitrary inherent optical properties within the water body. Monte Carlo method takes advantage of the statistical nature of photons behaviour and was used on a computer to simulate the fate of a large number of photons.

The underlying idea here is that if we know the probability of occurrence of each separate event in a sequence of events, then the probability that the entire sequence of events will occur can be determined. Random numbers were used in conjunction with appropriate cumulative frequency distributions based on the optical properties. The model is applied to both homogeneous and vertically stratified waters. A step by step explanation of the process and terms used for this simulation is given in the following section.

4.2 Random number generator

A random number generator is a number generated by a process, whose outcome is unpredictable. In 1951, Berkeley Professor D.H.Lehmer stated that:

A random sequence is a vague notion…in which each term is unpredictable to the uninitiated and whose digits pass a certain number of tests with traditional statistics.

When the expected value or average of a random process is taken into account, several important characteristics about how the process behaves in general are measured. The covariance and correlation are two important tools in finding the relationship between the different random processes. The covariance is a measure of how much the deviations of two or more variables or process match. For two processes X_i and X_{i+k}, if they are not closely related, then the covariance will be small and of they are similar, then the variance will be large. Mathematically, covariance is expressed as

$$\mathrm{cov}(X_i, X_{i+k}) = E[(X_i - \bar{X})(X_{i+k} - \bar{X})] \qquad 4.1$$

where k=0,1,2,3……..(N-i)

i=0,1,2,3,…… (N-1)

N=number of random points being considered

It should be noted that when k=0, the covariance is equal to the variance. But when $k \neq 0$, and if the two processes X_i and X_{i+k} are random, then the covariance is expected to be small.

The random number generator used in the Monte Carlo code is based on the Fortran program using a random function secnds(j)(it gives the number of seconds (minus j) since midnight. Fig. 4.1 shows the covariance for the sequence of random numbers generated by this random number generator.

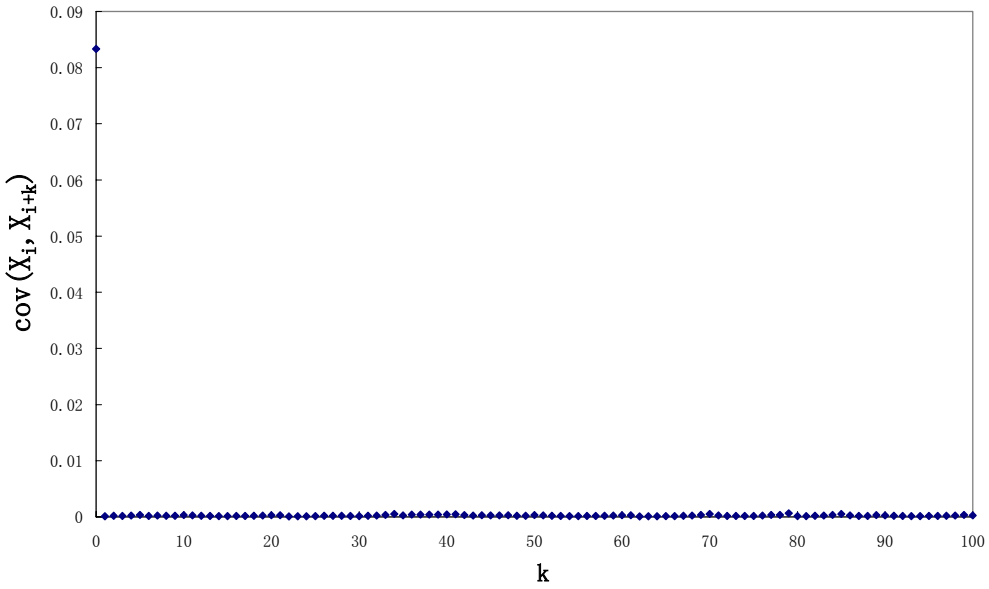

Figure 4.1 Plot showing the variance between two random processes X_i and X_{i+k} versus k

It is often useful to express the correlation of random variables with a range of numbers, like a percentage. For a given set of variables, the correlation coefficient is used to give an idea of the linear relationship between the variables. This provides a quick and easy way to view the correlation between our variables. If there is no relationship between the variables then the correlation coefficient will be zero and if there is a perfect positive match it will be one. If there is a perfect inverse relationship, where one set of variables increases while the other decreases, then the correlation coefficient will be negative one, as shown in the figures below.

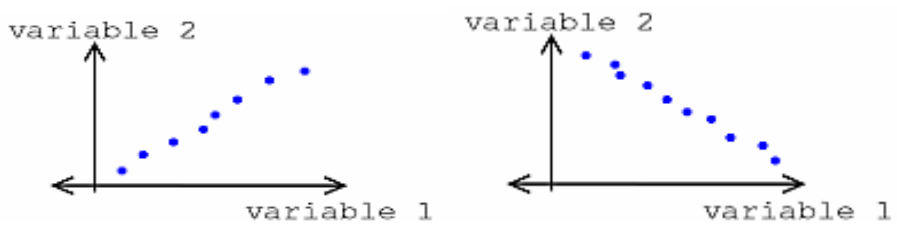

(a)positive correlation (b) negative correlation

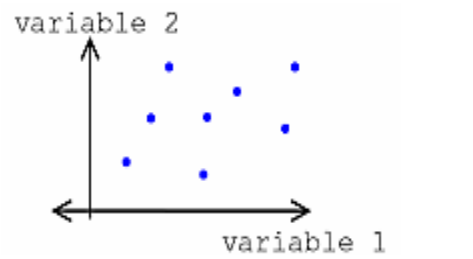

(c) uncorrelated(no correlation)

Figure 4.2(a)-(c) Types of correlation

In order to demonstrate that the random number generator employed here is of the uncorrelated type, two random numbers x and y generated by the used algorithm are plotted in Figure 4.3. A dot corresponds to a random coordinate (x,y). The number of dots in Figure 4.3 is 10000. From the figure, it can be clearly seen that there are gaps between the dots. This is because the number of random coordinate is not large enough to cover all the possible coordinates. As the number of random coordinates is increased, as shown in Figure 4.4, it is seen that all the spaces are covered with the dots.

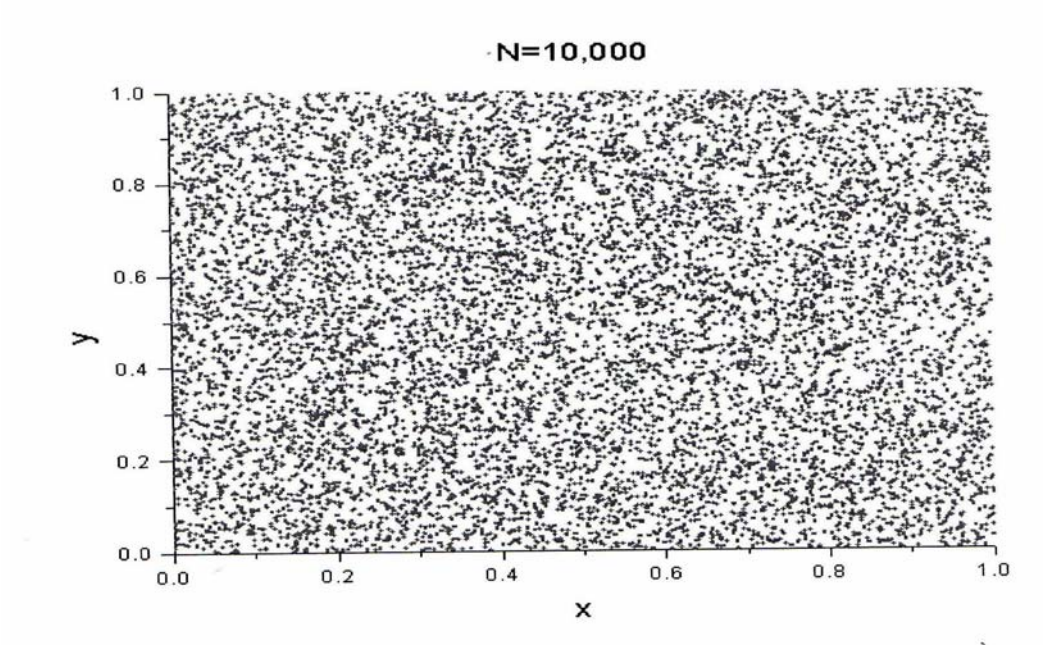

Figure 4.3 Random coordinate plot 1

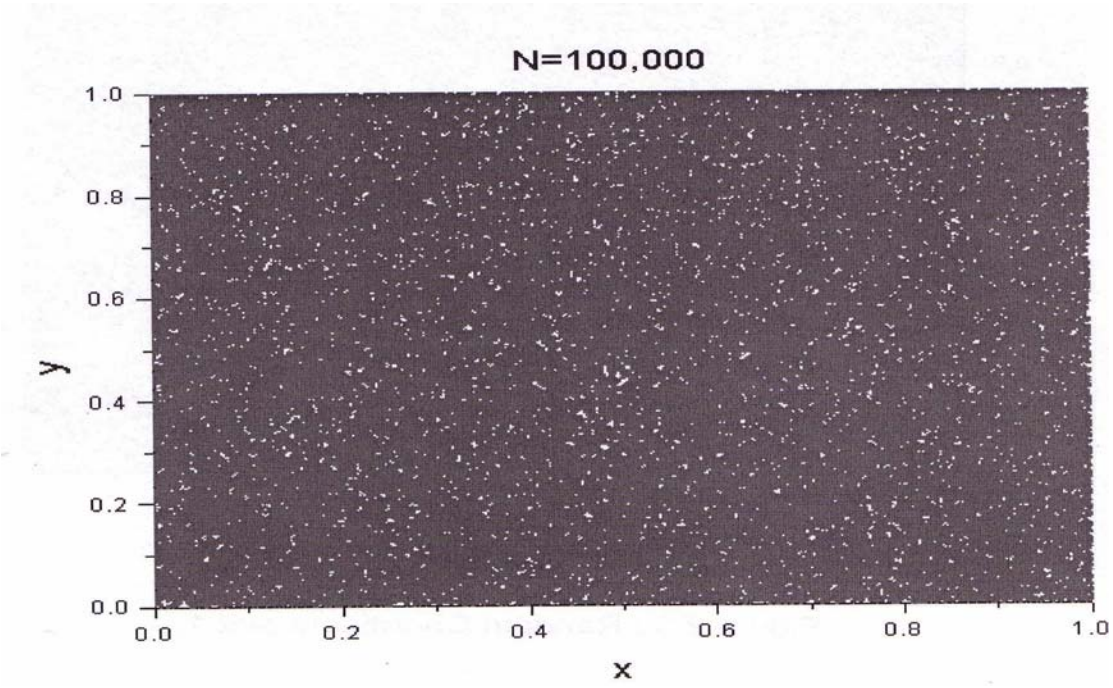

Figure 4.4 Random coordinate plot 2

4.3 Monte Carlo method

The method used in this simulation is the forward Monte Carlo method. According to this method, the measurement of downwelling plane irradiance E_d at some depth z below a random sea surface can be considered. Generally, each point on the sea surface is illuminated by an incident sky radiance $L(a, \hat{\xi})$. This concept is illustrated in Figure 4.5(a) to (d) and specific examples of the fate of four photons are given. As shown in Figure 4.5(a), after encountering the sea surface at point 1, photon d_1 is absorbed by a water molecule at position 2, as soon as it enters the water column. In Figure 4.5(b), photon d_2 encounters a scattering element at position 2 (example a phytoplankton cell, sediment particle, water molecule) and this causes the photon to scatter in a new direction. On the other hand, in Figure 4.5(c) photon d_3 enters the water, undergoes scattering interaction and travels upwards before eventually

reaching the surface of the water column. This event is recorded by a counter (according to the code set up). When photon d_4 enters the water (Figure 4.5(d)), it undergoes scattering and goes on to oceanic depths until it reaches the bottom. It is then absorbed by this bottom.

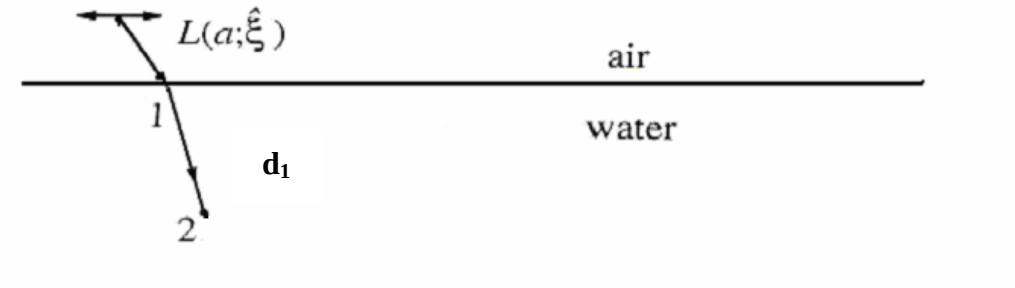

(a)

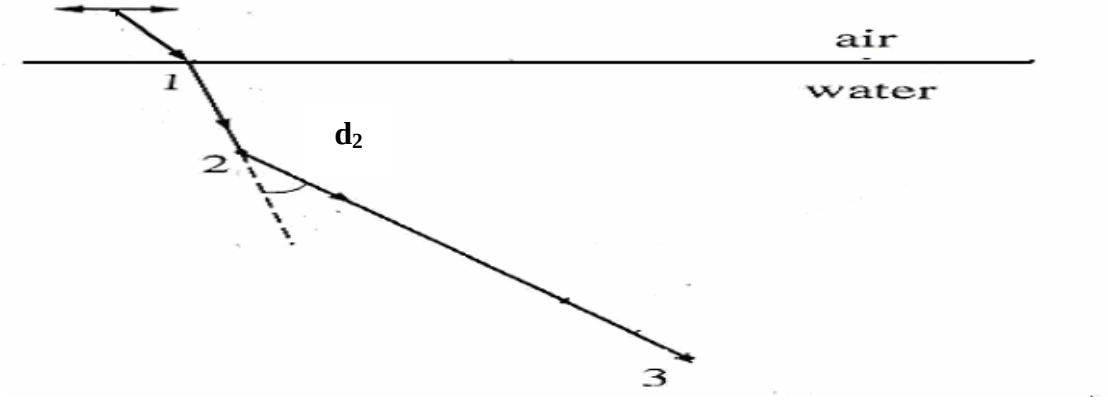

(b)

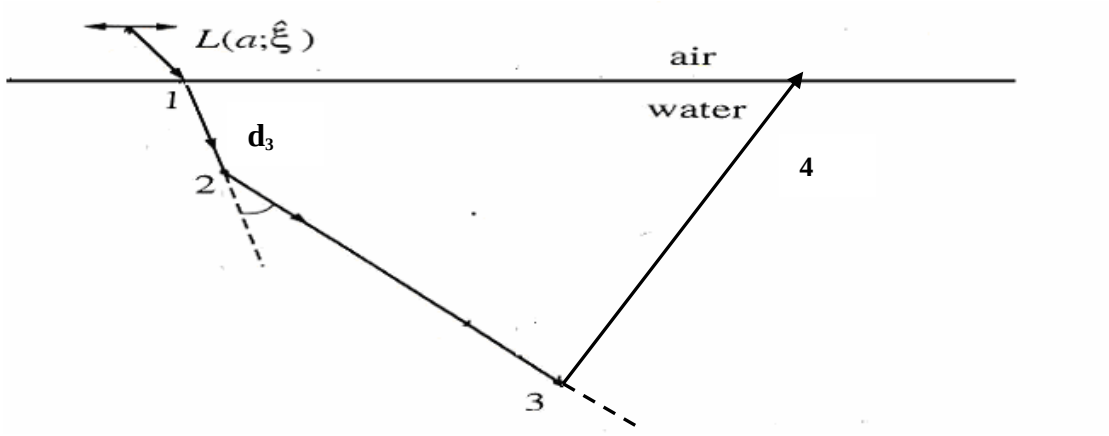

(c)

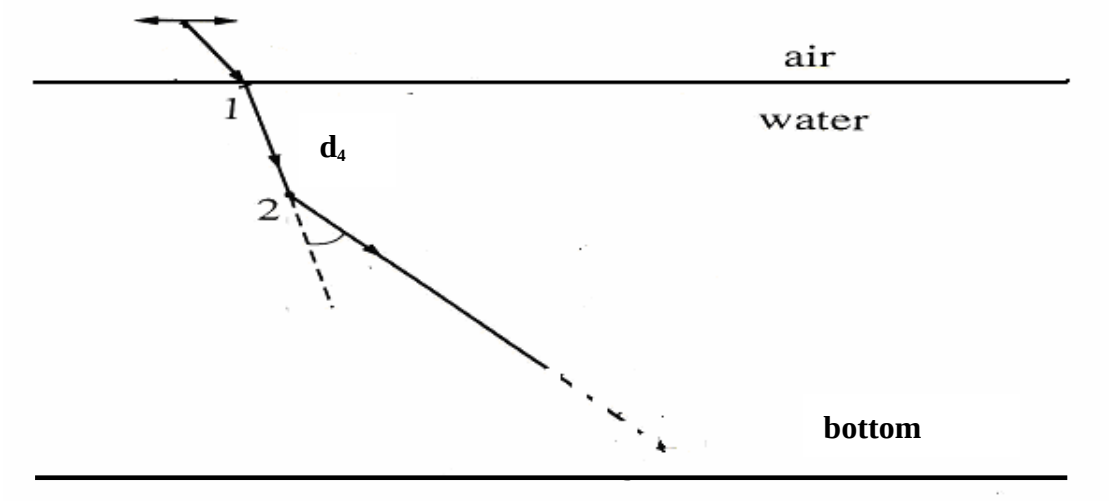

(d)

Figure 4.5(a)-(d) Illustration of 4 photon trajectories in a water column

4.3.1 Sampling photon path lengths

As a simplification, only the direct solar beam has been considered as under sunny conditions, 85 % or more of the irradiance comes from direct sunlight. The water surface was assumed to be flat and therefore, the angle to the vertical of a photon just below the surface is calculated from its angle just above the surface, permitting refraction. At this point, the azimuth angle of the photon is not taken into account. During the calculation, the trajectory of the

photon is expressed in term of its angle α to the horizontal. For each simulation run, an appropriate value of α′ the angle of the solar beam to the horizontal is chosen. Due to refraction at the surface, all photons just below the surface have trajectories at an angle to the horizontal given by

$$\alpha = \arccos[\frac{\cos\alpha'}{1.333}] \tag{4.2}$$

Once the photon is below the surface and its angle to the horizontal is known, its path can be followed in the water.

After a photon enters the water, its initial direction is known and its subsequent interactions and distance traveled within the water must be determined. Consider a collimated beam or a ray of many photons and this beam is assumed to have some radiance *L* which decreases with distance in the following way

$$\frac{dL}{ds} = -cL \tag{4.3}$$

where *s* is the distance along the path of the beam and c is the attenuation coefficient of the medium.

After traversing through a distance *l*, the radiance is reduced to

$$L = L(0)\exp(-cl) \tag{4.4}$$

Since l is the geometric distance along a specific direction, it can be measured from some reference point at *l*=0. In terms of optical pathlength, τ =cl

$$L = L\exp(-\tau) \tag{4.5}$$

This decrease in radiance is explained in terms of the fate of individual photons. If the probability of any particular photon being absorbed or scattered out of the beam between optical pathlengths τ and $\tau + \mathrm{d}\tau$ is

$$p(\tau)d\tau\exp(-\tau) \tag{4.6}$$

p(τ) must satisfy the following

$$\int_0^\infty \ p(\tau)\mathrm{d}\tau = 1 \tag{4.7}$$

as is required by any probability density function. The probability that a photon is absorbed or scattered somewhere between τ = 0 and τ =l is given by the cumulative distribution function P(τ)

$$p(\tau)=\int_0^\tau \ P'(\ \tau')\mathrm{d}\tau'=1\text{-}\exp(-\tau) \tag{4.8}$$

Suppose that now a random number r is drawn from the unit interval between 0 and 1 such that r is equally likely to have any value 0≤ r ≤1. In other words, r is uniformly distributed on the interval 0 to 1. The associated probability density function of r is given by

$$P_r(r) = \begin{cases} 1 & if \quad 0 \le r \le 1 \\ 0 & if \quad r < 0 \quad or \quad r \ge 1 \end{cases} \tag{4.9}$$

In this procedure, the randomly drawn r, which is a known number, is used to determine a value for τ . This can be done by regarding going from r to τ as a change of variables. Thus, the probability that r is in some interval r to r+dr is P(r)dr and the probability that τ is in a similarly corresponding interval τ to τ +dτ is P(τ)dτ . Then in the case these two probabilities are equal

$$\int_0^r \mathrm{P}(r')\mathrm{d}r' = \int_0^l \mathrm{P}(\tau')\,\mathrm{d}\tau' \tag{4.10}$$

Since *P(r)dr* is known, the left-hand integral can be evaluated and the preceding equation becomes

$$r= \ \int_0^\tau \ P(\tau')\mathrm{d}\tau'=P(\tau) \tag{4.11}$$

The fundamental Monte Carlo states that the equation $r=p(\tau)$ uniquely determines τ in such a manner that τ falls in the interval l to $\tau+d\tau$ with frequency $P(\tau)d\tau$

In the current case

$$r= P(\tau)=1-\exp(-\tau) \quad 4.12$$

gives

$$\tau =-\ln(1-r) \quad 4.13$$

This equation can be used to randomly determine the optical pathlength τ traveled by a photon between one scattering or absorption event and another.

It can be noted that

$P=-1/c\ ln(1-r)$ in terms of geometric distance $l=\tau/c$

The mean free path is obtained by

$$\langle l\rangle= \int_0^\infty l/c\ P(\tau)d\tau = \int_0^\infty 1/c\ e^{-l}\ d\tau =1/c \quad 4.14$$

and as can be seen, the beam attenuation coefficient is just the reciprocal of the photon mean free path. The depth, $l\sin\alpha$, at which the interaction occurs, is also calculated.

4.3.2 Sampling photon interaction types

When an interaction occurs, the nature of interaction must be decided. The photon then interacts with the medium and it is now to be decided whether the interaction is absorption or scattering event. This is done by drawing another random number r which is compared to the albedo of single scattering, ω_o=b/c. If r > ω_o, then the interaction is an absorption event and if r $\leq \omega_o$, the interaction results in scattering.

4.3.3 Sampling scattering directions

If the interaction results in absorption, the photon is terminated and a new photon is introduced. If however, the interaction is a scattering event, the new photon direction can be randomly determined. The random number selected is used to assign a value to the scattering angle θ, by reference to the cumulative distribution for θ. This cumulative distribution has been derived on the basis of the measured normalized volume scattering function $\tilde{\beta}(\theta)$ for some appropriate natural water and in the current case, the Petzold scattering phase function (Petzold, 1972) has been used. Thus the probability of scattering into an element of solid angle dΩ (ξ) centered on direction ξ is

$$\tilde{\beta}(\xi',\xi)\, d\Omega(\xi) = \tilde{\beta}(\theta,\varphi)\sin\theta d\theta d\varphi \qquad 4.15$$

In natural waters, $\tilde{\beta}$ depends only on the scattering angle θ. Therefore $\tilde{\beta}(\theta,\varphi) = \tilde{\beta}(\theta)$ and θ and φ are random variables, meaning that two random numbers must be drawn to determine both θ and φ. The independence of θ and φ also means that the joint probability density function can be written as a product of pdf's for θ and φ.

$$\tilde{\beta}(\theta,\varphi)\sin\theta d\theta d\varphi \equiv P(\theta)d\theta P(\varphi)d\varphi \qquad 4.16$$

The azimuthal angle φ which determinates the plane of the scattering event relative to some reference direction is uniformly distributed on the interval from 0 to 2π. Hence, $P(\theta)d\theta = \frac{1}{2\pi} d\varphi$. The result in equation 4.16 can be used to identify the pdf P(θ) for determining θ as follows

$$P(\theta) = 2\pi\, \tilde{\beta}(\theta) \sin\theta \qquad 4.17$$

For the scattering angle θ to be determined, a random number r is drawn from the uniform distribution on 0 to 1 and

$$r = P(\theta) = \int_0^{\theta} P(\theta')\,\mathrm{d}\theta' = 2\pi \int_0^{\theta} \tilde{\beta}(\theta')\sin\theta'\,\mathrm{d}\theta' \qquad 4.18$$

Similarly $\varphi = 2\pi r$, where r is another random number from the uniform distribution on 0 and 1. The angle of the new trajectory is

$$\sin\alpha' = \sin\alpha\cos\alpha + \cos\alpha\sin\theta\cos\varphi \qquad 4.19$$

as shown in Figure 4.6 below

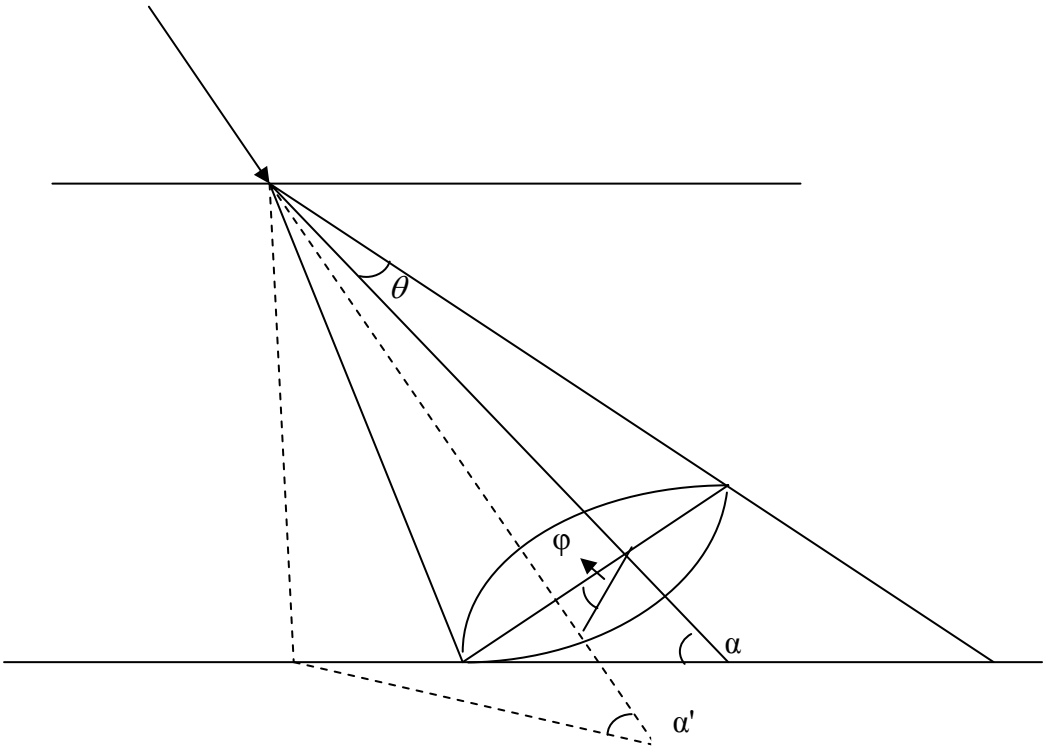

Figure 4.6 Diagram showing the relationship of the direction of a photon after scattering to the initial angle to the horizontal (α), the angle of deflection (θ) as well as the angle of rotation (φ)

Once the angle of the new trajectory has been determined, another random number is used to select the pathlength before the next interaction. As a consequence of a scattering event, when a photon has been made to travel in an upwards direction, then if there are no other interactions, it eventually reaches the surface. At this instance, a new random number should be used to

decide whether the photon would be reflected downwards or whether it would pass upwards through the interface, according to the relative probabilities of the two events. It should be noted that the proportion of light reflected at the air water interface from below changes quite steeply from complete reflection to a rather low value over a narrow range of angles: reflection is 100% for angle(to the surface) from 0 to 41.8^{o}(sea water), 15.3% at 45^{o}, 5.9% at 80^{o} and down to 2.1% from 55^{o} to 90^{o}. As a consequence, it has been assumed that any upward traveling photon that reaches the surface at an angle greater than or equal to 41.4^{o} passes through and all other photons incident at a smaller angle are reflected downwards. When a photon has escaped, a new photon is considered to enter the water. However, since the water surface was assumed to be flat and homogeneous here, only the photons reaching the water have been recorded.

4.3.4 Depth Effect

Throughout these calculations, it has been assumed that the water body has a finite depth. The size of the depth interval can be selected at the beginning of the run and is such that it is large enough to ensure that less than 0.1 % of the photons reach the bottom. Another major assumption is that the bottom is completely absorbing and as soon as the calculated depth for a specific photon exceeds the bottom depth, that photon is assumed to be absorbed and a new photon is started off.

4.3.5 Wavelength Range

Monte Carlo simulation was carried out within the photosynthetically active waveband from 400 to 700 nm, at 10-nm intervals. The total absorption coefficient due to water, dissolved humic substances, living (phytoplankton) and non living (tripton) particulate matter, at each wavelength, is considered. For idealized waters, these absorption coefficients must be calculated on the basis of the assumed composition of the water. Appropriate values for the scattering coefficients may be assigned as usual using the appropriate models.

4.3.6 Photon Statistics

The number of photons chosen in the simulation is 10^7 and the same number of photons was used for all the simulations. The number of photons is made large enough so that the intrinsic error obtained for each run is almost negligible. Thus, error bars have been omitted in the graphs showing the reflectance values. When the life histories of the 10^7 photons have been followed, the total number of photons that reach the surface are recorded. Suppose that N is the number of photons (per m^2 per second) impinging on the water surface (either from above or below the air water interface). Then, at a given wavelength, the irradiance would be the product of N and $h\nu$ (the photon energy, where h is the Planck's constant and ν is the frequency of light). At any wavelength, the ratio of the upwelling and downwelling photon numbers would then be equal to the ratio of the respective irradiances. The remote sensing reflectance is then calculated as the ratio of the number of photons reaching the surface to the number of photons that enter the water

column, divided by π (assuming the surface to be Lambertian). The total accumulated flux of photons that pass each depth marker in a downwards or upwards direction is then recorded and, after multiplication by the photon energy, is taken to be a measure of the downwards (E_d) or upwards (E_u) irradiance respectively. The code also records the angle of each photon passing a depth marker.

The typical remote sensing reflectance of water ranges from about 0.001 sr^{-1} to 0.02 sr^{-1}.Using the lower limit of reflectance, 10^7 incident photons would yield about 30000 photons scattered back to the surface. Assuming Poisson statistics, the standard deviation of the detected photon number is about $(3 \times 10^4)^{0.5} = 144$, giving an uncertainty in the reflectance value of about 0.5%.

4.4 Simulation conditions for homogeneous water

At the beginning of each simulation, a set of absorption and scattering coefficients, including the values of the coefficients for pure sea water are read in. The number of photons chosen for the simulation is subdivided in to the number of wavebands according to the assumed spectral distribution of incident radiance. Simulation begins with a specific waveband and continues until all the photons allotted to that waveband are used up and it then continues with the next waveband and so on. The photons of all wavelengths passing at each depth marker are added together and the irradiances and other parameters are calculated in the usual way. In this case, the water column is assumed to be of a constant depth.

4.5 Simulation conditions for vertically stratified water

In this case, the water column is separated into N layers, and each layer is assigned a specific(example 1m, 1.5m ,2m etc…) and uniform thickness. At the start of each simulation, different sets of absorption and scattering coefficients are allocated to each depth. The number of photons chosen for the simulation is once again subdivided into the number of wavebands according to assumed spectral distribution of incident radiance. The simulation will start with a specific waveband and will continue until all photons assigned to that waveband are used up and then the next waveband is taken up.

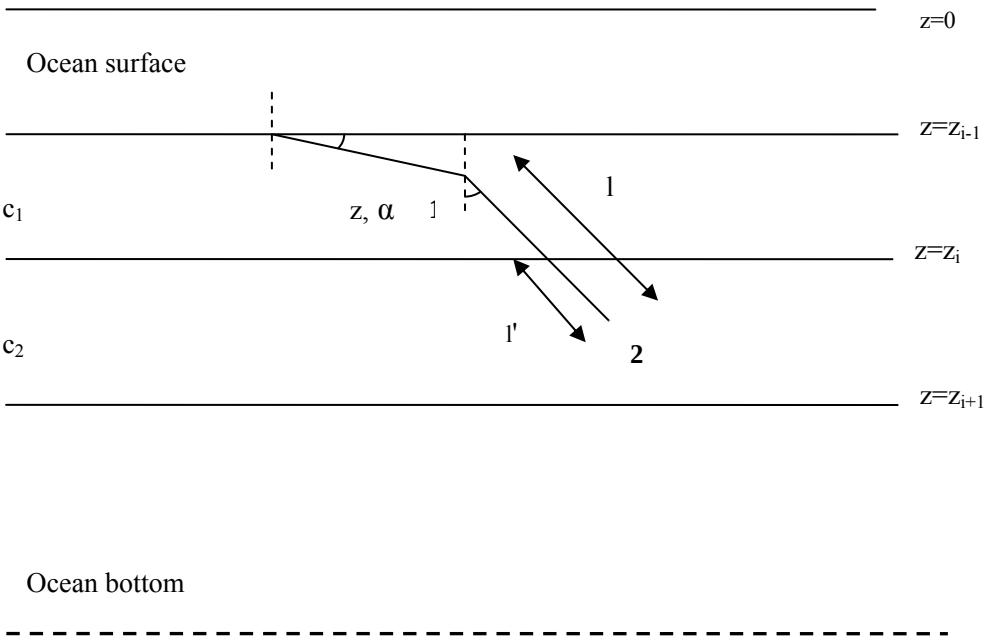

Figure 4.7 Sketch showing the initial and final directions before and after scattering interaction

The above diagram shows the stratification that is present in the water column. The water column is separated into N layers with uniform thickness. The layers are assigned different values of absorption and scattering

coefficients and hence have different values for the attenuation coefficient (example c_1 and c_2). The diagram shows a photon that starts at position 1 with coordinates z with angle α to the vertical. It reaches the boundary at z=i(the depth interface between i-1 and i layer) after traversing a pathlenth l. The pathlength that it has traversed in the new layer is given by

$$l' = \frac{z_i - z}{\cos\alpha} + \frac{c_1}{c_2}[l - \frac{(z_i - z)}{\cos\alpha}] \qquad 4.20$$

The water surface was assumed to be flat and homogeneous. The wave effects, surface effects and influence of white foams were ignored. The sun was considered at zenith angle of 30^o unless specified otherwise. The Petzold phase function was used for all layers and all wavelengths. All the simulations include Rayleigh scattering by water molecules. The surface boundary conditions assumed a clear sky. Surface effects of the water have been ignored.

4.6 Validation of code

Once the Monte Carlo has been set up, the next step is to test for its accuracy. For this purpose a synthetised data set containing both inherent and apparent optical properties was used. This data set was produced by the Ocean-Color Algorithm Working Group (OCAWG) of the International Ocean-Colour coordinating group (IOCCG).

IOCCG was established in 1996 under the auspices of the Intergovernmental Oceanographic Commission (IOC), following a resolution endorsed by the Committee on Earth Observation Satellites (CEOS), to act as

a liaison and communication channel between users, managers and agencies in the Ocean Colour arena. One major focus of the IOCCG has been the formation of specialized working groups investigating various aspects of ocean-colour technology and its applications. The Ocean-Colour Algorithms working group (OCAWG) chaired by Dr. ZhongPing Lee from the Naval Research Laboratory, USA, is among the seven working groups. The objectives of the group are to perform algorithm cross comparisons, to make recommendations on specific algorithms and to report on the progress of algorithm development.

The OCAWG synthetized data set contains both inherent optical properties (IOPs) and the corresponding apparent optical properties (AOPs). IOPs are generated with various available/reasonable optical/bio-optical parameters/models (Ocean Colour Algorithm Working Group, 2003) (Appendix C). For the simulation of the apparent optical properties, AOPs, which include the remote-sensing reflectance (R_{rs}, ratio of water-leaving radiance to downwelling irradiance just above the surface) and the sub-surface remote-sensing reflectance (r_{rs}, ratio of upwelling radiance to downwelling irradiance just below the surface), the Hydrolight numerical simulation code was used. In the Hydrolight runs, the solar input was simulated with the Gregg and Carder (1990) model and the sky was assumed cloud free. A wind speed of $5ms^{-1}$ was applied and the water body was assumed to be homogeneous. Data sets for solar zenith angles of 30^o and 60^o were created.

The same set of the inherent optical properties from the OCAWG synthesized data set (with 30^o solar angle) was used in the Monte Carlo code

for the simulation of the following AOPs; the remote-sensing reflectance (R_{rs}, ratio of water-leaving radiance to downwelling irradiance just above the surface) and the sub-surface remote-sensing reflectance (r_{rs}, ratio of upwelling radiance to downwelling irradiance just below the surface). Similarly, the water body was also assumed to be homogeneous. Spectral bands were set from 400 and 750nm with a spacing of 10nm.

The results obtained from the Monte Carlo code and Ocean-Colour Algorithms of the IOCCG (using Hydrolight) were then compared and this comparison was used as a validation to the Monte Carlo code. The results for the remote-sensing reflectance (R_{rs}) and the sub-surface remote-sensing reflectance (r_{rs}) are displayed in Figures 4.8 [(a) to (h)] and 4.9[(a) to (h)] respectively. Next to each graph, the values of the chlorophyll concentration(*Chl*), the detrital matter exponent coefficient (S_{dm}), the coloured dissolved organic matter and (S_g) , the total absorption coefficient at 440nm, a(440), and the total backscattering at 550nm, $b_b(550)$, are denoted.

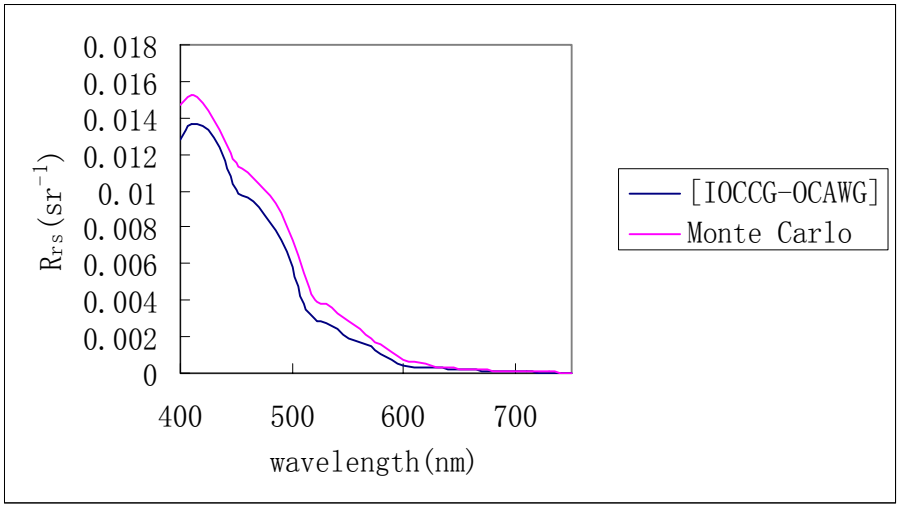

Chl=0.03 μ g/l
Sg=0.0193 nm^{-1}
Sdm=0.00804 nm^{-1}
a(440)=0.0181 m^{-1}
$b_b(550)$=0.002424 m^{-1}
RMSD=0.0008871

Figure 4.8 (a)graph of above surface remote sensing reflectance

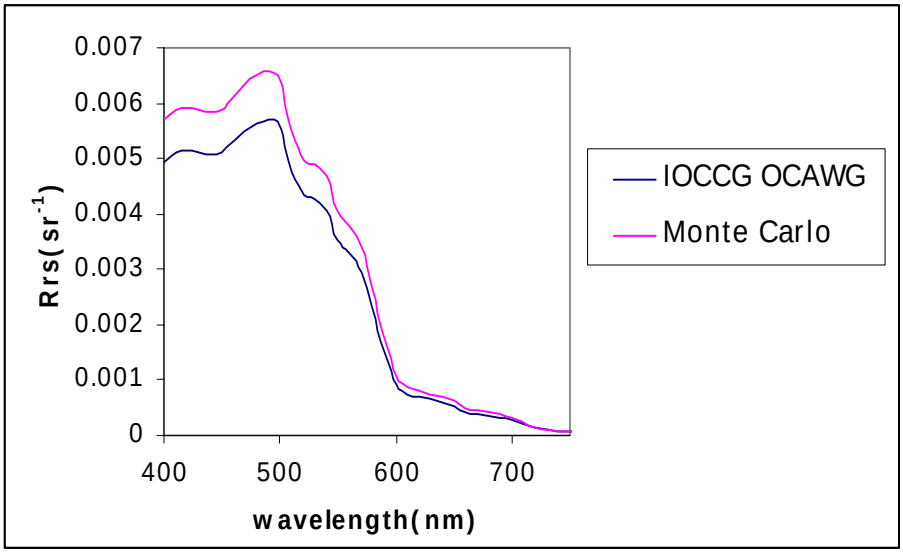

Chl=0.3 μ g/l
S_g=0.011 nm^{-1}
S_{dm}=0.01436 nm^{-1}
a(440)=0.0717 m^{-1}
$b_b(550)$=0.005379m^{-1}
RMSD=0.000643

Figure 4.8 (b) graph of above surface remote sensing reflectance

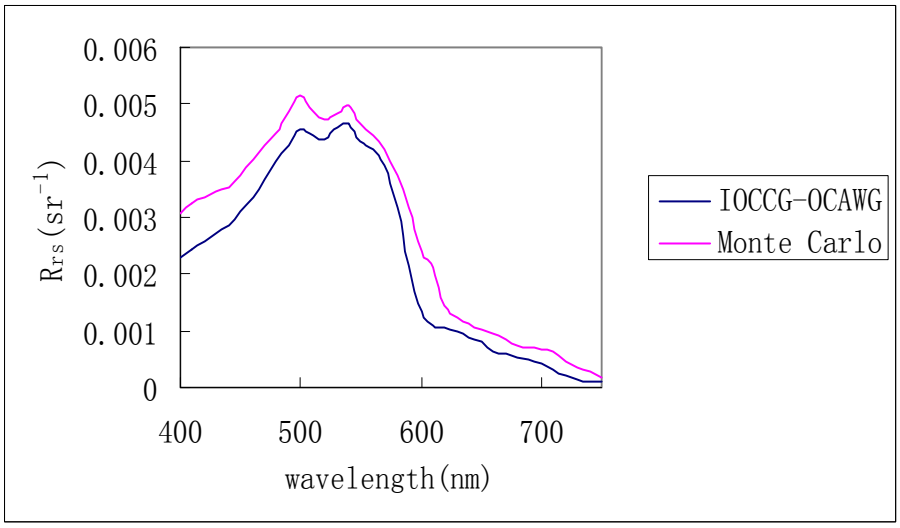

Chl=0.7 μ g/l
S_g=0.0151 nm^{-1}
S_{dm}=0.0137 nm^{-1}
a(440)=0.1630 m^{-1}
$b_b(550)$=0.0079 m^{-1}
RMSD=0.0005260

Figure 4.8 (c) graph of above surface remote sensing reflectance

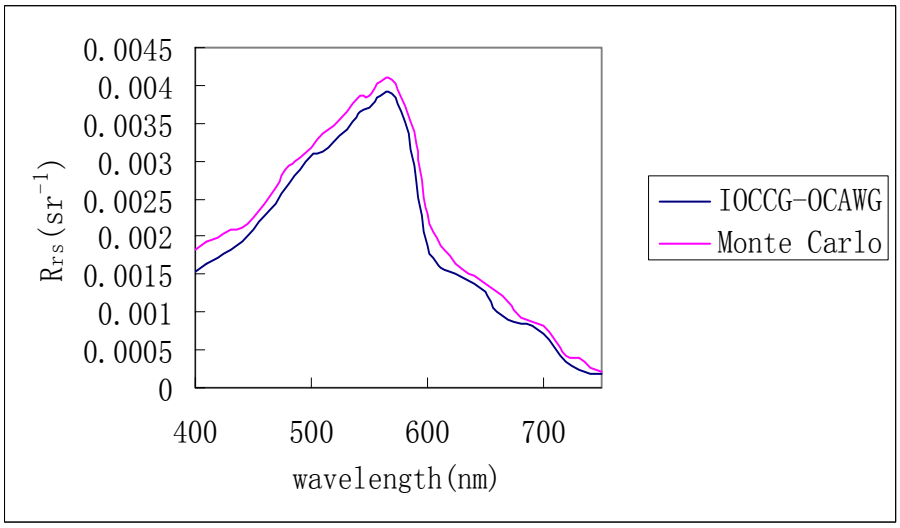

Chl=1.5 μ g/l
S_g=0.0117nm^{-1}
S_{dm}=0.0102nm^{-1}
a(440)=0.2177m^{-1}
$b_b(550)$=0.0127m^{-1}
RMSD=0.000517

Figure 4.8 (d) graph of above surface remote sensing reflectance

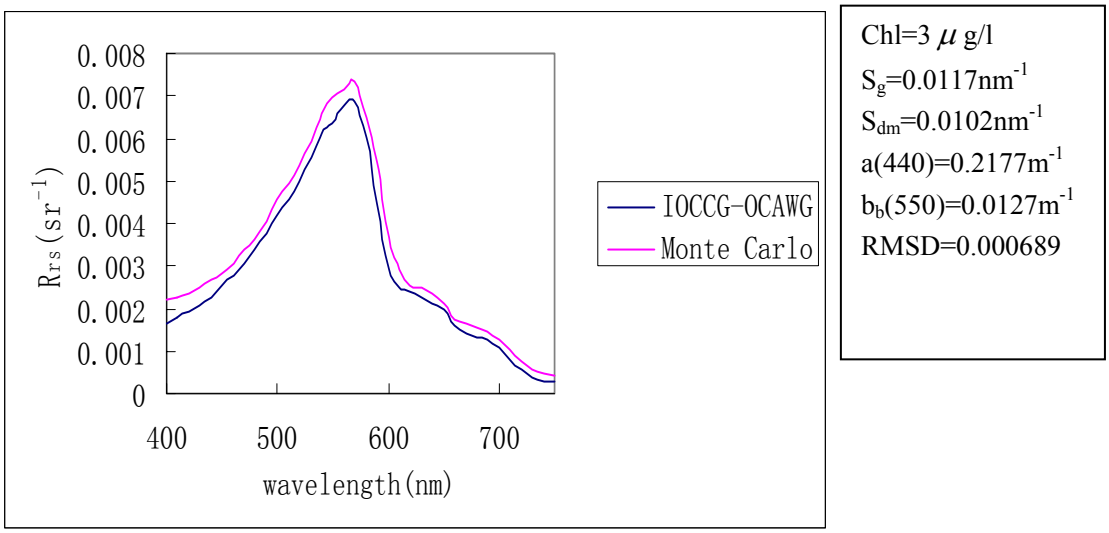

Figure 4.8 (e) graph of above surface remote sensing reflectance

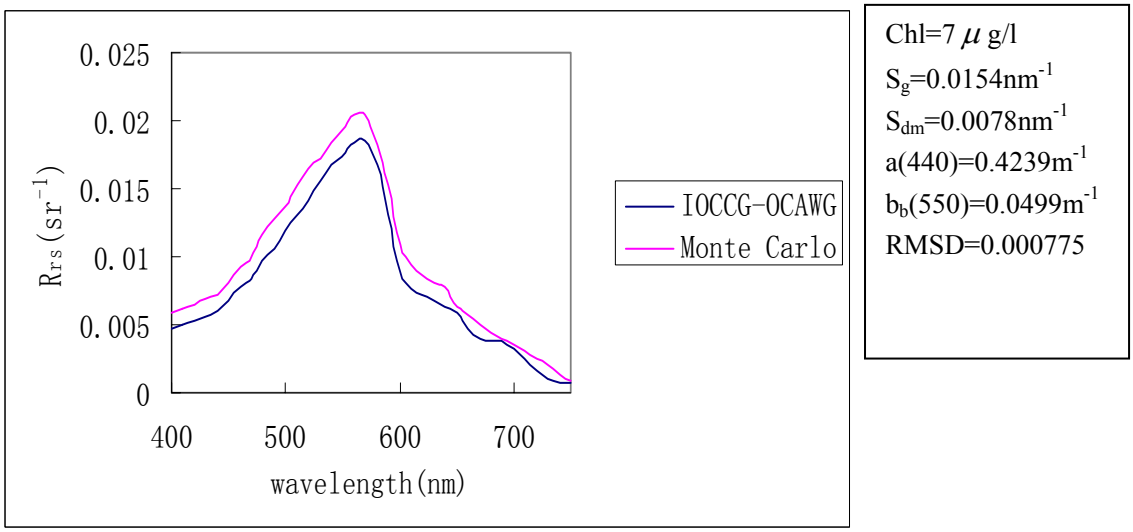

Figure 4.8(f) graph of above surface remote sensing reflectance

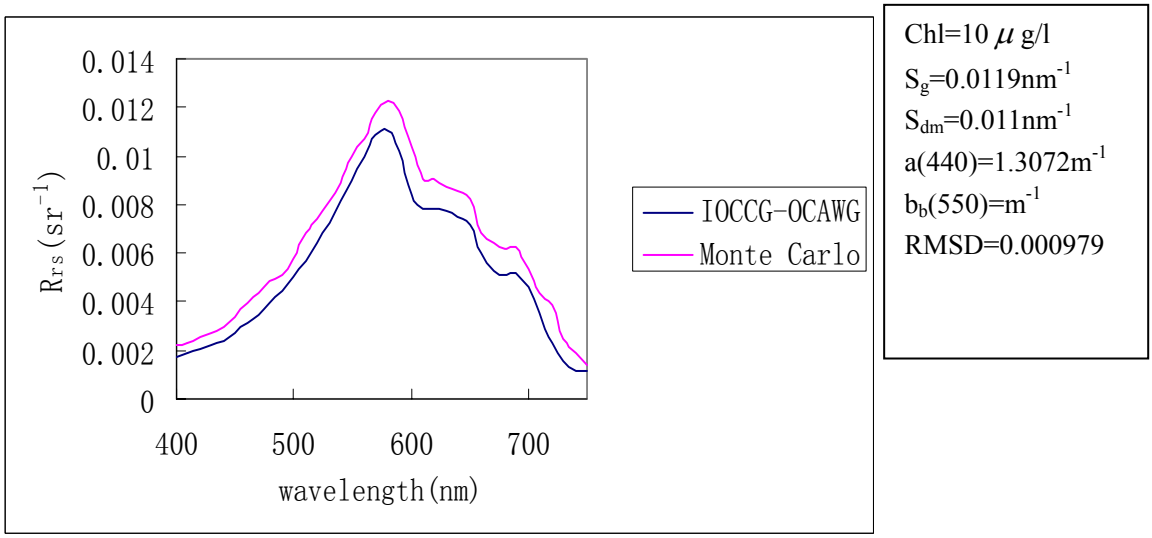

Figure 4.8 (g) graph of above surface remote sensing reflectance

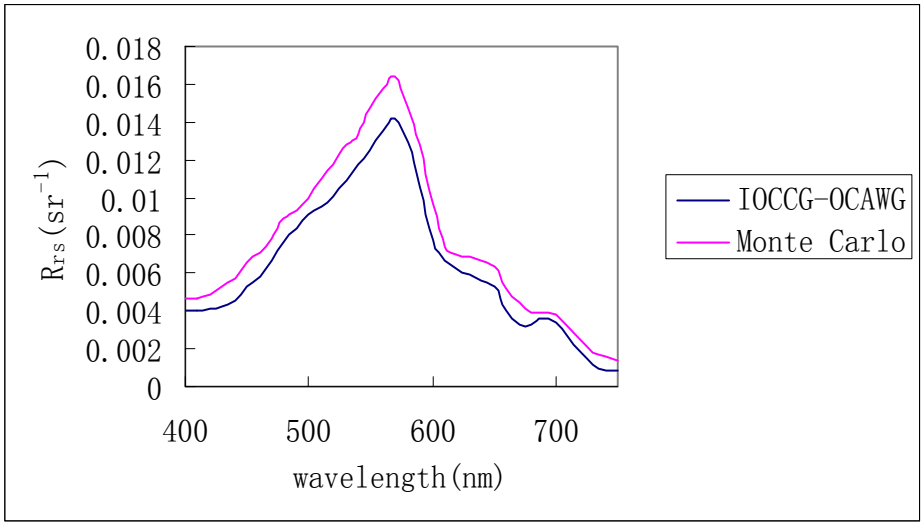

Figure 4.8 (h) graph of above surface remote sensing reflectance

The root mean square difference (RMSD) between the reflectance obtained by Hydrolight in the OCAWG data set and that simulated by the Monte Carlo code and is used to characterise the closeness of the two reflectance spectra. The RMSD is evaluated as,

$$RMSD = \sqrt{\frac{1}{N}\sum_{i=1}^{N}(R_{H(\lambda_i)} - R_{MC(\lambda_i)})^2} \qquad 4.21$$

where

N= number of wavelengths at which the value of reflectance is generated

R_H=reflectance values obtained by the Ocean –Colour Algorithm Working Group using Hydrolight

R_{MC}=reflectance values obtained by Monte Carlo

Since the remote sensing reflectance values are already small, the RMSD values seem negligible. However when this RMSD value for each graph is compared to the mean remote sensing reflectance values of the IOCCG group, the %error obtained is quite substantial, ranging from 8.84-26.92%. The %error for each graph was calculated as follows

$$\%error = \frac{RMSD}{MEAN} X\ 100 \qquad 4.22$$

where MEAN is the mean value of the remote sensing reflectance of the IOCCG group.

Graph	MEAN	RMSD	% error
4.8(a)	0.0069	0.0008871	12.85
4.8(b)	0.002785	0.000643	23.08
4.8(c)	0.002325	0.000526	22.62
4.8(d)	0.00192	0.000517	26.92
4.8(e)	0.003455	0.000689	19.94
4.8(f)	0.008766	0.000775	8.84
4.8(g)	0.0075	0.00979	13.2
4.8(h)	0.00697	0.0009127	13.09

Table 4.1 showing the percentage error for graphs 4.8(a) to 4.8(h)

The graphs in Figure 4.8 (a - h) show the comparison for the above surface remote sensing reflectance derived ($R_{rs}=L_u(0^+)/E_d(0^+)$) against wavelength. The differences in both sets of reflectance values can be explained by the fact that the surface conditions for the Monte Carlo code differed from those employed by the IOCCG group for Hydrolight. It is to be noted that generally Hydrolight takes into account the wave slopes due to wind speed, the radiance distribution (including sky, clouds) and the bottom boundary specified via the bidirectional reflectance distribution function. All these factors were neglected in the Monte Carlo code.

Hence, to generate a more reasonable comparison, the comparison was drawn for the below surface remote sensing reflectance, where these surface effects are no longer the source of error.

The graphs in Figure 4.9(a-h) show that the results generated from the Monte Carlo code can reasonably be compared to those generated by Hydrolight. It can be seen that the RMSD was reduced as opposed to that for the above surface remote sensing reflectance comparison, for the same sets of input conditions. This indicates that the Monte Carlo code that has been set up has been validated for the ideal case of homogeneous ocean, based on the results shown.

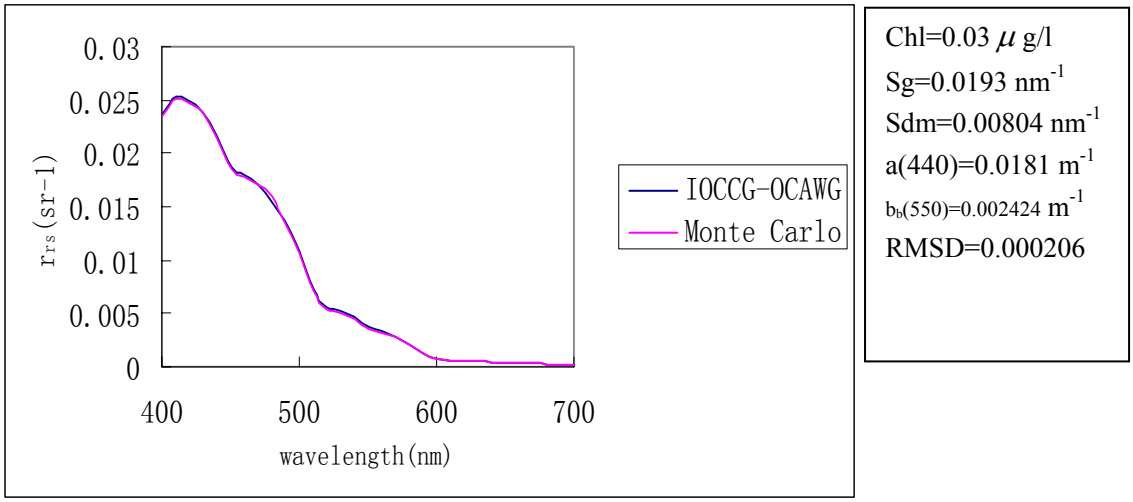

Figure 4.9 (a)graph of below surface remote sensing reflectance

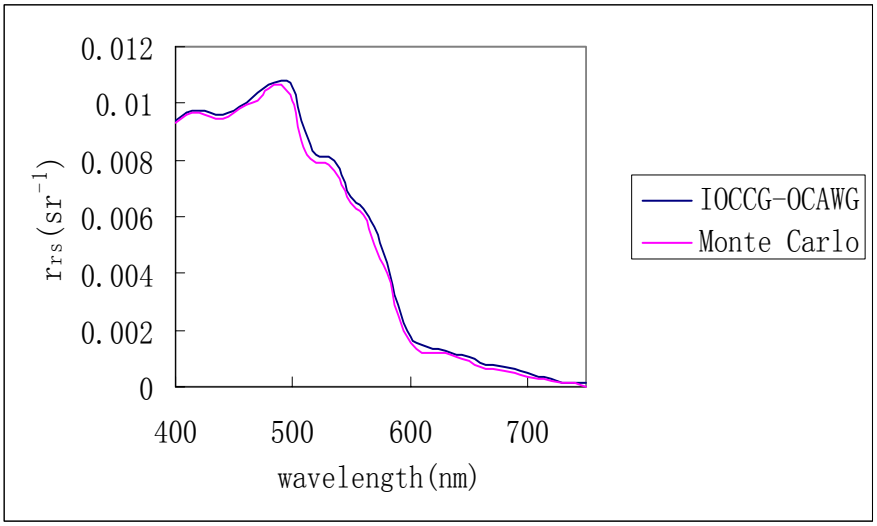

Figure 4.9 (b) graph of below surface remote sensing reflectance

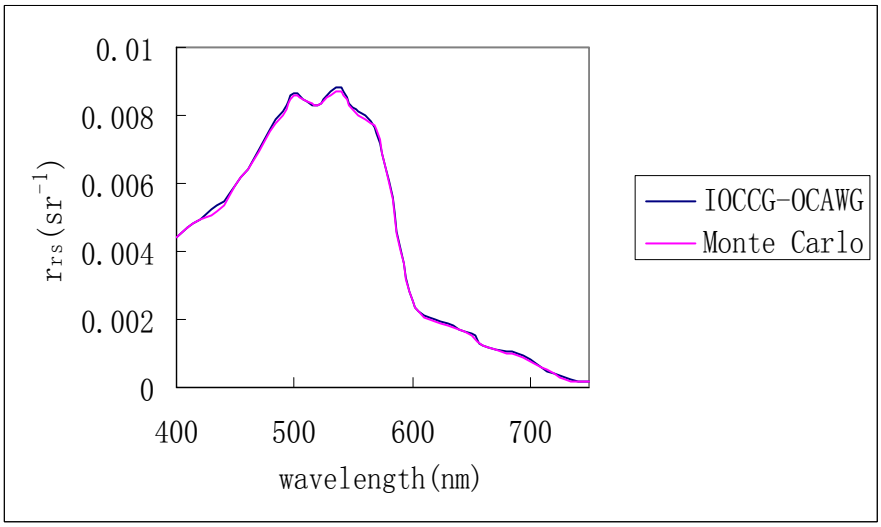

Figure 4.9 (c) graph of below surface remote sensing reflectance

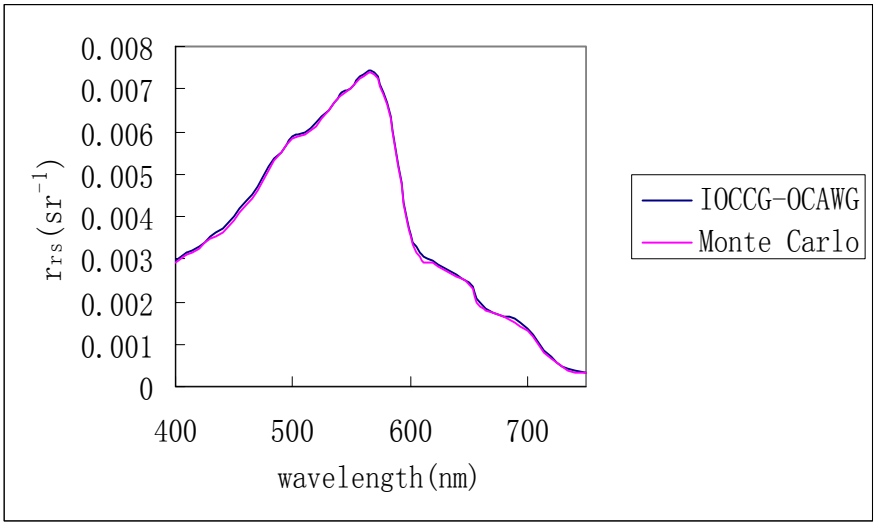

Figure 4.9 (d) graph of below surface remote sensing reflectance

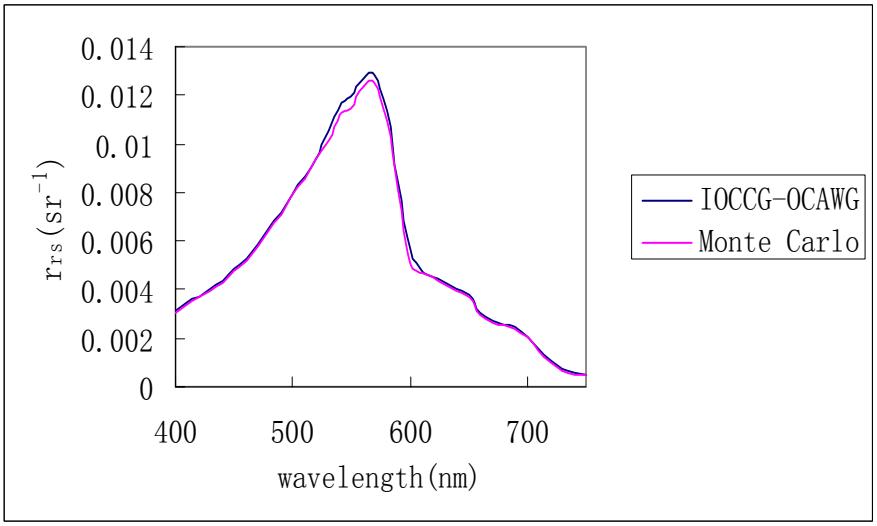

Figure 4.9 (e) graph of below surface remote sensing reflectance

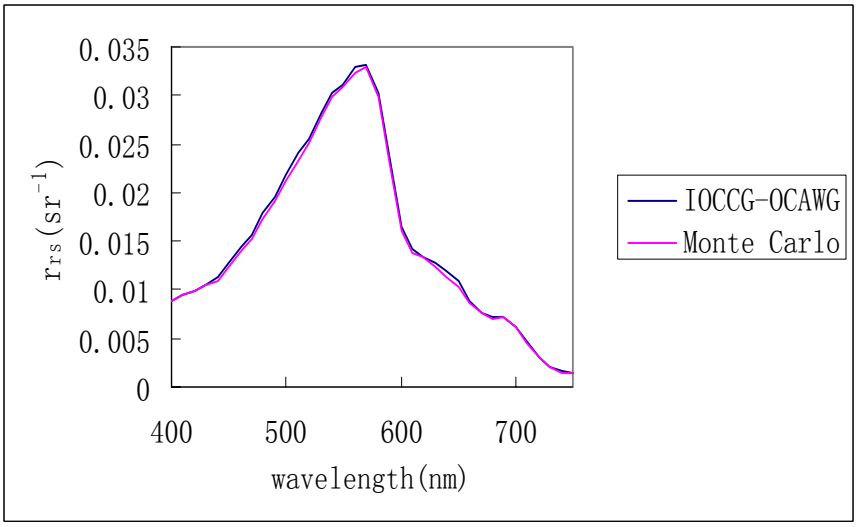

Figure 4.9 (f) graph of below surface remote sensing reflectance

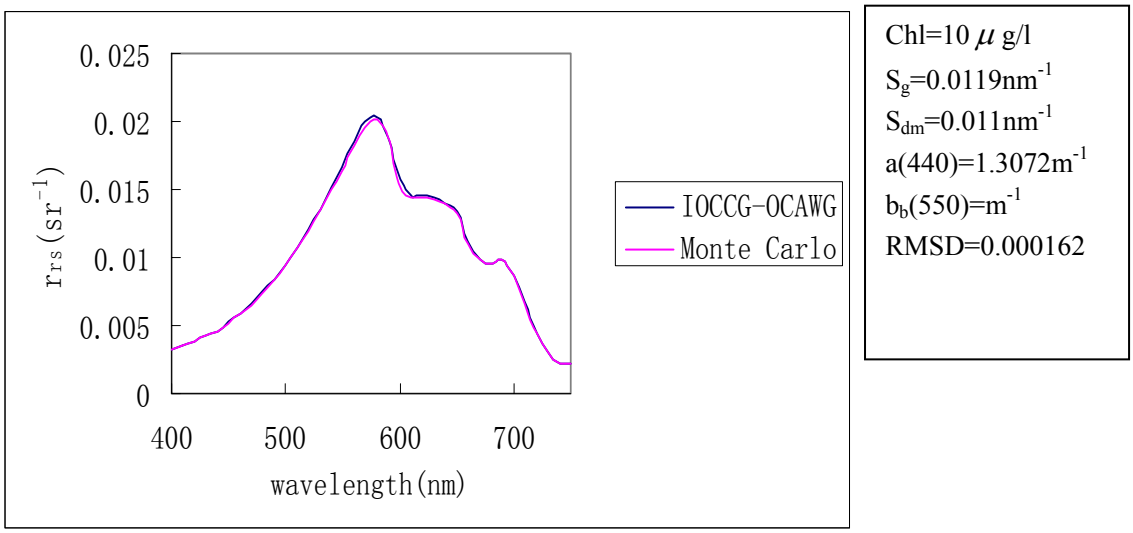

Figure 4.9 (g) graph of below surface remote sensing reflectance

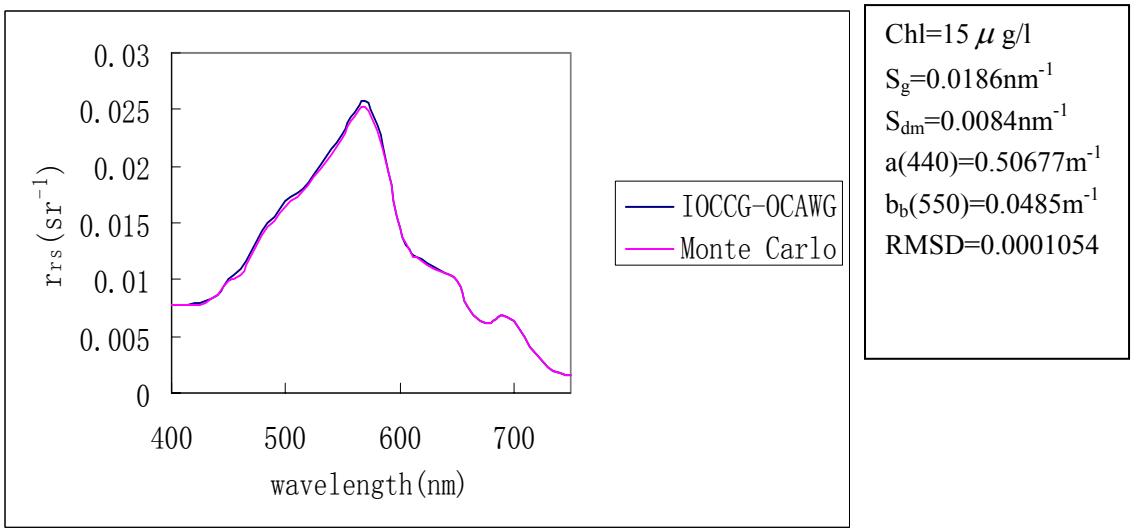

Figure 4.9 (h) graph of below surface remote sensing reflectance

Table 4.2 below shows the percentage error for the below surface remote sensing cases. It can be seen that there is a decrease in the %error for below surface remote sensing cases (0.81%–3. 36%) as opposed to the above surface remote sensing cases (8.84%–26.92%).

Graph	MEAN	RMSD	% error
4.8(a)	0.01261	0.000206	1.633
4.8(b)	0.00735	0.000247	3. 36
4.8(c)	0.004475	0.000526	1.39
4.8(d)	0.003915	0.000794	2.02
4.8(e)	0.0065	0.000194	2.98
4.8(f)	0.0169	0.00159	0.94
4.8(g)	0.0109	0.000162	1.486
4.8(h)	0.0013	0.0001054	0.81

Table 4.2 showing the percentage error for graphs 4.9(a) to 4.9(h)

Chapter 5

Monte Carlo Simulation of remote sensing reflectance of waters with homogeneous and vertically inhomogeneous optical properties

---

5.1 Introduction

In Chapter 3, it was seen that when interpreting the reflectance data, it is usually assumed that the whole water column is vertically homogeneous. But, from oceanographic observations of the upper ocean, the presence of vertical stratification has been observed. Also, retrieval algorithms assume that the water body being examined is homogeneous and gives no indication of the stratification present.

In this chapter, Monte Carlo simulations will be used to simulate the reflectance of stratified oceans (with different types of stratification) and see how it compares with the reflectance of a homogeneous ocean. The Monte Carlo method is used as it is conceptually easy to use and the computations carried out are very fast. One advantage of this method is that it allows the simulation of reflectance for a wide range of conditions that mimic those found in nature. For each run, a large number of photons can be considered and the error for each run is only about 0.5% (as was shown in Chapter 4).This chapter consists of four subsections and the work done in each subsection is listed here.

1. It will be demonstrated that interpreting the reflectance of a stratified

ocean in terms of an equivalent homogeneous one work well for a two layer ocean but shows slightly more deviations for a multi layered ocean.

2. The effects of a nonuniform vertical pigment profile of the inherent optical properties of the water column associated with the depth dependent chlorophyll concentration ,*Chl(z)* will be studied. The Gaussian function described in Chapter 3 will be used to model this non uniform chlorophyll profile.
3. A retrieval algorithm will then be applied to both homogeneous and inhomogeneous(described by the Gaussian profile)water to see how the retrieved values of the optical coefficients compare with the actual values found in the water body. The retrieval algorithm used is the Quasi Analytical Algorithm which has been fully described in Appendix B.
4. It will then be seen how the reflectance of a stratified ocean compares with a hypothetical homogeneous one with a pigment concentration (<*Chl*>) that is the depth weighted average of the actual depth varying concentration *Chl(z)*.

5.2 The effect of vertical structure on diffuse reflectance for a stratified ocean

In an earlier study, Gordon (1973) investigated the diffuse reflectance of a flat homogeneous ocean as a function of its optical properties using Monte Carlo. He found that the diffuse reflectance could be expressed in terms of the parameter *u* as,

$$R(\lambda) = 0.0001 + 0.3244u(\lambda) + 0.1425u(\lambda)^2 + 0.1308u(\lambda)^3 \quad 5.1$$

Where

$$u(\lambda) = \frac{b_b(\lambda)}{a + b_b(\lambda)} \quad 5.2$$

The inverse relation was also be fitted to a cubic equation,

$$u(\lambda) = -0.003 + 3.0770R(\lambda) - 4.2158R(\lambda)^2 + 3.50R(\lambda)^3 \quad 5.3$$

In a vertically stratified ocean with depth dependent IOPs, the parameter *u(z)* is also depth dependent. Suppose that Equation 5.3 is applied to the reflectance of this stratified ocean, then the value of u obtained would represent the equivalent value that would be obtained from a homogeneous ocean with the same reflectance. This equivalent u would be notated as u_e for the stratified ocean. Gordon and McCluney (1975) have shown that for the case of a homogeneous ocean, 90% of the diffuse reflection originates from the depth above which the in water downwelling irradiance falls to 1/e of its value at the surface. Gordon and Clark ((1980) proposed that u_e is related to the average value of *u* over that penetration depth z_{90} calculated by,

$$u_{av} = \frac{\int_0^{z_{90}} g(z)u(z)dz}{\int_0^{z_{90}} g(z)dz} \quad 5.4$$

u is related to the single scattering albedo ω_o = b/a by

$$u = \frac{\omega_o B}{1 - \omega_o(1 - B)} \quad 5.5$$

where *B* is the backscattering probability which is the ratio of the backscattering coefficient to the total scattering coefficient. The weighted average function is given as $g(z) = [\frac{E_d(z)}{E_d(0)}]^2$

The average single scattering albedo can be obtained in the same way as,

$$\omega_{0av} = \frac{\int_0^{z_{90}} g(z)\omega_o(z)dz}{\int_0^{z_{90}} g(z)dz} \qquad 5.6$$

Assuming the backscattering probability B to be the same at all depth, then an equivalent single scattering albedo, ω_e can be calculated from u_e using Equation 5.5.

In the following sections, Monte Carlo simulations are carried out to obtain the reflectance for several cases of stratified waters. It is assumed that the inherent optical properties of the ocean can be described by one-parameter model pertaining to case 1 waters. Thus the inherent optical properties of the ocean are given in terms of the concentration of chlorophyll a. The total absorption coefficient $a(\lambda)$ and the total scattering coefficient $b(\lambda)$ was calculated using the biooptical model described in Chapter 2 (Section 2.8). The value of the chlorophyll concentration Chl was made to vary from 0.03-1.2 mg m^{-3}

The range of ω_o that is being considered is from 0 (no scattering) to 0.9 (almost no absorption). The total number of photons that pass each depth marker in the upwards and downwards direction is taken to be a measure of the downwards (E_d) and upwards (E_u) irradiance respectively. The penetration depth (described in Appendix A) is taken as the depth at which E_d falls to 1/e (about 36%) of its subsurface value.

5.2.1 A two-layered water column

The first case to be considered for the vertical structure of the water is

described by a two layer model as shown in Figure 5.1 below.

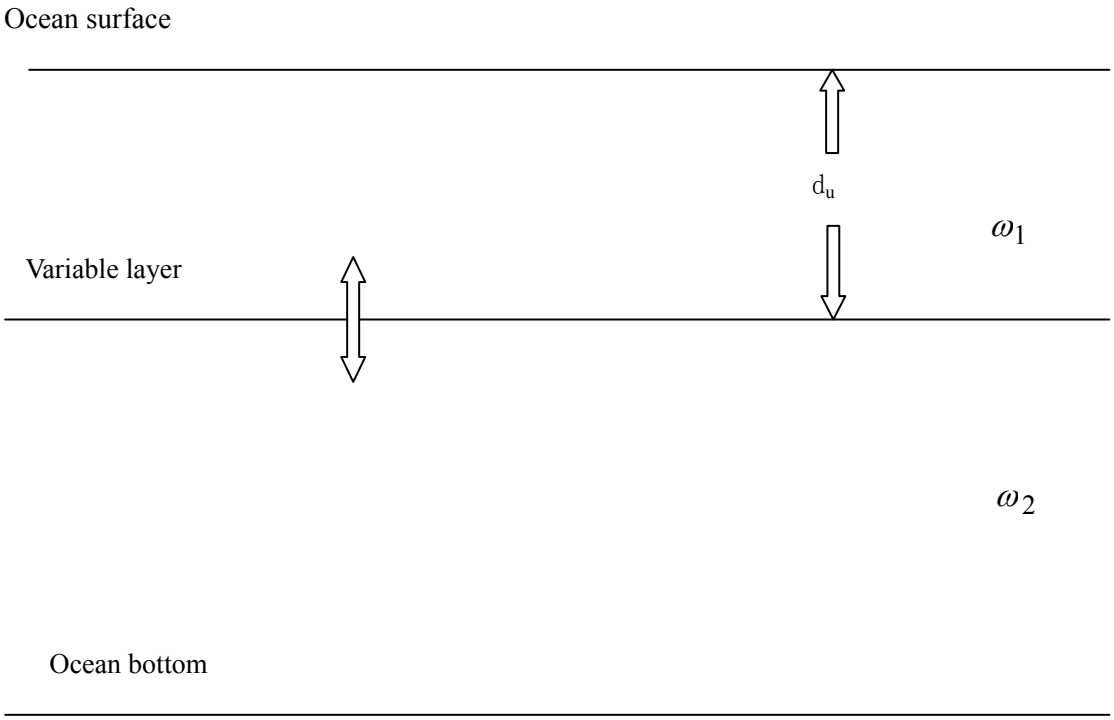

Figure 5.1. Sketch of two layered water column

The two layers are made to differ in their values of *a* and *b* (and hence ω_o), which are denoted by ω_1 and ω_2 for the top and bottom layers respectively. The computations have been carried out for various combinations of ω_1 and ω_2 (between 0 and 0.9) where $\omega_1 \neq \omega_2$. The chlorophyll concentrations of the two layers were assigned randomly and the corresponding values of *a*, *b*, and ω_0 were calculated from the bio-optical model described earlier. The values were accepted provided the ω_0 values were not the same for both layers. The thickness of the upper layer (d_u) was made to vary and was given the following values: 1.5 m, 2.5 m and 3.5 m. The second layer was assumed to stretch to the bottom, which was taken to be at 20m.

Figure 5.2 shows the relation between *b/a* of the top layer and the values of reflectance, both at 440 nm.

As can be seen, there is a nearly linear relationship between R and b/a for b/a less than 2. However, when the value of b/a increases, this linearality is no longer apparent.

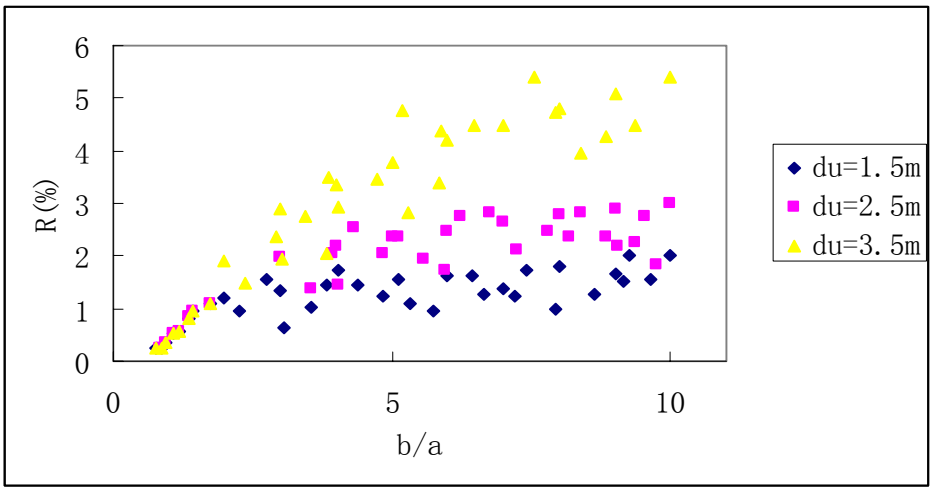

Figure 5.2 The diffuse reflectance of a two layer ocean as a function of the thickness (in metres) and the ratio of the backscattering to absorption of the upper layer

Using equation 5.2, the equivalent u, i.e. u_e, is calculated from the reflectance for each case of the two layer water system. It is not a-priori known how this quantity is related to the vertical structure of the water. Fig. 5.3 shows the values of R plotted against the values of u_e(calculated from equation 5.3) and the values of u_{av}(calculated from Equation 5.4)

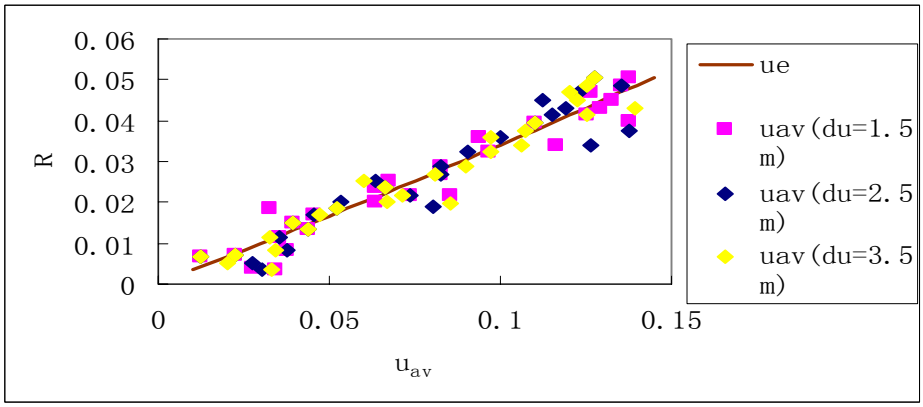

Figure 5.3 The diffuse reflectance, R, of a two layer ocean as a function of u_{av}(calculated from Equation 5.4). The solid line in the plot of R versus u_e (calculated from Equation 5.3)

In Figure 5.3, the points show u_{av} (calculated from equation 5.4) against the diffuse reflectance of a stratified ocean, R and the solid line is u_e(calculated from Equation 5.3) plotted versus R. If Gordon's hypothesis was exactly satisfied, all the points would have fallen on the line. It is seen that almost all of the points cluster along the line, even though some slight deviations are seen. This indicates that the general trend of the hypothesis is satisfied.

Figure 5.4 shows the graphs of u_e and u_{av} for a two layer ocean (calculated from the %R)

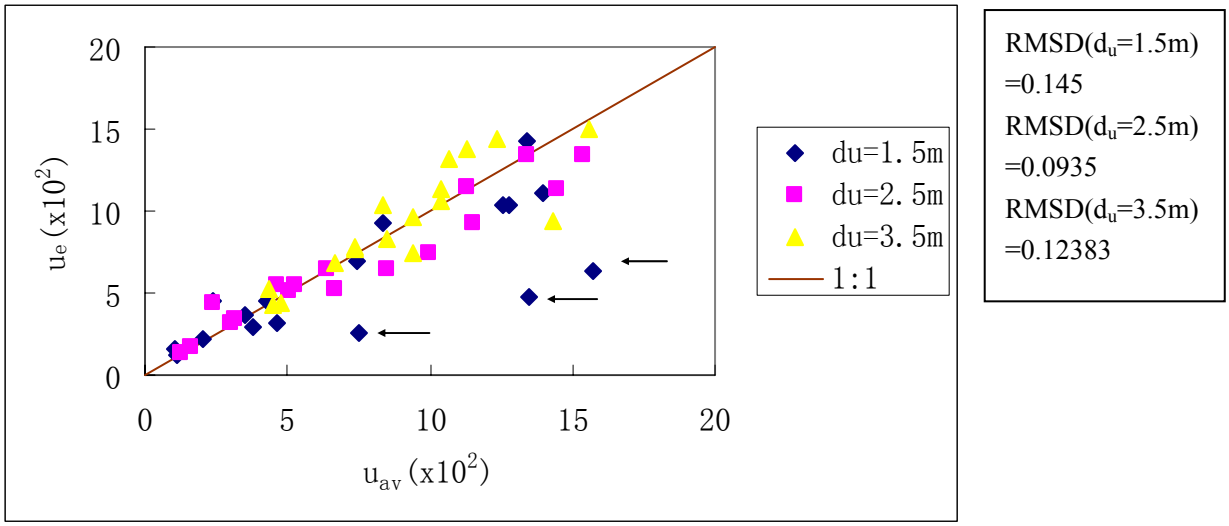

Figure 5.4. Comparison between u_{av} and u_e for a two layer ocean

The above graph in Figure 5.4 shows that for most of the cases tested, u_e is highly correlated to u_{av}. In fact, the data points lie close to the $u_e = u_{av}$ line, except for a few outliers (indicated by the arrow in Figure 5.2). These points are due to values ω_1 and $\omega_2 \approx 0.83$ -0.87 for an upper layer thickness of 1.5m. The conclusion that can be derived here is that $u_e \approx u_{av}$ except for the case of thin upper layers with high scattering

Figure 5.5 shows the plot of u_e versus u_{av} when these outliers have been removed. It is seen that for all the depth of the upper layer considered, the

correlation between u_e and u_{av} is of a quite good degree, when the oddities are not considered.

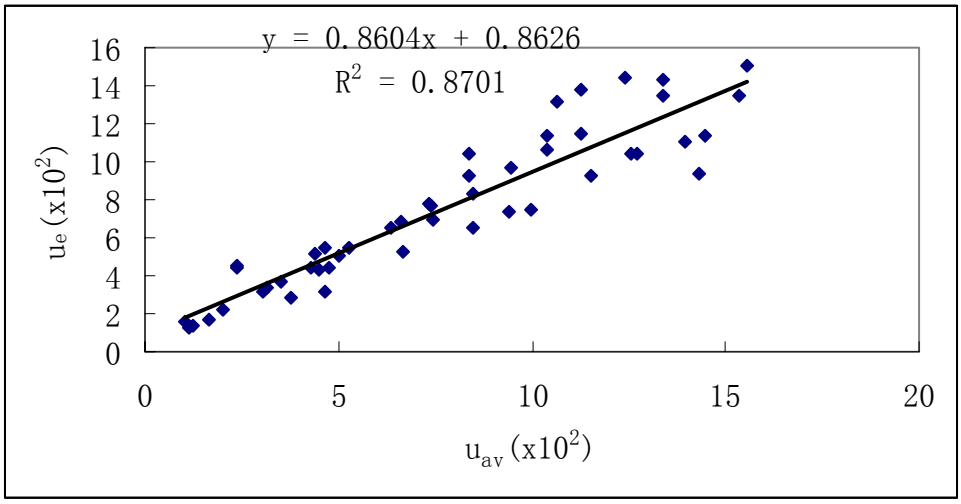

Figure 5.5. Comparison between u_{av} and u_e for a two layer ocean, without the outliers in Figure 5.4

Figure 5.6 shows the plot of ω_e and ω_{0av} .In this graph, ω_e was calculated from u_e by inverting Equation 5.5 i.e.

$$\omega_e = \frac{u_e}{B + u_e(1-B)} \qquad 5.7$$

with the value of B equals to 0.0183, i.e. the backscattering probability for the Petzold phase function used in the Monte Carlo simulation. The value of ω_{0av} is calculated from Equation 5.6

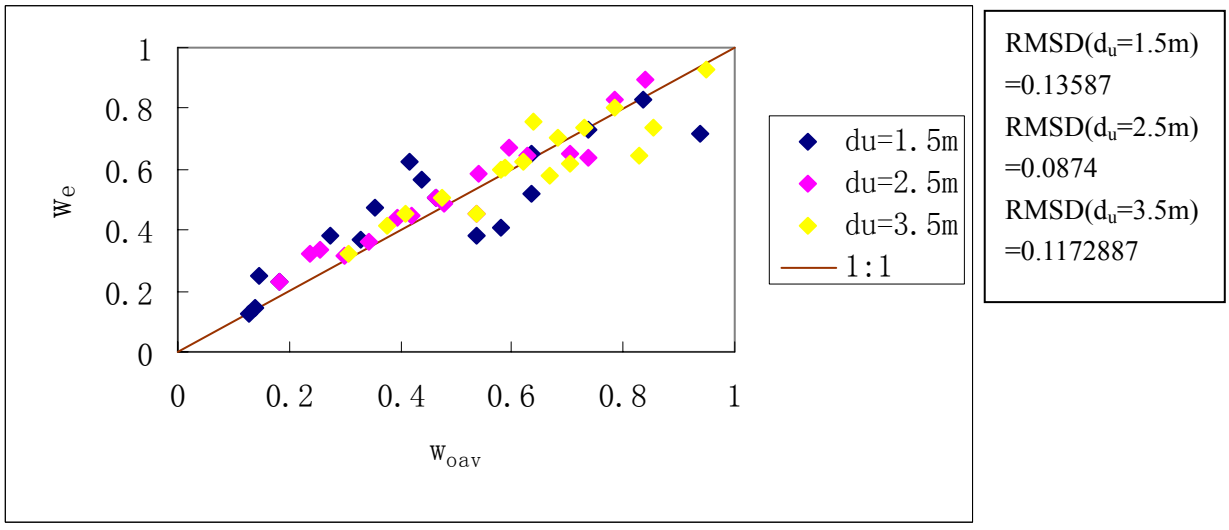

Figure 5.6. Comparisons between ω_e and ωo_{av} for a two layer ocean

It can be seen that ω_e is nearly equal to $\omega_{0av,}$ even for the outliers shown in Figure 5.5. It should be noted that in practical situation, it is difficult to compute ω_e from u_e because the backscattering probability, *B*, of the scattering phase function needs to be known and the values of *B* may be different for different types of waters. Here the scattering phase function was taken to be the Petzold one and was assigned to both layers.

5.2.2 A multi-layered water column

In the second case, the same procedure is now applied to a stratified water column. Instead of being divided in two layers, the water column is now divided into several layers of the same thickness (1m each). Only the thickness of the upper layer is allowed to vary (from 1.5m to 3.5m, similar to the case of a two layer ocean). The sketch for the multi layered ocean is shown in Figure 5.7 below.

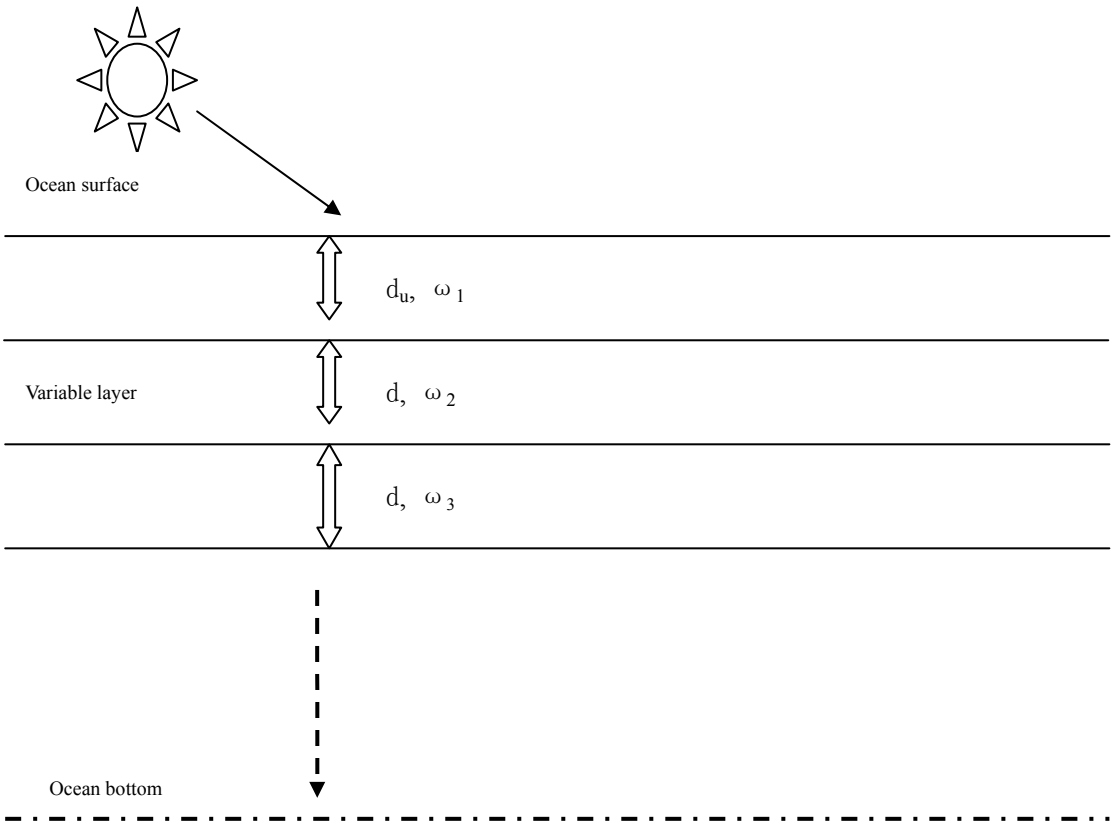

Figure 5.7. Sketch of a multi layered water column

The calculations are again carried out using the Monte Carlo technique to trace the life history of the photons. Detectors are now placed at several depths in the medium to measure the upwelling and downwelling irradiances (below the water surface). The several layers differed only in their values of ω_o. The computations have been carried out for 3 values of the upper layer thickness, d_u=1.5m, 2.5m, 3.5m and various combinations of ω_o. The water column was stratified and the bottom was assumed to be at a depth of 20.5m and apart from the upper layer, the rest of the other layers had the same thickness of 1m (i.e. d_u =1m)

Fig. 5.8 shows the values of R plotted against the values of u_e(calculated from equation 5.3) and the values of u_{av}(calculated from Equation 5.4)

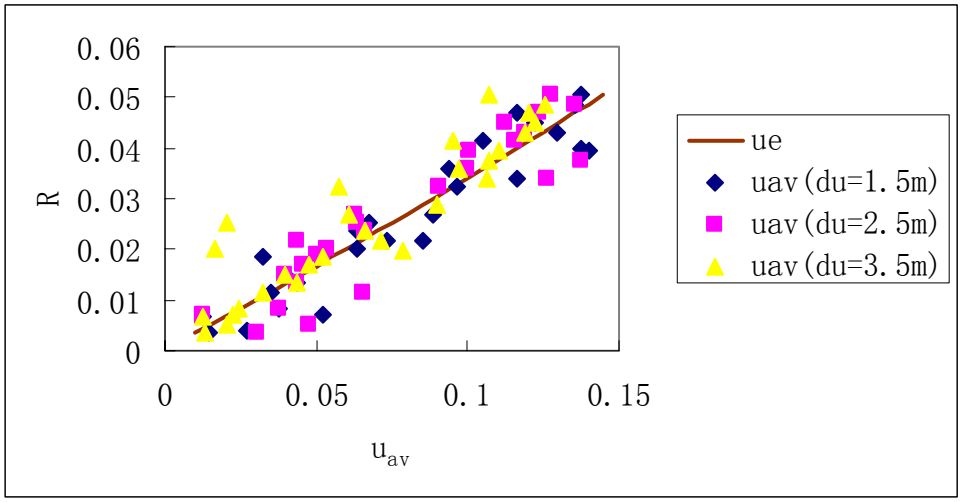

Figure 5.8 The diffuse reflectance, R, of a multi layered two layer ocean as a function of u_{av}(calculated from Equation 5.4). The solid line in the plot of R versus u_e (calculated from Equation 5.3)

Even in the case of a multilayered ocean, Gordon's hypothesis is satisfied, as almost all the points cluster along the line. However, more deviations are seen when the result is compared to that obtained for the case of a two layer ocean.

The results obtained for u_e versus u_{av} and ω_e versus ω_{0av} are illustrated in Figures 5.9 and 5.10 respectively.

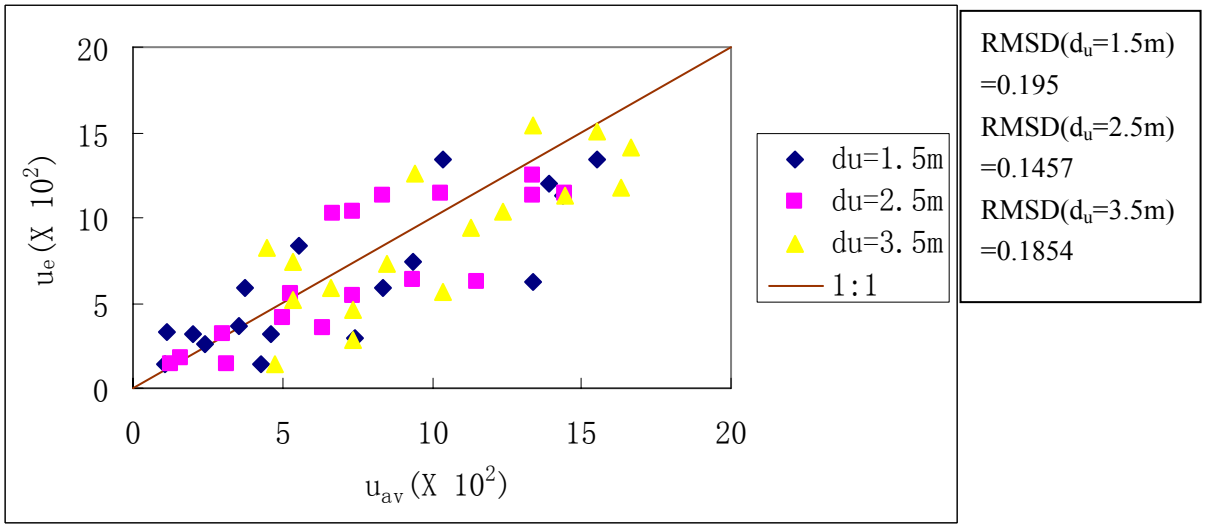

Figure 5.9 Comparison between u_{av} and u_e for a multi layered ocean

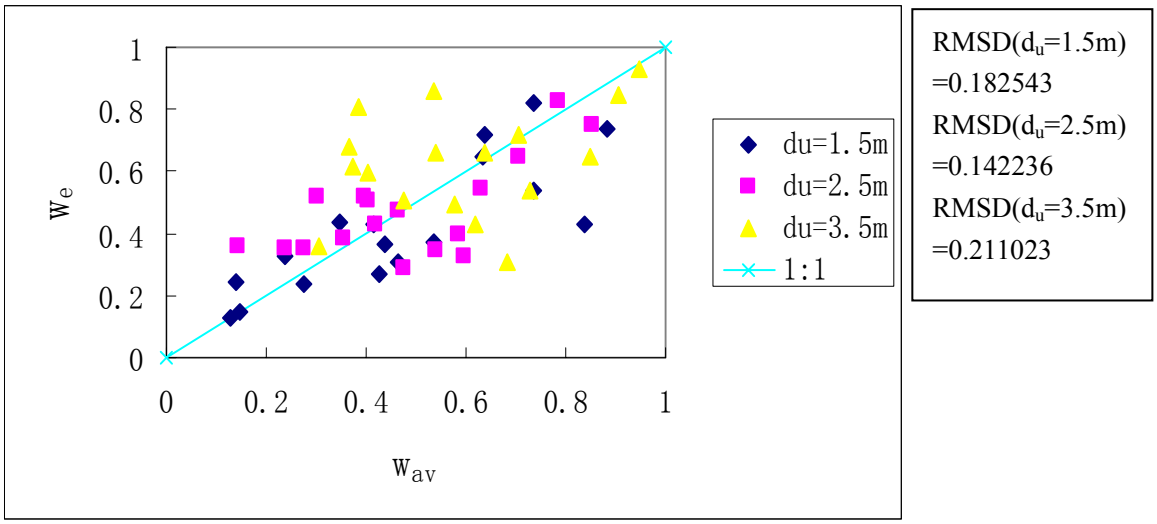

Figure 5.10 Comparisons between ωe and ωoav for a multi layered ocean

The above graph (Figure 5.9) shows that for most of the cases tested, u_e is nicely correlated to u_{av}. In fact, the data points lie close to the $u_e = u_{av}$ line. Unlike for the case of a two layer ocean, there are no outliers here. It can also be seen that ω_e is nearly equal to ω_{0av} (Figure 5.10) but it should be noted than in both cases, the comparisons show larger deviations than those of the two layer ocean. The root mean square difference between the equivalent values and the ones averaged over the penetration depth is higher as compared with the two layer model.

The introduction of vertical inhomogeneities can strongly influence the diffuse reflectance of the oceans. However for a two layer ocean, the reflectance is still a linear function of the scattering coefficient of the upper layer as long as its thickness remains constant and the phase function is the same for both layers. However, the case of continuous stratification, the assumption of comparing the diffuse reflectance of a stratified water body to that of a homogeneous ocean shows slightly larger deviations.

5.3 Effects of an inhomogeneous chlorophyll concentration with a vertical Gaussian profile

As was discussed in Chapter 3, vertical profiles obtained from diverse regions and environments usually show a subsurface maximum in chlorophyll concentration, commonly referred to as the deep chlorophyll maximum. It was also explained how a Gaussian function could be used to model the profile of this subsurface chlorophyll maximum.

In this section , Monte Carlo simulations will be used to examine the effects of a nonuniform vertical profile of the inherent optical properties of the water column associated with the vertical profile of chlorophyll concentration, *Chl(z)*, on the spectral remote-sensing reflectance, $R_{rs}(\lambda)$, of the ocean. This will be carried out by using the Gaussian function that describes the *Chl(z)* profile, to simulate a relatively broad range of open ocean conditions characterized by the presence of a subsurface *Chl* maximum at depths greater than or equal to 20 m. The simulations for a vertically nonuniform *Chl(z)* are then going to be compared with reference simulations for a homogeneous ocean whose chlorophyll concentration, *Chl*, was identical to the surface *Chl* of inhomogeneous cases.

The Gaussian function used to model the depth dependent chlorophyll concentration, *Chl(z)* was be expressed as

$$Chl(z) = Chl_0 + \frac{h}{\sigma(2\pi)^{0.5}} \exp[\frac{-(z - z_{\max})^2}{2\sigma^2}] \qquad 5.8$$

where Chl_0 is the background value of chlorophyll, z_{max} is the depth of the chlorophyll maximum, σ is the standard deviation that controls the thickness

of the chlorophyll peak and $\frac{h}{\sigma(2\pi)^{0.5}}$ is the amplitude of the chlorophyll maximum above the value of Chl_0 (ie Chl_{max}).

Two examples of the chlorophyll profiles are shown below in Figures 5.11(a) and (b).

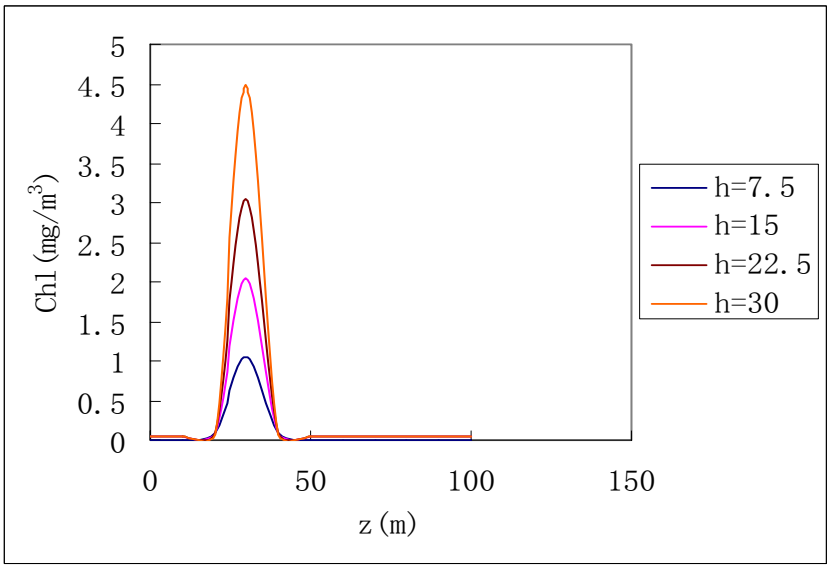

(a)Chl_o=0.05mgm^{-3}
z_{max}=30m
σ=3m

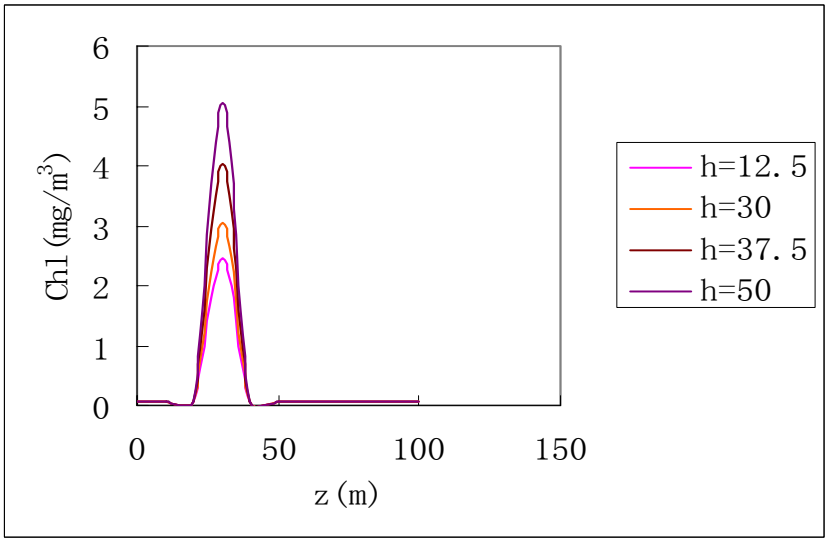

(b)Chl_o=0.05mgm^{-3}
Zmax=30m
σ=5m

Figure 5.11 (a) and (b): Examples of chlorophyll profiles for one selected pair of z_{max} and Chl_o values and different combinations of σ and h values as specified.

In order to analyse the sensitivity of the remote sensing reflectance to the vertical structure of chlorophyll concentration *Chl(z)*, Monte Carlo simulations were once again carried out . The same conditions attributed to the running of the code, as explained in chapter 4, were used here.

Chlorophyll profiles were used to determine the vertical distributions of the inherent optical properties (IOPs) within the upper ocean. The water column was divided into several layers, all with a constant thickness of 1m and the bottom was fixed at a depth of 60 m. The chlorophyll concentration was evaluated at the midpoint of each layer (using the Gaussian function for the vertical profile of chlorophyll in Equation 5.8). Once the chlorophyll concentration in each specific layer was obtained, the spectral absorption coefficient $a(\lambda)$ and scattering coefficient $b(\lambda)$ coefficients, as functions of depth, were calculated. The description of the biooptical model used to simulate the total absorption and scattering coefficients was given in section 2.6 .The values of the chlorophyll concentration, *Chl*, used will be specified below.

The analysis of variations in remote sensing reflectance caused by the *Chl(z)* profiles was carried out in the following way. Firstly, four Monte Carlo simulations were carried out for cases of homogeneous ocean and these were used as references. These reference simulations were carried out for a uniform distribution of chlorophyll with depth. The values of the chlorophyll concentration employed in the simulation are 0.05, 0.1, 0.2 and 0.3mgm^{-3} and these correspond to the typical values found in open oceans. The whole water

column was assigned only one value of the chlorophyll concentration and hence had only one set of $a(\lambda)$ and $b(\lambda)$. The reflectance values obtained for the four chlorophyll concentration values used are shown in Figures 5.12(a)-(d) below.

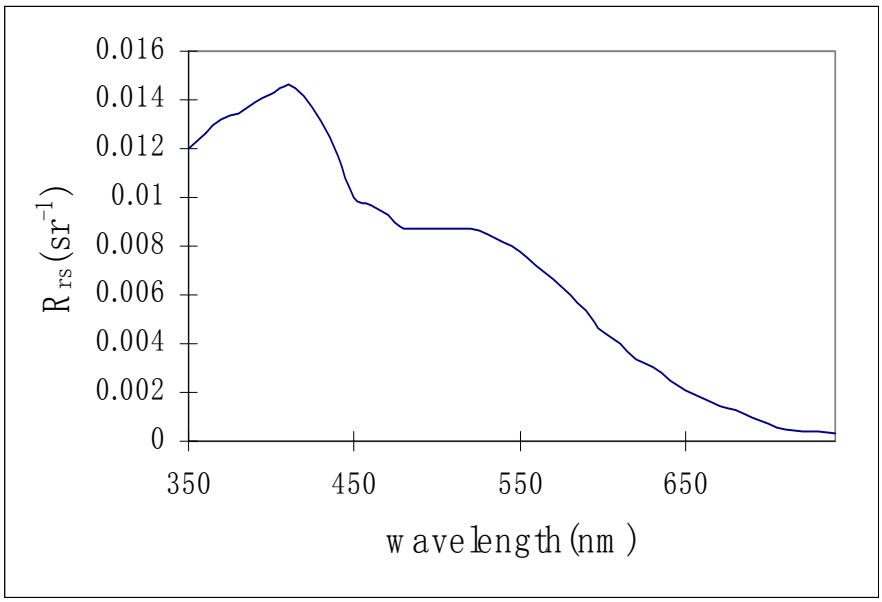

Figure 5.12(a) The reflectance $R_{rs}(\lambda)$ for a homogeneous ocean with a uniform pigment profile(Chl=0.05mgm^{-3})

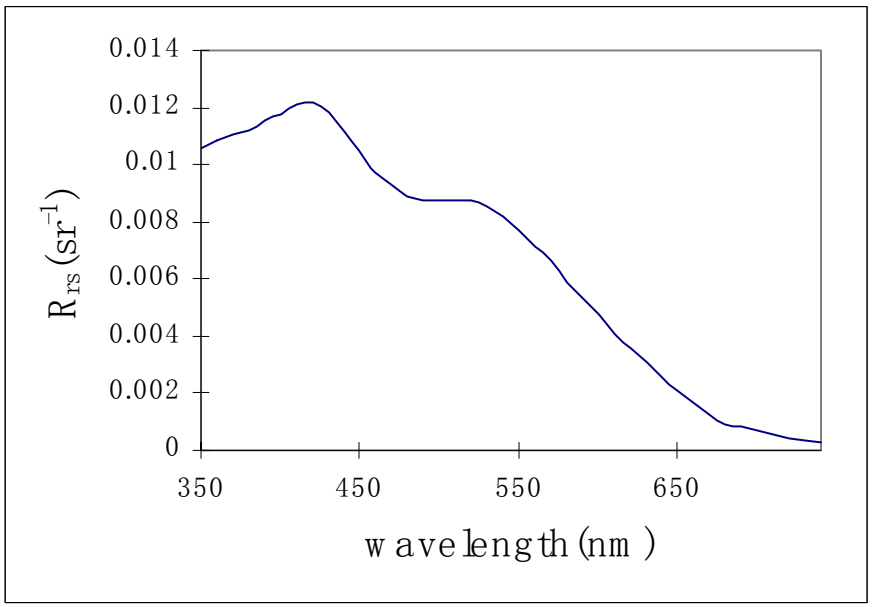

Figure 5.12(b) The reflectance $R_{rs}(\lambda)$ for a homogeneous ocean with a uniform pigment profile(Chl=0.1mgm^{-3})

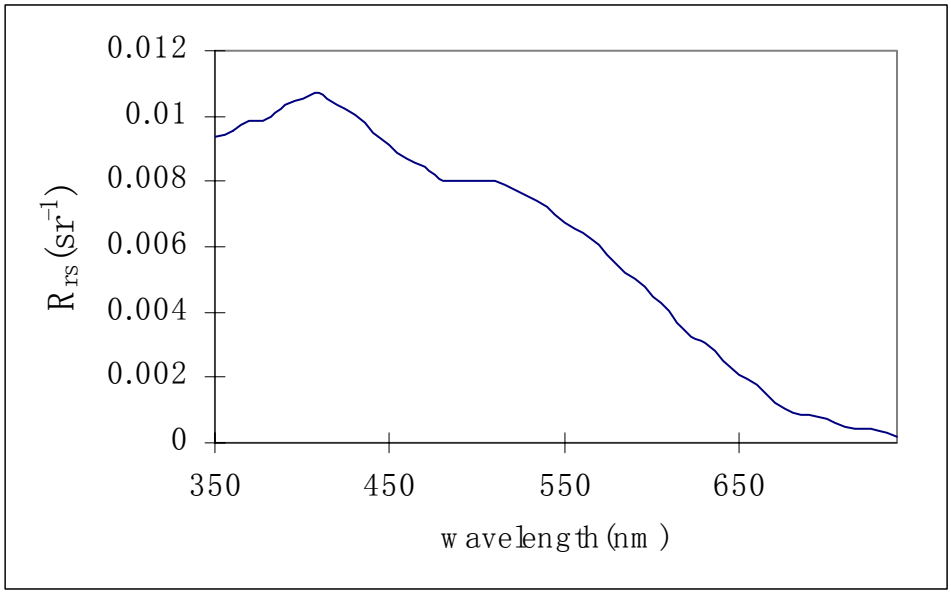

Figure 5.12(c) The reflectance $R_{rs}(\lambda)$ for a homogeneous ocean with a uniform pigment profile(Chl=0.2mgm^{-3})

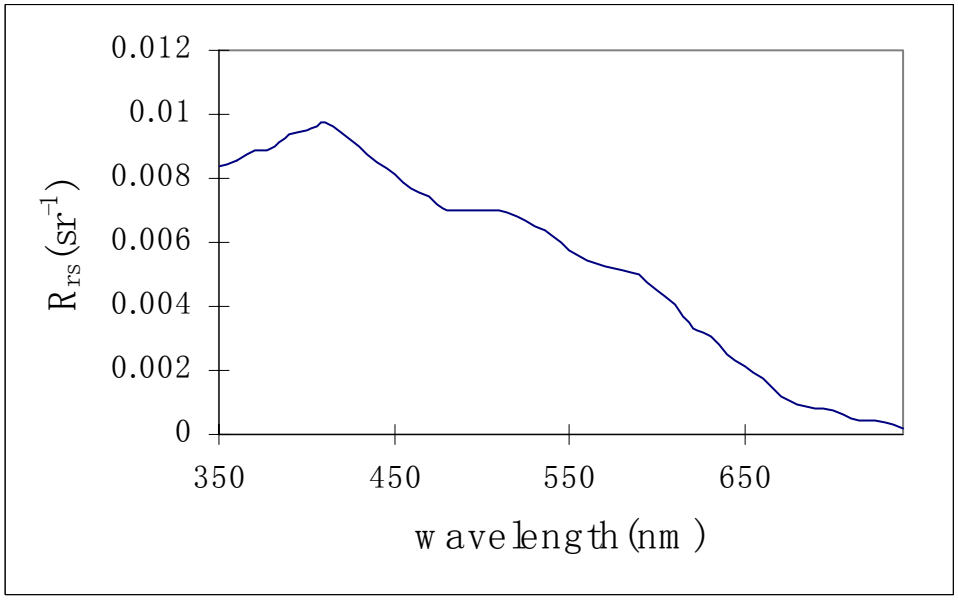

Figure 5.12(d) The reflectance $R_{rs}(\lambda)$ for a homogeneous ocean with a uniform pigment profile(Chl=0.3mgm^{-3})

Then the Gaussian function describing the chlorophyll profile was superimposed on each of the background values of chlorophyll concentration (0.05, 0.1, 0.2 and 0.3 mgm^{-3}). For each Chl_o value, σ was assigned the

following values; 2, 3, 4 and 5 m. For each σ, four values of h were used such that $\frac{h}{\sigma}$ =2.5, 5, 7.5 and 10 mgm^{-3}. Then for each Chl_o values, the specific values of z_{max} that were used are given below

Chl_o =0.05 mgm^{-3} ; z_{max} = 20,25,30 and 35m

Chl_o =0.1 mgm^{-3} ; z_{max} = 20,25 and 30m

Chl_o =0.2 mgm^{-3} ; z_{max} = 20,25, and 30m

Chl_o =0.3 mgm^{-3} ; z_{max} = 20 and 25m

The case for $z_{max} > 35$m was not considered because when the Chl_{max} is located at such large depths, the effect of *Chl(z)* profile on surface reflectance is negligible. The situations with near surface stratifications ($z_{max} < 20$m) are not considered because these situations are somewhat unrealistic in the sense that it would be difficult to maintain such stratifications in the presence of vertical mixing caused by wind through wind action (Gordon, 1992).

It should be noted that the parameters of the profiles were selected to cover a relatively broad range, representative of the ocean conditions characterized by the presence of a subsurface chlorophyll maximum located at depths greater than or equal 20m. In total, 748 cases of inhomogeneous water column were simulated.

5.3.1 Simulation results

The influence of parameters σ and h on the remote sensing reflectance is

examined first. The results are expressed as the relative change in reflectance at 445 nm, $R_{rs}(445)$, and the reflectance at 555 nm, $R_{rs}(555)$. The value of the relative change is given as

$$R_{change}(\%) = [\frac{(R_{nu} - R_u)}{R_u}]x100$$

where R can either denote $R_{rs}(445)$ or $R_{rs}(555)$ and the subscript nu and u refer to the non uniform and uniform profile respectively, where the uniform profile has a chlorophyll concentration equal to the background concentration of the non-uniform profile. The examples of this change are illustrated in Figure 5.13 for three combinations of z_{max} and Chl_0.

(i)z_{max}=30, Chl_o=0.2mgm^{-3}

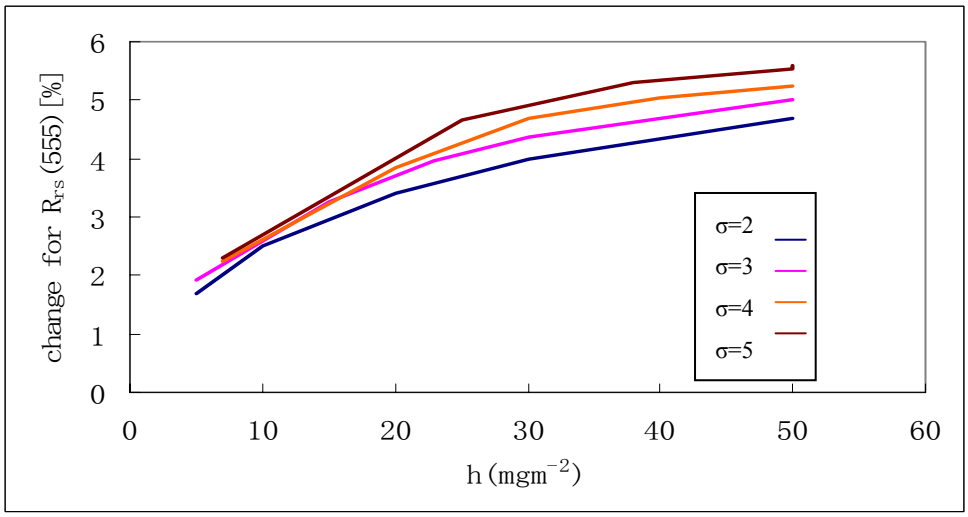

(a)

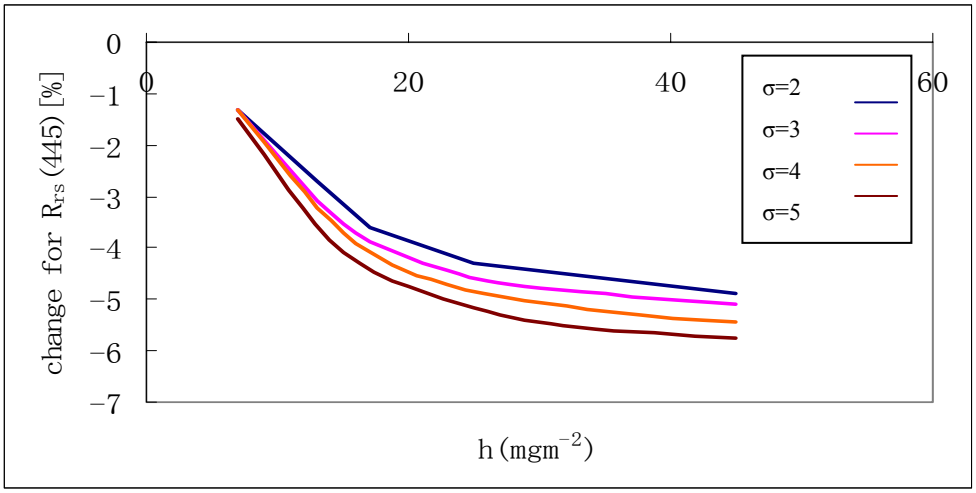

(b)

(ii) z_{max} =30, Chl_o =0.05mgm^{-3}

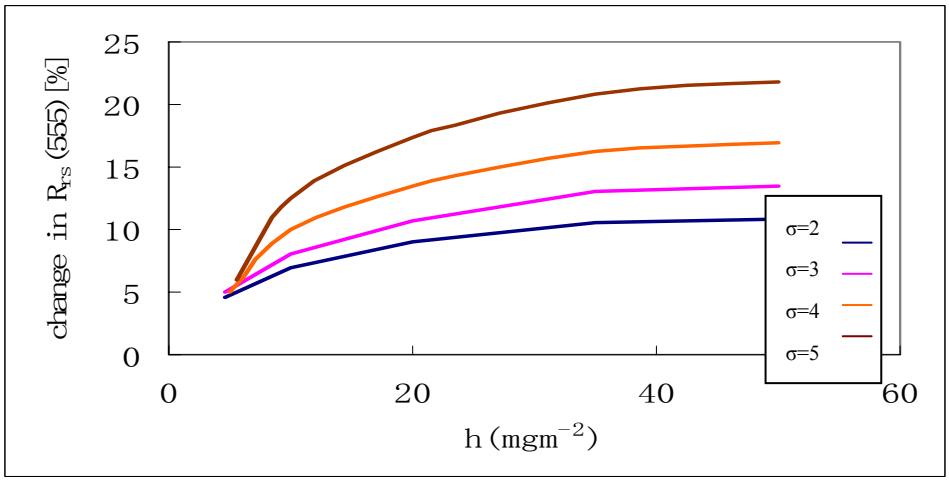

(c)

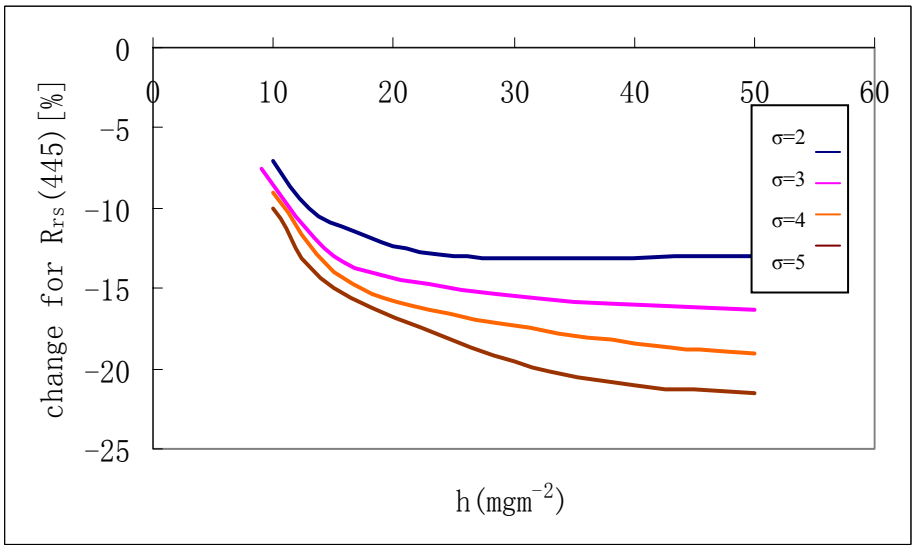

(d)

(iii)z_{max} =20, Chl_o=0.05mgm^{-3}

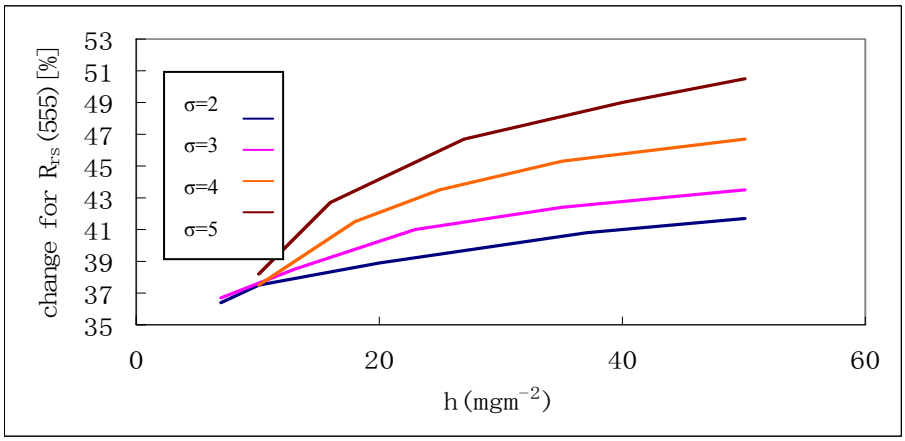

(e)

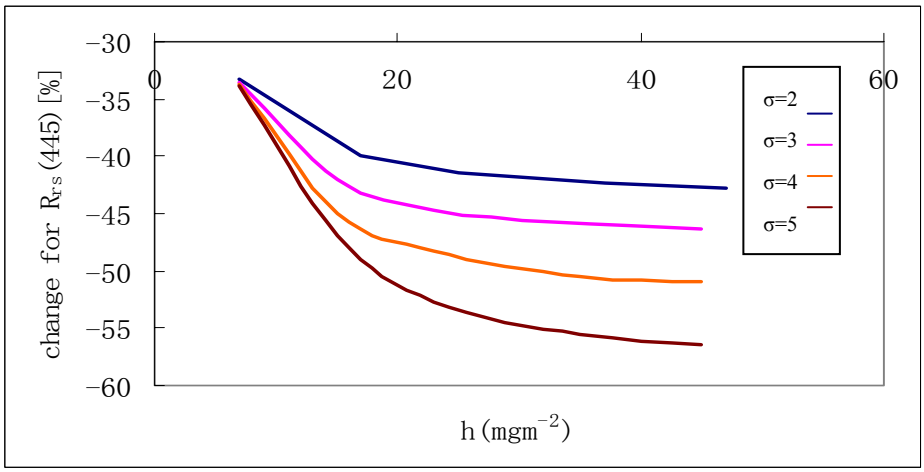

(f)

Figure 5.13: Example results of Monte Carlo transfer simulations, showing how the relative difference between nonuniform and homogeneous ocean values of *Rrs(445)* and *Rrs(555)* for various values of z_{max} , Chl_o, h and σ

The main consequences of variation in parameters σ and h are follows. When h increases, the magnitude of R_{change} increases as well. Increasing σ broadens the *Chl* maximum and also results in an increase in R_{change}. The first case considered is that of z_{max}=30m and Chl_0=0.2mgm^{-3}. When σ=5 m and h=50 mg m^{-2} (Chl_{max}=4mg m^{-3}), $R_{rs}(445)$ is lower by 5.7 % and $R_{rs}(555)$ is

higher by 5.3%. If however, the chlorophyll peak is narrow (σ=2 and h=5(Chl_{max}=1mgm^{-3}), then $R_{rs}(555)$ is higher by 1.8% and $R_{rs}(445)$ is lower by 1.3%

The second case considered is for high value of z_{max} (30m) and low value of Chl_0(0.05 mgm^{-3}). When σ=5m and h =50 mgm^{-2} (Chl_{max}=4mgm^{-3}), $R_{rs}(445)$ is lower by 22 % and $R_{rs}(555)$ is higher by 23%.when both σ(=2) and h(=5 i.e.Chl_{max}=1mgm^{-3})) are low, then $R_{rs}(555)$ is higher by 5% and $R_{rs}(445)$ is lower by 7%.

The third case consists of both low values of z_{max}=20m and Chl_0=0.05mgm^{-3}. When σ=5 and h=50(Chl_{max}=4mgm^{-3}), $R_{rs}(445)$ decreases by 56 % and $R_{rs}(555)$ increases by 51.8%. If however, the chlorophyll peak is narrow (σ=2 and h=5(Ch_{lmax}=1), then $R_{rs}(555)$ is higher by 36.2% and $R_{rs}(445)$ is lower by 33%.

In extreme cases of low surface chlorophyll of 0.05mgm^{-3} and a shallow chlorophyll maximum at 20m, R_{change} can exceed 50% when both h and σ are high. However, in cases where both surface Chl is high (0.2mgm^{-3}) and z_{max} is high, the influence of σ and h are quite small, regardless of whether they have high or low values.

Figure 5.14 (a-d) shows four examples of reflectance spectra representing chlorophyll profiles with several combinations of z_{max} , Chl_0 , h and σ values, compared with reflectance spectra of homogeneous water with uniform $Chl(z)$ profile, $Chl(z)=Chl_0$. It can be seen that the effect of the subsurface chlorophyll maximum is to decrease R_{rs} in the blue spectral region

and cause an increase in the green spectral region as compared to the case of uniform *Chl* profile. Consequently, $R_{rs}(\lambda)/R_{rs}(555)$ ratio in the presence of the chlorophyll maximum is reduced for wavelengths λ from the blue spectral region. This implies that the blue to green ratio can be significantly lower in the presence of the subsurface chlorophyll maximum than in a uniform profile. The effect of chlorophyll maximum becomes more pronounced with a decrease in z_{max} and Chl_0 (for the case z_{max} = 20m and Chl_0=0.05mgm^{-3}). In the case where z_{max} or Chl_0 or both are quite high, the differences between $R_{rs}(\lambda)$ observed in a vertically homogeneous[$Chl(z)=Chl_0$] ocean and a vertically inhomogeneous ocean[with a background concentration of chlorophyll] are small (the case where z_{max}=30m and Chl_0=0.4mgm^{-3}). The root mean square difference between the reflectance of the non uniform (*nu*) and uniform(*u*) case is calculated as

$$RMSD = \sqrt{\frac{1}{N}\sum_{i=1}^{N}(R_u - R_{nu})^2} \qquad 5.9$$

where N is the number of wavelengths(in nanometers) used. R_u is again the reflectance of a homogeneous ocean with a uniform chlorophyll profile and R_{nu} is the reflectance of a non homogeneous ocean characterized by a non uniform chlorophyll profile.

(a)

z_{max} =20m

Chl_0=0.05mgm^{-3}

σ =2m

h=5 mgm^{-2}

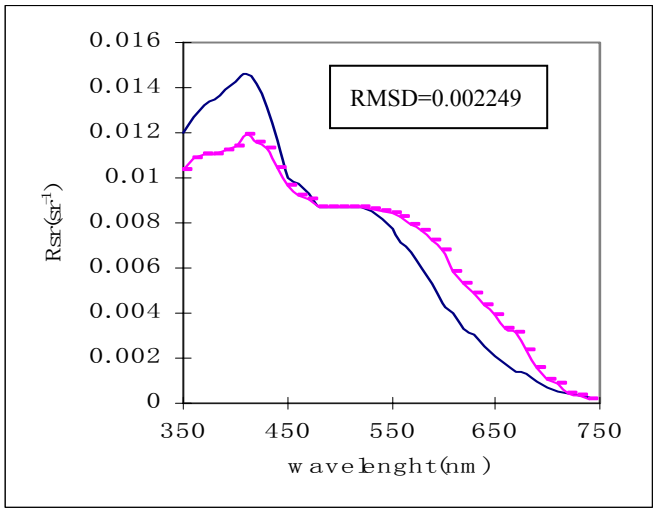

(b)

z_{max} =20m

Chl_0=0.05mgm^{-3}

σ =2m

h=5 mgm^{-2}

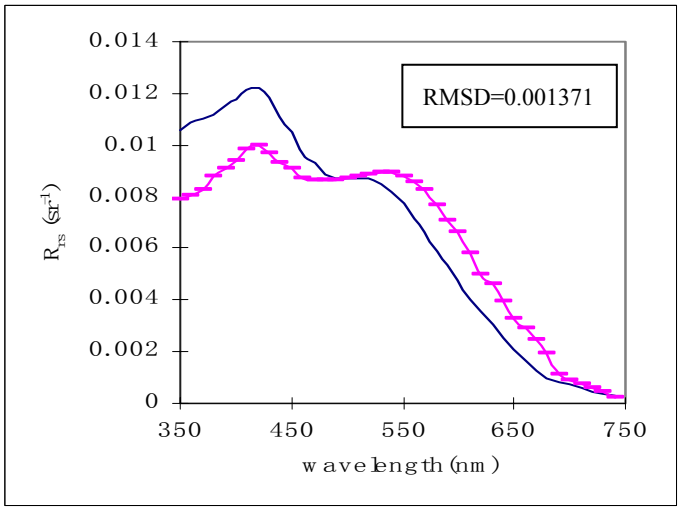

(c)

z_{max} =30m

Chl_0=0.2mgm^{-3}

σ =2m

h=5mgm^{-2}

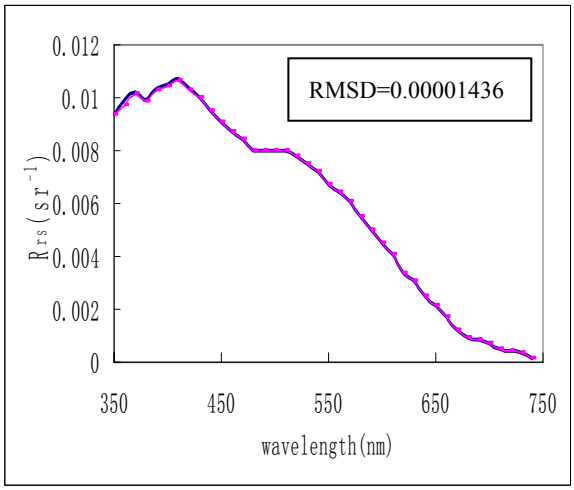

(d)

z_{max} =30m

Chl_0=0.1mgm^{-3}

σ =2m

h=5mgm^{-2}

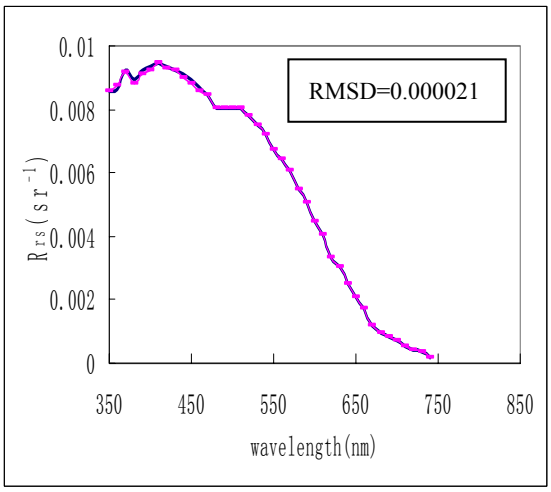

Figure 5.14: example results of radiative transfer simulations, showing the difference in reflectance $R_{rs}(\lambda)$ between the homogeneous ocean with a uniform pigment profile and the inhomogeneous ocean with a distinct subsurface chlorophyll maximum (dotted curve)

The empirical ocean colour algorithms for estimating chlorophyll are

typically based on the correlation between the measured spectral reflectances R_{rs} and the measured surface chlorophyll concentration, *Chl*. This type of correlation cannot account for the vertical structure of inherent optical properties. This means that it is possible that two water bodies with the same surface *Chl* but with different vertical distributions of *Chl(z)* and associated IOPs can have different values of $R_{rs}(\lambda)$ at any wavelength λ or different spectral ratios of R_{rs}. In that sense the vertical distribution of *Chl(z)* may introduce errors into the algorithm derived surface chlorophyll. Here it was shown that the percentage difference in $R_{rs}(\lambda)$ or in the spectral ratios of $R_{rs}(\lambda)$ between a vertically homogeneous and a vertically inhomogeneous ocean (with the surface *Chl* identical to a homogeneous case) can be significantly larger than 25% in many situations. The magnitude of these differences is expected to depend strongly on the parameters that describe the *Chl(z)* profile. It is tricky to gauge to what extent the non uniform *Chl(z)* profile might affect the performance of the present empirical algorithms like OC2 and OC4 (O'Reilly et al. 1998)

The at-launch Sea Viewing Wide field of view Sensor, SeaWiFS, chlorophyll a algorithm, named OC2 for Ocean chlorophyll 2-band algorithm, is an empirical equation relating remote sensing reflectances, R_{rs}, in the 490 and 555nm bands to chlorophyll a concentration, *Chl* (O'Reilly et al. 1998). OC2 was derived from a large data set (n = 1174) of coincident in situ remote sensing reflectance and chlorophyll a concentration measurements, $\tilde{R}_{rs}(\lambda)$ and $\tilde{Chl}$, respectively. This large data set covered a $\tilde{Chl}$ range of 0.02–32

mgm^{-3} from a variety of oceanic provinces, and was assembled during the SeaWiFS Bio-Optical Algorithm Mini-Workshop(SeaBAM) (1996). The main SeaBAM objective was to evaluate a variety of biooptical algorithms and produce an at-launch operational algorithm suitable for producing chlorophyll a images at global scales from SeaWiFS data (Firestone and Hooker, 1998). The OC2 algorithm was chosen by the SeaBAM participants, because it represented a good compromise between simplicity and performance over a wide range of Chl.

The formulation of the OC2 algorithm is given as:

$$\text{Chl} = 10^{(a_0 + a_1 R + a_2 R^2 + a_3 R^3)} + a_4 \qquad 5.10$$

where $R = \log 10 \frac{R(490)}{R(555)}$ and $R_{\lambda_j}^{\lambda_i}$ is a compact notation for the $\frac{R_{rs}(\lambda_i)}{R_{rs}(\lambda_j)}$ band ratio and a_0=0.2974,a_1=-2.2429,a_2=0.8358,,a_3=-0.0077,a_4=-0.0929

The first version of OC4 (O'Reilly and Guza, 1998) was formulated as a modified cubic polynomial (i.e., a third order polynomial plus an extra coefficient), however, the current version of OC4 uses a fourth order polynomial (five coefficients), because this yielded better statistical agreement between model (Chl) and $\tilde{C}hl$. The fourth order polynomial equation for OC4 version 4 (OC4v4), is:

$$\text{Chl} = 10.0^{(0.366 - 3.067R4 + 1.930R\_4\_2 + 0.649R\_4\_3 - 1.532R\_4\_4)} \qquad 5.11$$

where $R_4 = \log 10\ (R_{555}^{443} > R_{555}^{490} > R_{555}^{510})$, where the argument of the logarithm is a shorthand representation for the maximum of the three values.

The algorithms mentioned above are based on a large amount of field

data that were collected in various oceanic regions throughout different seasons. Thus it is possible that some of these data were collected in the presence of significant effects of a non uniform *Chl(z)* profile on ocean reflectance and that some data were collected in regions devoid of such effects i.e. under nearly homogeneous conditions in the ocean's upper layer. These algorithms are also mostly representative of case 1, non polar waters.

Figure 5.15 provides an indication of the relationship between the OC4 and OC2 algorithms and the data affected by nonuniform Chl(z) profiles. The graph shows the comparison of OC4 and OC2 curves with the data obtained from the Monte Carlo simulations.

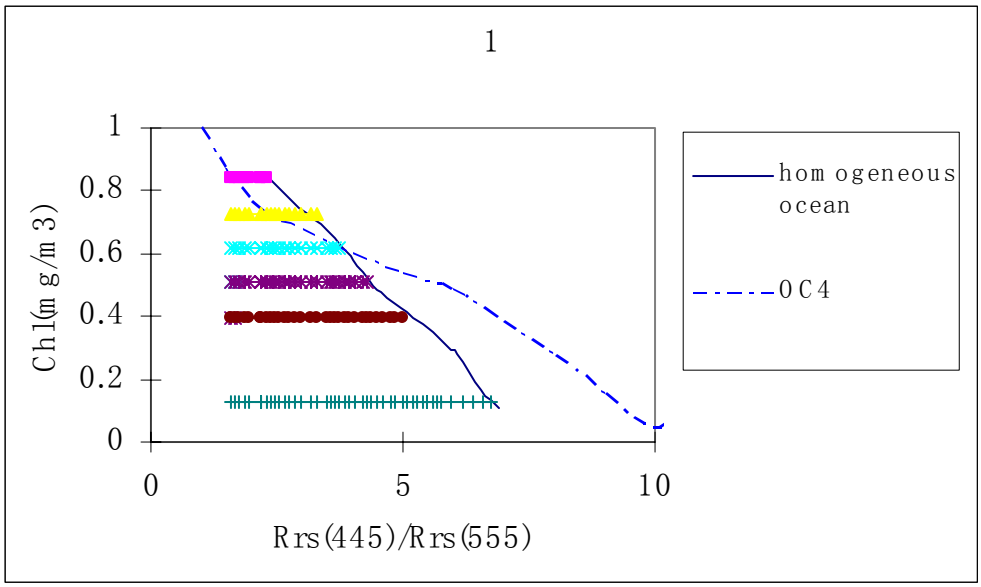

(a)

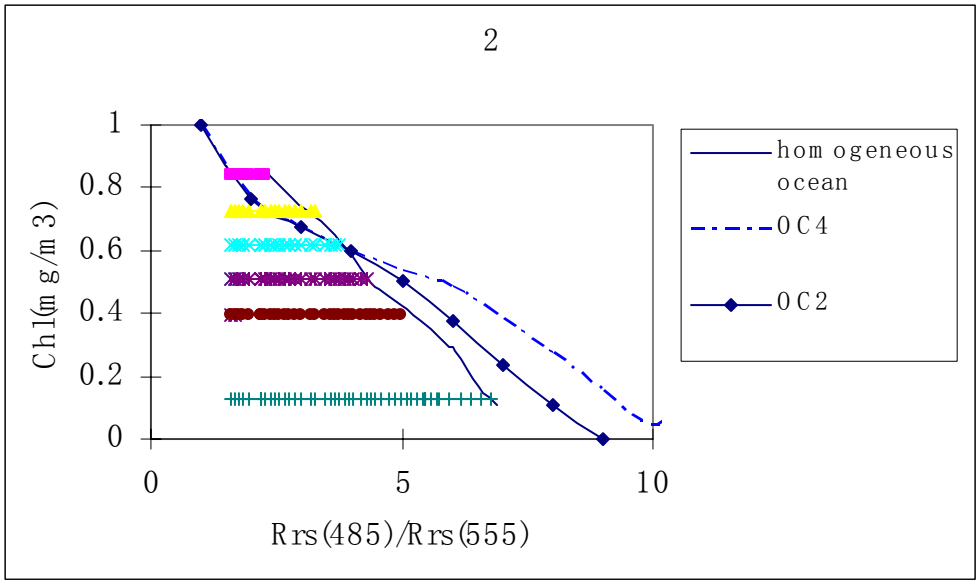

(b)

Figure 5.15: (a), Chlorophyll concentration at the sea surface as a function of the blue to green ratio if remote sensing reflectance $R_{rs}(445)/R_{rs}(555)$.(b) same but for the ratio $R_{rs}(485)/R_{rs}(555)$. Solid curve represents the homogeneous ocean. The spread of the data points to the left from the solid curve shows the effects non uniform *Chl(z)* profiles.

The solid line representing the homogeneous ocean in Figures 5.15 (a) and (b) has been computed from the background values of chlorophyll concentration, Chl_0, used in the simulations. The points on the left side of the solid line representing the homogeneous ocean For a given surface chlorophyll, the data points on the right corner correspond the values of *Chl(z)* that has been superimposed on this surface chlorophyll concentration using different values of z_{max}, h and σ. The curved for OC2 and OC4 have been calculated for the background chlorophyll concentrations used. It can be seen that the general slope of the solid curve differs from those of OC4 and OC2. This

shows that there are some differences in the surface *Chl*-versus-reflectance ratio relationships between the database of the OC4 and OC2 algorithms and that of the Monte Carlo simulations. This cause may lie in the fact that the Monte Carlo computations simulated in a specific range of conditions that was not as broad as that concerning the OC4 and OC2 algorithm development.

Despite these differences from the above graphs, it can be seen that most of the data points for the inhomogenous chlorophyll profiles from the Monte Carlo simulation lie on the left hand side of the OC4 and OC2 curves. This illustrates that the application of OC4 or OC2 when the nonuniform *Chl(z)* profile influences the reflectance ratio can lead to a sizeable overestimation in the algorithm derived surface *Chl*. This inconsistency associated with correlating the surface value of *Chl* with reflectance values that depend on the vertical structure of inherent optical properties will continue to produce errors in the estimation of surface chlorophyll from the existing ocean colour algorithms.

5.4 Applying inverse modelling to homogeneous and inhomogeneous water columns

In remote sensing, the accurate retrieval of the absorption and backscattering coefficients is very important. This is because, when combined with the downwelling light from the sun and the sky, these coefficients help in determining the appearance of water colour (normally measured from the remote sensing reflectance). Because these inherent optical properties are

directly linked to the constituents on the water, their values can be employed to determine the type of water, turbidity, pigment concentration etc.

The previous work done showed how the reflectance of a stratified ocean (modelled using a Gaussian curve) differed from that of a homogeneous ocean. In this section, a multi band quasi analytical algorithm, QAA, (described fully in appendix B) developed for the retrieval of absorption and backscattering coefficients will be made use of. The purpose here is to analyse how the properties of a stratified water column, distributed over different depths contribute to the overall reflectance and how they compare with their retrieved values. The work done will focus on both homogeneous and inhomogeneous water columns. The multiband quasi analytical algorithm was developed for the retrieval of absorption and backscattering coefficients, as well as absorption coefficient of phytoplankton and gelbstoff. The algorithm here is based on relationships between remote sensing reflectance and inherent optical properties of the water derived from the radiative transfer equation. It is then seen how the retrieved values compare with the true values used in the simulations.

5.4.1 Homogeneous water column

This series of Monte Carlo simulations concerns a homogeneous water column, with the same values of the IOPs for the entire water column. The absorption and scattering coefficient of this water column was assumed to be independent of depth and were calculated using the bioptical model

explained in Chapter 2 (Section 2.8). In this case, the chlorophyll concentration, *Chl*, was varied from 0.03 to 1 mgm^{-3}. The bottom was assumed to be at a depth of 45m.

The Monte Carlo code was used to generate values for the below surface remote sensing reflectance, $r_{rs,}$ by using the bio optical models described above. Once these values were obtained, the following was derived

1. The backscattering coefficient of particles at 555nm, $b_{bp}(555)$
2. The total absorption coefficient, $a(\lambda)$
3. The combined absorption coefficient of gelbstoff and detritus at 440nm, $a_g(440)$
4. The absorption coefficient of phytoplankton pigments at 440nm , $a_\varphi(440)$
5. the spectral power for backscattering, Y

The difference between the retrieved values and those used as input is calculated as

$$RMSD = \sqrt{\frac{1}{N}\sum_{i=1}^{N}((V_{R_i} - V_{I_i})^2} \qquad 5.12$$

where

V_R is the retrieved values by the QAA

V_I is the input values and,

N is the number of points, corresponding to the different chlorophyll concentration values.

Here, V can be $b_{bp}(555)$, Y, $a(440)$, $a_g(440)$ and $a_\varphi(440)$

The linear percentage difference is given as

$$\varepsilon = 10^{RMSD_{\log 10}} - 1 \qquad 5.13$$

where $RMSD_{log10} = \{\frac{\sum_{i=1}^{N}[\log_{10}(V_{R_i}) - \log_{10}(V_{I_i})]^2}{N}\}^{\frac{1}{2}}$

The graphs (Figure 5.16) can be interpreted as follows; the x axis is representative of the input values calculated from the bio optical model and hence has been labelled [Model values used as input]. The y axis represents the QAA derived values from the subsurface reflectance values obtained from the Monte Carlo code and has been labelled as [QAA retrieved values].

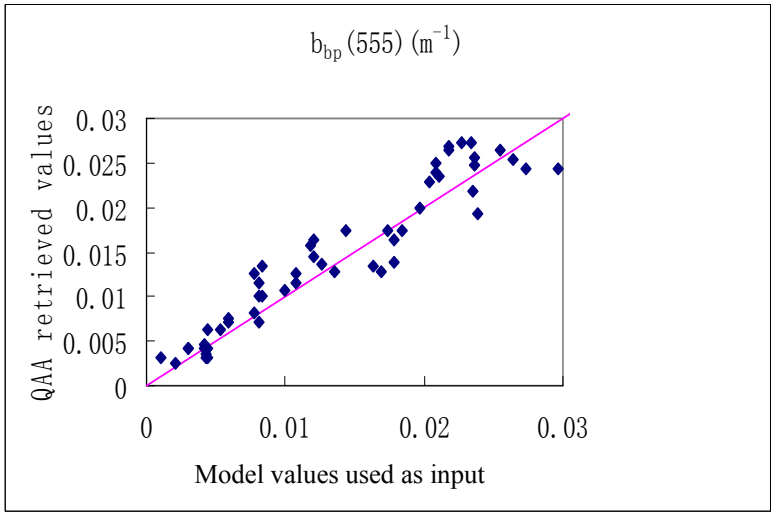

Figure 5.16(a) QAA retrieved values versus values used as input for $b_{bp}(555)$

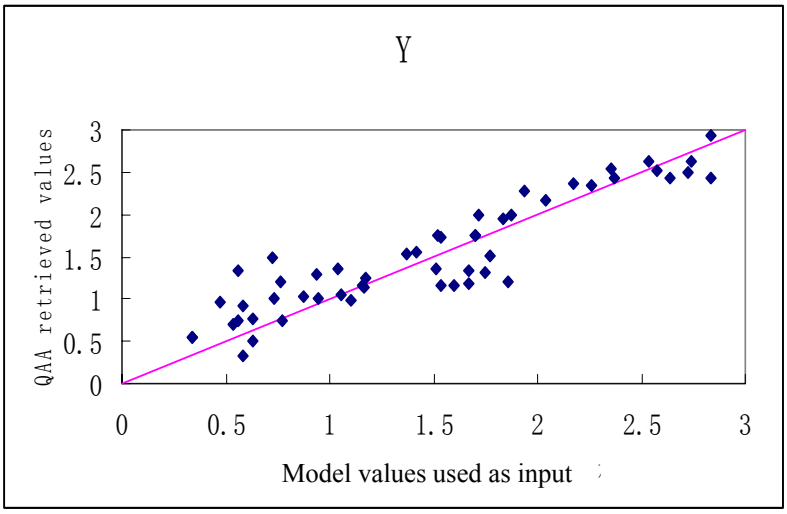

Figure 5.16(b) QAA retrieved values versus values used as input for *Y*

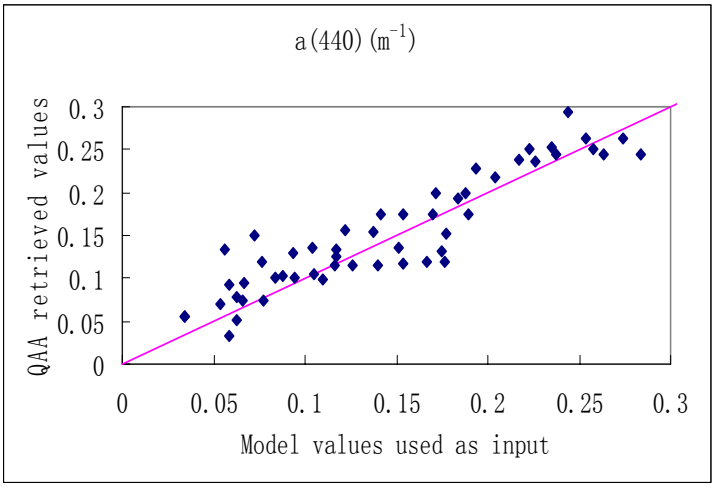

Figure 5.16(c) QAA retrieved values versus values used as input for *a(440)*

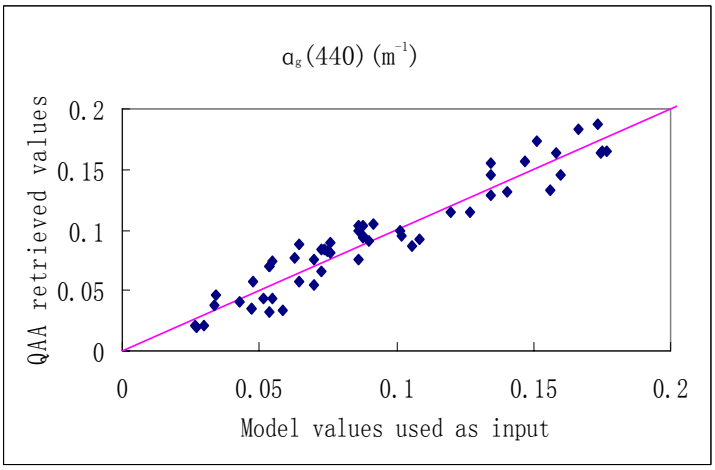

Figure 5.16(d) QAA retrieved values versus values used as input for $a_g(440)$

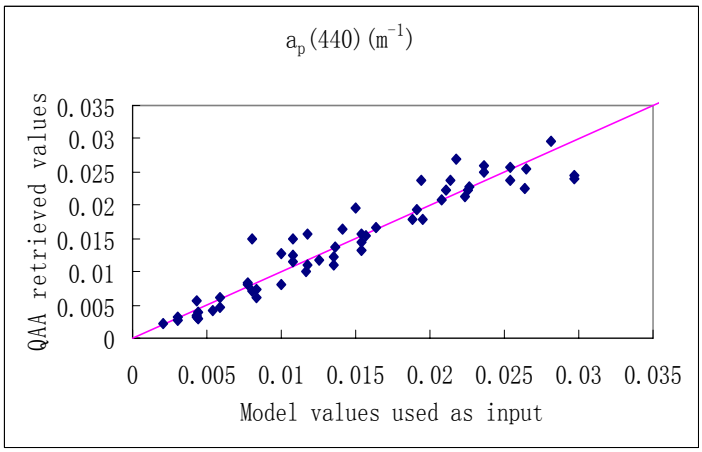

Figure 5.16(e) QAA retrieved values versus values used as input for $a_p(440)$

Figure 5.16:QAA retrieved values versus values used as input for (a)$b_{bp}(555)$, (b)Y (c) $a(440)$

(d) $a_g(440)$ and (e) $a_p(440)$

Figure 5.16(b) represents the empirically derived *Y* values versus the true values. This derivation produced quite an accurate return (ε=5.48%). Still, this property is of second order importance and hence does not affect the end result

Figure 5.16(c) shows the comparison of the retrieved absorption coefficients at 440nm with their values used as input. Clearly the *a(440)* values match their true values for the 440nm wavelength (ε=6.95%) for almost the entire data set.

For clearer waters, [$a(440) < 0.15 m^{-1}$], the retrieved $b_{bp}(555)$ values show less error and ε=7.99% for the entire data set. The errors for $a_p(440)$[ε=7.71%]and $a_g(440)$ [ε=4.95%]are slightly higher, and this can be explained by the fact that additional error is introduced when a is partitioned into a_p and a_g

The situation just examined shows that when a water body is homogeneous, the retrieved values of the optical constituents show relatively less deviation when compared to the actual values found in the water column. The QAA retrieval algorithm performs very well for homogeneous waters. However, as has been discussed in the previous chapters, that water bodies actually do show vertical inhomogeneity. Retrieval algorithms commonly used always assume that the water column being examined is of a homogeneous nature and hence cannot give any indication of the stratification present. The retrieval of optical properties from vertically stratified ocean using the same QAA will be examined in the section below.

5.4.2 Inhomogeneous water column

In this series on Monte Carlo simulations, the water column was assumed to be stratified and this stratification was included by the use of a Gaussian function to model the vertical profile of the depth dependent chlorophyll concentration, *Chl(z)* as given in equation 5.14.

The Gaussian function was modeled as

$$Chl(z) = Chl_o + Chl_1 \exp[\frac{-(z_m - z)^2}{2\sigma^2}] \qquad 5.14$$

and the values of Chl_0, Chl_1 ,z_{max} and σ are given in table 5.1

Property	**Value**
Chl_0	0.03, 0.05, 0.1, 0.2, 0.5mgm^{-3}
Chl_1	1,2,3,4,5 mgm^{-3}
z_{max}	20,25,30,35m
σ	5,6,7 mgm^{-2}

Table 5.1: C_o, C_1, z_{max} and σ employed in the simulations

Chlorophyll values shown in Table 5.1 were used to determine the vertical distributions of the inherent optical properties (IOPs) within the upper ocean. The water column was divided into several layers, all with a constant thickness of 1m and the bottom was fixed at a depth of 60m. The chlorophyll concentration was evaluated at the midpoint of each layer (using the Gaussian function for the vertical profile of chlorophyll in Equation 5.14). Once the chlorophyll concentration in each specific layer was obtained, the spectral absorption, *a(λ)*, and scattering ,*b(λ)*, coefficients for each layer, as a function of depth, were calculated. The description of the biooptical model used to

simulate the total absorption and scattering coefficients is given in Section 2.8 of Chapter 2.

The QAA retrieved values for *a(440)* and $b_{bp}(555)$ were then compared to their vertically weighted average values of the optical coefficients for the different values of z_{max} and σ. The table below each graph show the root mean square error (RMSD) and the linear error (ε) for each value of σ used.

Gordon and Clark (1980) [as discussed in Chapter 3] found that the reflectance of a stratified ocean, R_i, could be approximated with good accuracy to that of a homogenous ocean, R_h, by

$$R_i = R_h\, f(u_{av}) \quad \text{here}$$

u_{av} is the weighted average of u given by

$u_{av} = \frac{\int_0^{z_{90}} g(z)u\,dz}{\int_0^{z_{90}} g(z)\,dz}$ (similar to equation 5.4) and $u = \frac{b_b}{a + b_b}$, is the ratio of the backscattering coefficient to the sum of the backscattering and absorption coefficient.

The weighted average function is given as $g(z) = [\frac{E_d(z)}{E_d(0)}]^2$. They suggested that u_{av} could be computed from the weighted valued of Chl_i defined by

$$< Chl_i >= \frac{\int_0^{z_{90}} g(z)Chl_i(z)\,dz}{\int_0^{z_{90}} g(z)\,dz} \qquad 5.15$$

The table below each graph show the root mean square error (RMSD) and the linear error (ε) for each value of σ used.

(i)z_{max} =20m, σ =5, 6, 7m

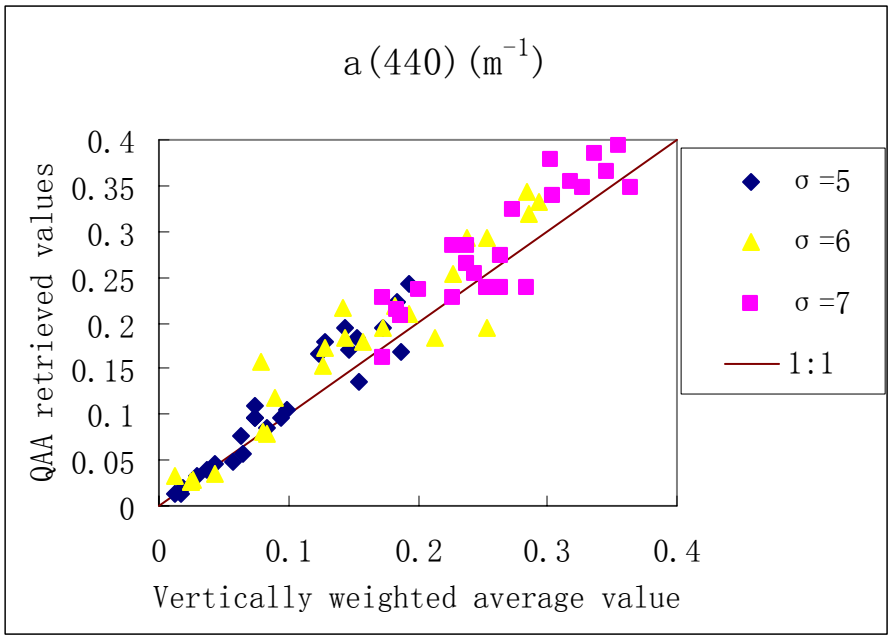

5.17(a) QAA retrieved *a(440)* values versus the vertically weighted values when z_{max}=20m

σ	5	6	7
RMSD	0.00331	0.00464	0.00491
ε	0.138	0.159	0.245

(ii) z_{max} =25m, σ =5, 6, 7m

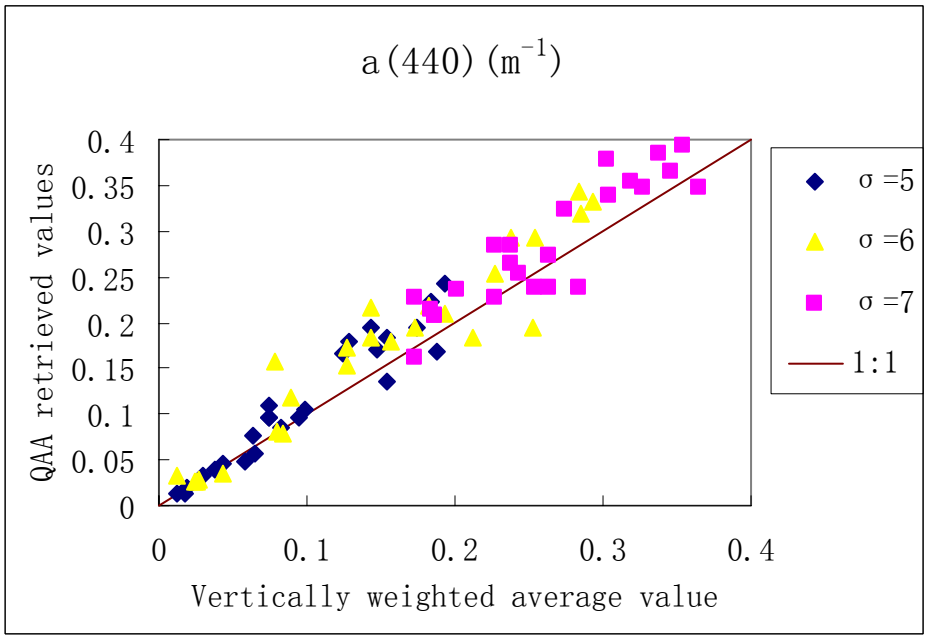

5.17(b) QAA retrieved *a(440)* values versus vertically weighted values when z_{max}=25m

σ	5	6	7
RMSD	0.00579	0.00624	0.00677
ε	0.168	0.294	0.167

(iii) z_{max} =30m, σ =5, 6,7m

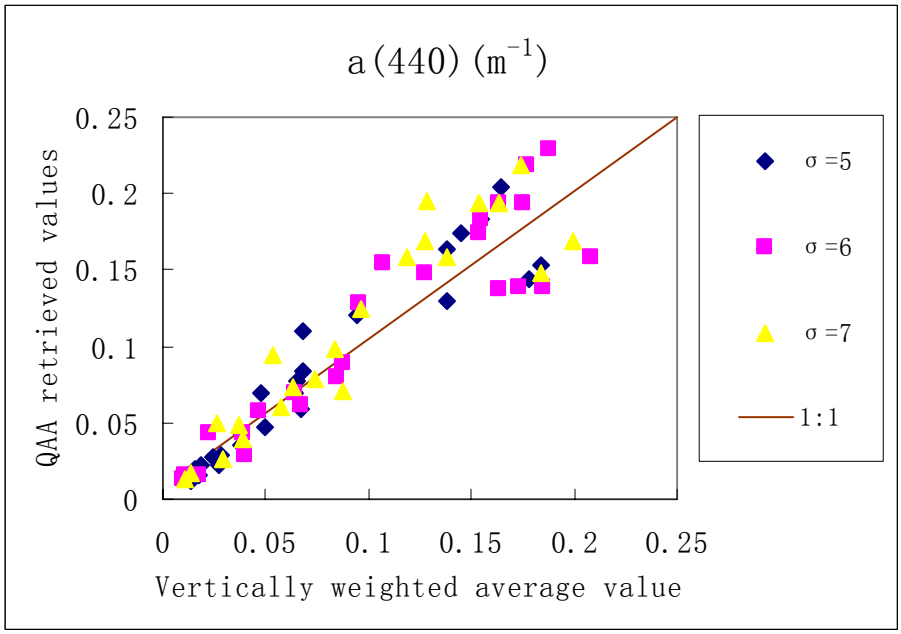

5.17(c) QAA retrieved *a(440)* values versus vertically weighted values when z_{max}=30m

σ	5	6	7
RMSD	0.00683	0.00719	0.0072
ε	0.172	0.187	0.193

(iv)z_{max} =35m, σ =5,6,7m

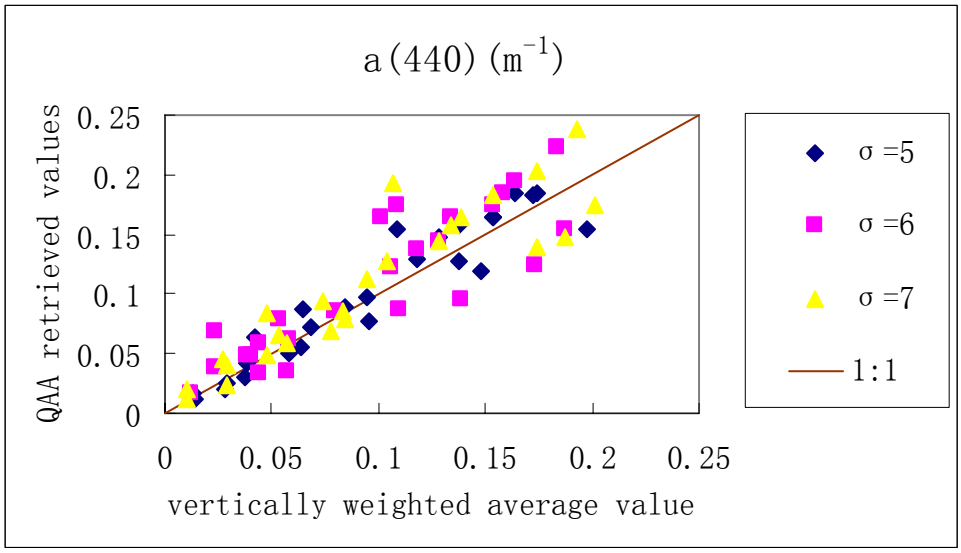

5.17(d) QAA retrieved *a(440)* values versus vertically weighted values when z_{max}=35m

σ	5	6	7
RMSD	0.0074	0.00781	0.00801
ε	0.197	0.217	0.245

Figure 5.17(a)-(d) QAA retrieved *a(440)* values versus vertically weighted values when z_{max}=20, 25,30 and 35m

The results generated here show that the QAA retrieved values have a good correlation with the vertically weighted average values. It is seen that when the chlorophyll peak is shallow (z_{max}=20m) the correlation is better and hereafter decreases as the depth of the chlorophyll peak increases. This observation was also made by Andre (1992) who stated that the influence of the vertical structure on remote sensing is more significant only when such structure is found higher in the water column.

Figure 5.17(a), 5.17(b), 5.17(c) and 5.17d) represent the QAA retrieved a(440) values versus the vertically weighted average values. As can be seen,

the correlation decreases with depth of the chlorophyll maximum with an increased error from ~13% to 24%. When σ is increased, there is an increase in the difference between the retrieved values and the input ones. In all cases considered above, the situation with the lowest value of σ showed the least deviations.

Figure 5.18(a), 5.18(b), 5.18(c) and 5.18(d) represent the QAA retrieved $b_{bp}(555)$ values the vertically weighted average values. Again it can be seen that for the correlation for the shallow water case (z_{max}=20m) is better. The correlation decreases with depth of the chlorophyll maximum with an increased error from ~11% to 27%. It can be said that the weighted average value is a good measure of the surface concentration if the location of the chlorophyll concentration peak is shallow.

(i) z_{max} =20m, σ =5,6,7m

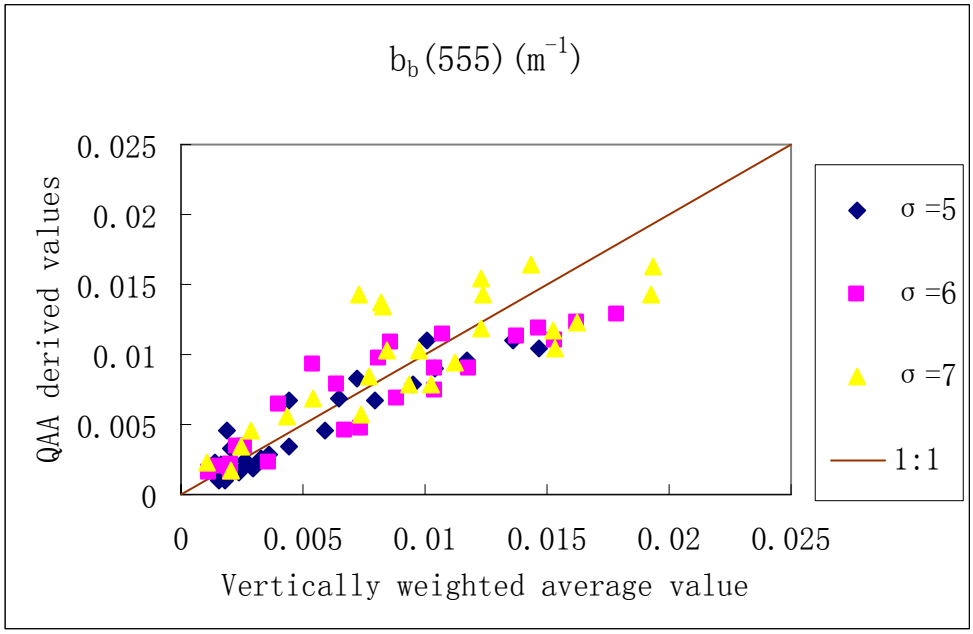

5.18 (a) QAA retrieved $b_{bp}(555)$ values versus vertically weighted values when z_{max}=20m

σ	5	6	7
RMSD	0.00308	0.00438	0.0057
ε	0. 117	0. 157	0. 16

(ii)z_{max}=25m, σ =5,6,7m

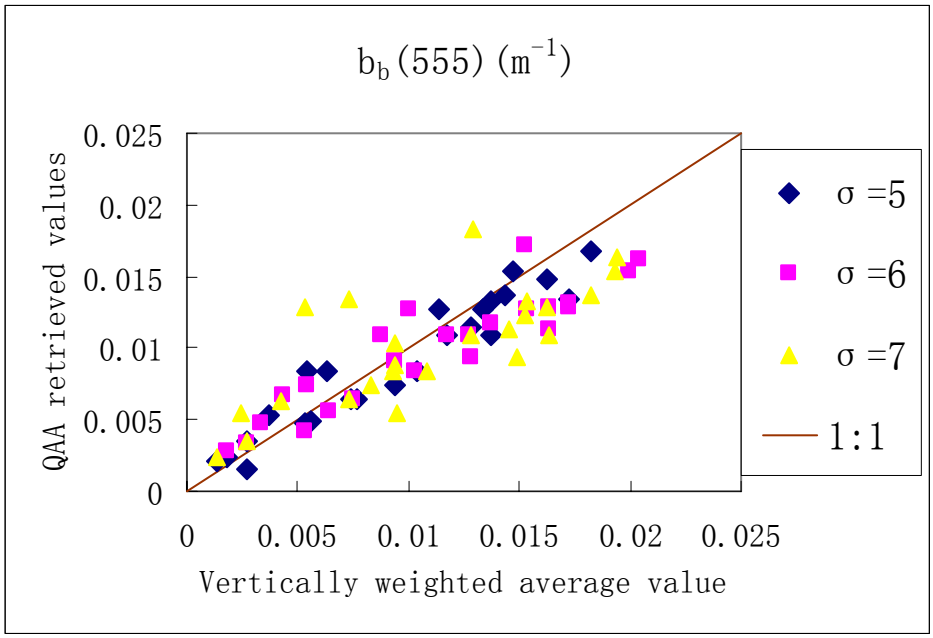

5.18(b) QAA retrieved $b_{bp}(555)$ values versus vertically weighted values when z_{max}=25m

σ	5	6	7
RMSD	0.00494	0.0058	0.00662
ε	0.248	0.273	0.295

(iii)z_{max} =30m, σ =5, 6, 7 m

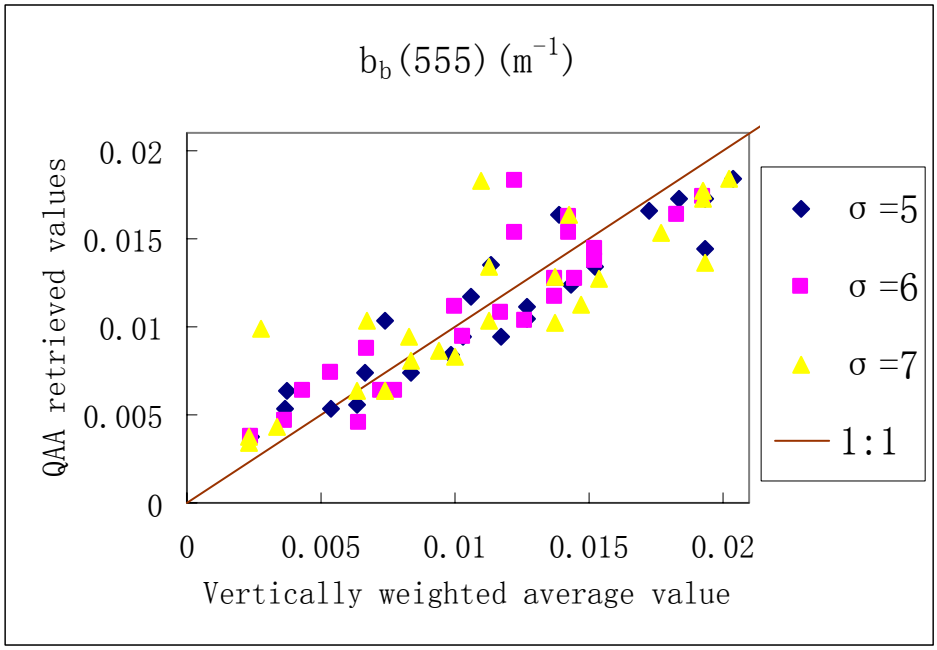

5.18(c) QAA retrieved $b_{bp}(555)$ values versus vertically weighted values when z_{max}=30m

σ	5	6	7
RMSD	0.00603	0.00663	0.0077
ε	0.167	0.1709	0.195

(iv)z_{max} =35m, σ =5,6,7m

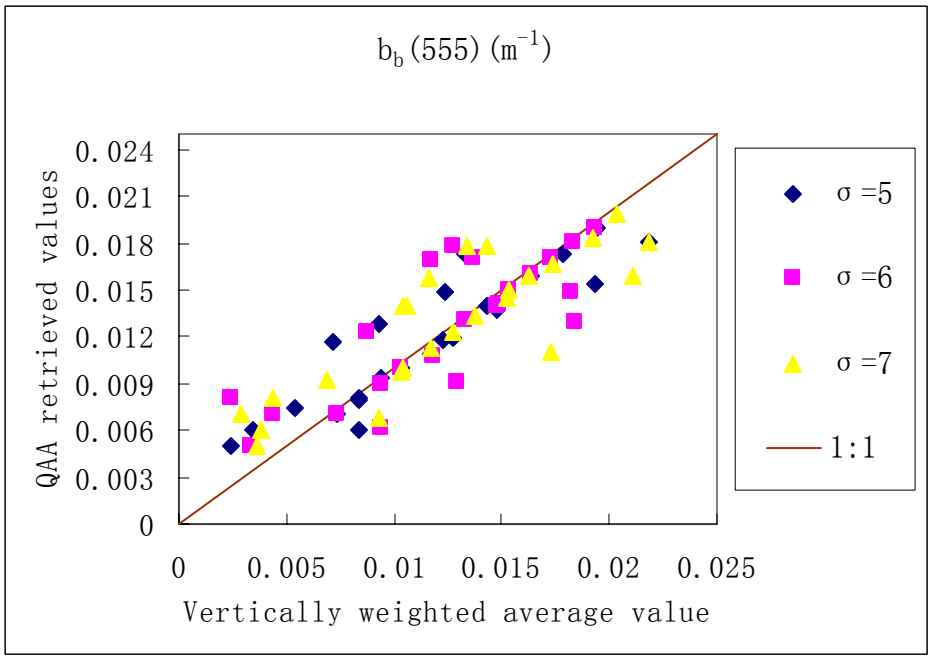

5.18(d) QAA retrieved $b_{bp}(555)$ values versus vertically weighted values when z_{max}=35m

σ	5	6	7
RMSD	0.00805	0.0085	0.0087
ε	0.247	0.269	0.273

Figure 5.18(a)-(d) QAA retrieved $b_{bp}(555)$ values versus vertically weighted values when z_{max}=20, 25,30 and 35m

5.5 Influence of nonuniform pigment profile on the diffuse reflectance of the ocean

In this section, it is seen how the reflectance of a stratified ocean, R_i, compares with the reflectance of a hypothetical homogeneous ocean, R_h, having a pigment concentration $<Chl>$, which is the weighted average of the actual depth varying concentration $Chl(z)$.

Gordon and Clark (1980) [as discussed in Chapter 3] found that the reflectance of a stratified ocean, R_i, could be approximated with good accuracy to that of a homogenous ocean, R_h, by

$$R_i = R_h f(u_{av}) \quad \text{where}$$

u_{av} is the weighted average of u given in equation 5.4.

The weighted average function is given as $g(z) = [\frac{E_d(z)}{E_d(0)}]^2$. u_{av} could be computed from the weighted valued of Chl_i defined by $< Chl_i >= \frac{\int_0^{z_{90}} g(z) Chl_i(z) dz}{\int_0^{z_{90}} g(z) dz}$ and the reflectance of a stratified ocean was expected to be equivalent to that of a homogeneous ocean with $Chl_i = <Chl_i>$ for all i.

Chlorophyll profiles were once again used to determine the vertical distributions of the IOPs within the upper ocean and for the calculation of the spectral absorption *a(λ)* and scattering *b(λ)*, as a function of depth. The bio optical model described in Chapter 2(Section 2.6) was again employed here. The profiles of chlorophyll concentrarion characteristics of the actual variation in the ocean is given as

$$Chl(z) = Chl_0 + Chl_1 \exp[-\frac{1}{2}(\frac{z - z_{\max}}{\sigma})]^2 \qquad 5.16$$

The water column was divided into several layers, all with a constant thickness of 1m and the bottom was assigned a depth of 60m. The chlorophyll concentration was evaluated at the midpoint of each layer (using the Gaussian function for the vertical profile of chlorophyll in Equation 5.16). Once the chlorophyll concentration in each specific layer was obtained, the spectral absorption, *a(λ)*, and scattering ,*b(λ),* coefficients, as a function of depth, were calculated. The IOPs at 440 and 550 nm were then used with the Monte Carlo code to compute the reflectance *R* just beneath the surface. This is R_i for a given stratification. The total accumulated photon flux that that passes each depth marker (at every 1m in this case) in the downward direction is taken to be a measure of E_d, from which the weighted average function, *g(z)* and hence the <*Chl*> was computed. Then computations for the homogeneous case (the whole water column has the same set of IOPs) were carried out with each <*Chl*>, to give the reflectance of a hypothetical homogenous ocean, R_h.

It was suggested by Kitchen and Zaneveld (1990) that the vertical profile of backscattering b_b does not covary with the pigment concentration in

the open ocean. This was based on their observation that the depths of chlorophyll a maximum and that of particle maximum are often separated by tens of meters (experiment carried out in the Pacific Central Gyre). They argued that the chlorophyll maximum is due to an increase in the quantity of chlorophyll a in the individual plankton cells and not in the concentration of cells. They applied scattering theory for spherical particles to measured particle size distributions and concluded that the absorption coefficient at depth z should covary with the pigment concentration in a similar way as it does near the surface. In 1980, Gordon and Clark hypothesised that in many cases, the backscattering coefficient is constant down to the bottom of the mixed layer, increases slightly in the particle maximum and decreases slowly through the chlorophyll maximum

Therefore, for the study of the comparison of the reflectance of a stratified ocean and a hypothetical homogeneous ocean, the two following scenarios will be considered; in the first case, both the particle absorption and backscattering coefficients are allowed to vary with *Chl(z)* and in the second scenario, only the particle absorption coefficient is allowed to vary with *Chl(z)*. In the second case thus, the particle backscattering coefficient is made independent of depth and is calculated from the background chlorophyll concentration, Chl_o(in Tables 5.2 and 5.3), in each run.

5.5.1 Case 1: Water column with deep stratification.

The first case considered is that where the depth of the chlorophyll

maximum, $z_{max,}$ is greater than 10m. The values of $z_{max,}$ $Chl_{0,}$ Chl_{1} and σ employed are given in Table 5.2

Chl_0	0.05,0.1,0.5,1 mgm^{-3}
Chl_1	2,4,7 mgm^{-3}
σ	8m
z_{max}	17,25,30m

Table 5.2 Values of $Chl_{0,}$ $Chl_{1,}$ z_{max} and σ used in simulations

Computations of R_h and R_i were carried out at 440 and 550nm. The values of R_h and R_i are then plotted against one another and the values of R_i are also plotted against <*Chl*>.

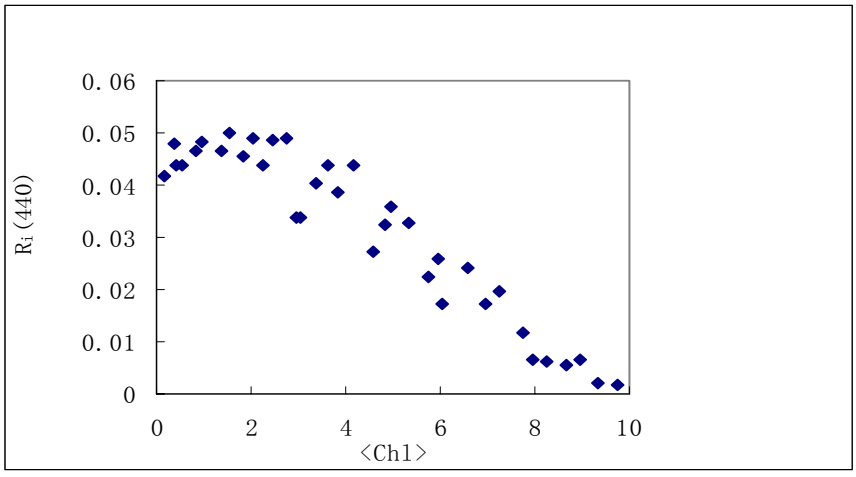

(a)

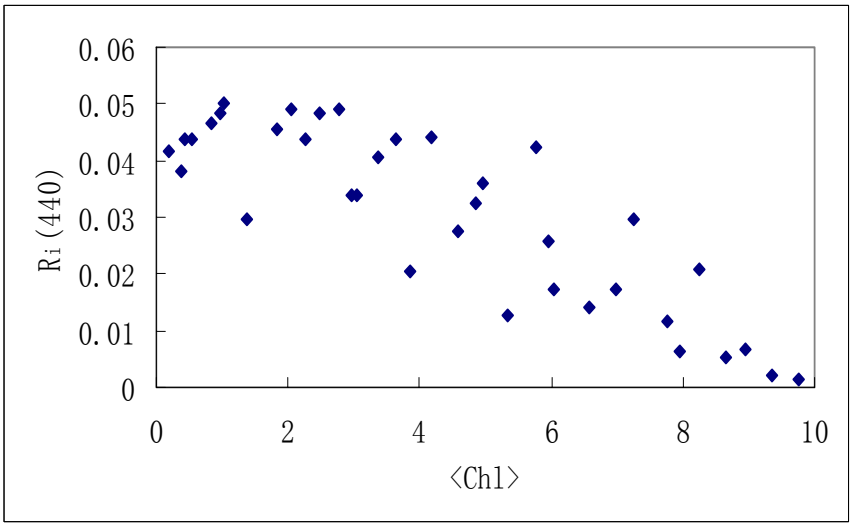

(b)

Figure 5.19; comparison between R_i at 440 nm computed for a stratified ocean with a weighted pigment concentration <*Chl*> (a) both *a* and *b* covary with *Ch(z)*;(b) *a* covaries with *Chl(z)* but *b* is independent of z

The absorption of chlorophyll is characterized by strong absorption at 430nm and 665nm. Therefore from Figure 5.19 (a) it can be seen that at 440nm, there are less deviations when both *a* and *b* covary with *Chl(z)*. However, in accordance with the Kitchen and Zaneveld theory, the computations in the case where b is independent of *Chl(z)*, more deviations are seen.

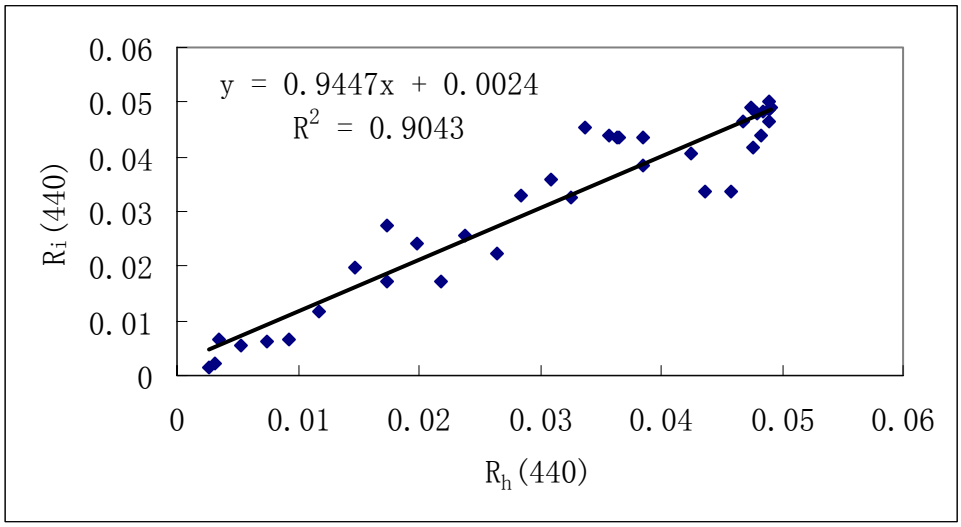

Figure 5.20(a) Comparison between R_i and R_h at 440 nm computed for a stratified ocean with a weighted pigment concentration <*Chl*> and that of a uniform ocean with *Chl*=<*Chl*> when both a and b covary with *Chl(z)*.

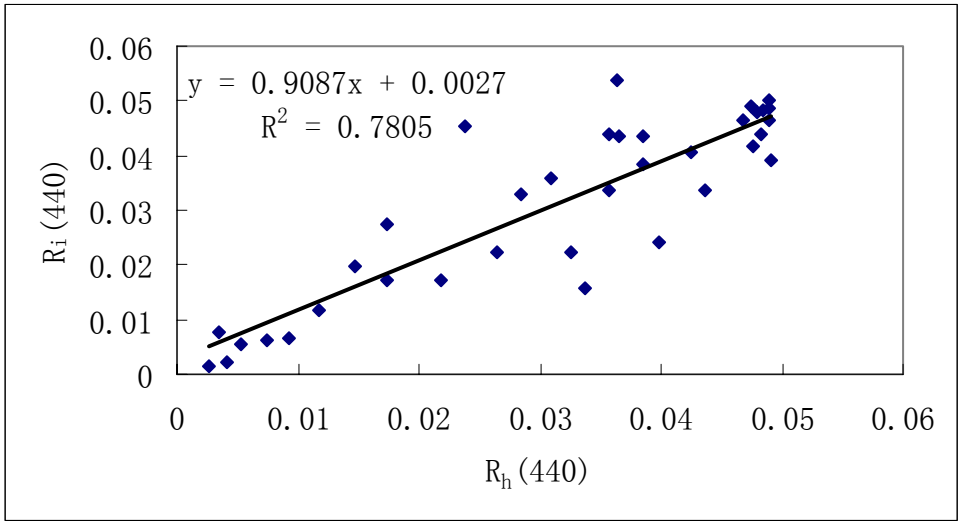

Figure 5.20(b) Comparison between R_i and R_h at 440 nm computed for a stratified ocean with a weighted pigment concentration <Chl> and that of a uniform ocean with *Chl*=<*Chl*>when a covaries with *Chl(z)* but *b* is independent of z

Figure 5.20(a)-(b) Comparison between R_i and R_h at 440 nm computed for a stratified ocean with a weighted pigment concentration <*Chl*> and that of a uniform ocean with *Chl*=<*Chl*>.(a) both *a* and *b* covary with *Chl(z)*;(b) *a* covaries with *Chl(z)* but *b* is independent of z

The resulting comparisons between R_i and R_h shown in Figure 5.20 (a) indicates that the reflection of a stratified ocean is to an excellent approximation identical to that of a homogeneous ocean with pigment concentration <*Chl*>. In graph 5.20(b), the absorption coefficient is allowed to vary with *Chl(z)* while the scattering coefficient is taken to be independent of depth and is provided by the surface pigment concentration. It is seen that deviations from the Gordon and Clark hypothesis begin to appear.

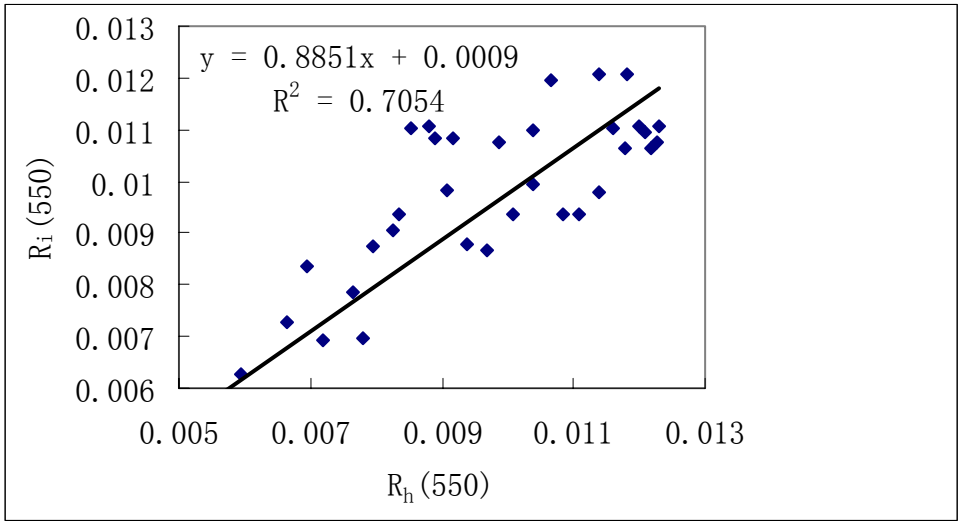

(a)

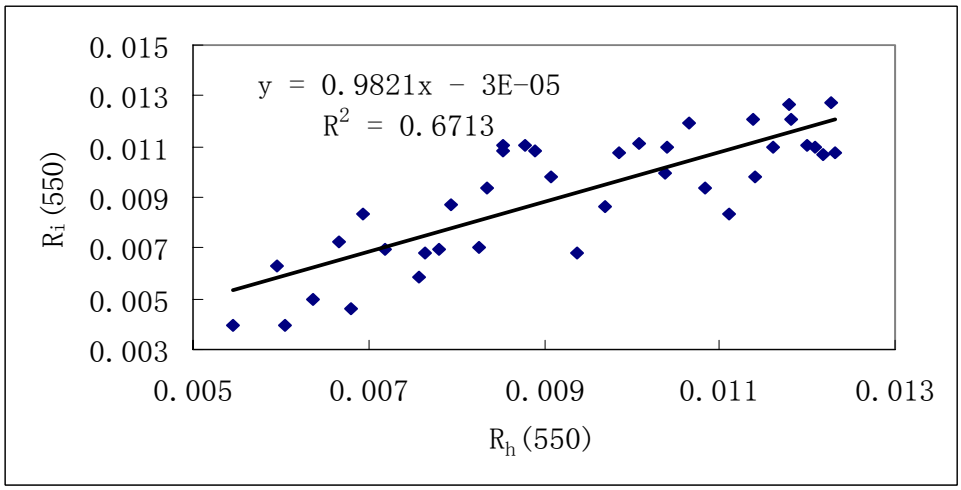

(b)

Figure 5.21(a)-(b); comparison between R_i and R_h at 550 nm computed for a stratified ocean with a weighted pigment concentration <Chl> and that of a uniform ocean with *Chl*=<*Chl*>.(a) both *a* and *b* covary with *Chl(z)*;(b) *a* covaries with *Chl(z)* but *b* is independent of z

Between 550nm and 650nm, there is relatively little absorption by chlorophyll and the absorption minimum near 600nm~10 to 30% of the value at 440nm. Hence, the comparisons between R_i and R_h shows a lesser degree of correlation as opposed to the case where the comparison was done at 440nm. Figures 5.20(a) and 5.21(a) suggest that for the model in which both *a* and *b* covary with *Chl(z)*, the reflectance ratio at 440 and 550nm, $R_i(440)$ and

$R_i(550)$, will not be influenced by the vertical profile of *Chl*. In contrast, when *b* is constant and not correlated with *Chl(z)*, Figures 5.20 (b) and 5.21(b) have shown the differences in $R_i(440)$ and $R_i(550)$, indicating that the reflectance ratio will depend on the vertical profile of *Chl*. Computations of $R_i(440)/R_i(550)$ for this case(*b* independent of depth) as functions of the weighted pigment concentration were carried out with the weighting function *g(z)* determined at 440nm. The results in Figure 5.22 show that the influence of stratification on the reflectance ratio is small and this can be explained by the fact that when *R* is directly proportional to *b* and when *b* is not dependent on z and is << *a*, it will tend to cancel out.

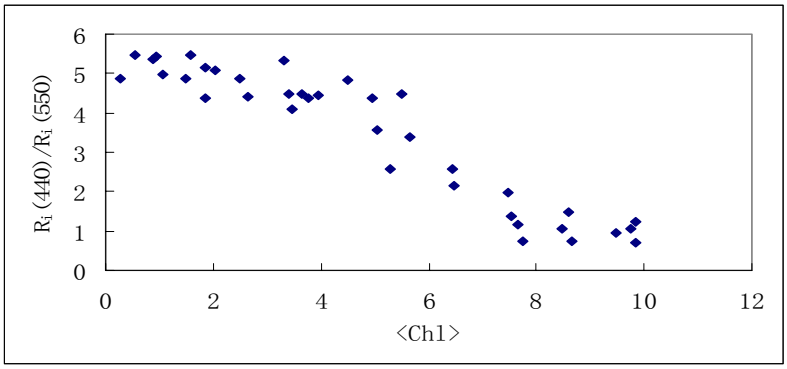

Figure 5.22 Ratio $R_i(440)/R_i(550)$ as a function of <*Chl*> evaluated at 440nm for *b* is independent of *Chl(z)*

5.5.2 Case 2: Water column with shallow stratification.

So far, the situations applicable to open oceans have been studied. This section deals with cases having shallow stratifications i.e z_{max} < 10m. The stratification model is the same one used earlier. The new parameters were selected so that the maximum value of *Chl(z)* was near the surface as shown in Table 5.3

Chl_o	0.05,0.1,0.5,1 mgm^{-3}
Chl_1	2,4,7 mgm^{-3}
σ	2m
z_{max}	5,7,9m

Table 5.3 Values of Chl_o, Chl_1, z_{max} and σ used in the simulation

These situations are quite unrealistic in nature and it would be unusual to find them in open ocean waters. In real life it is difficult to get such kind of situations because of the presence of vertical mixing caused by wind due to wind action.

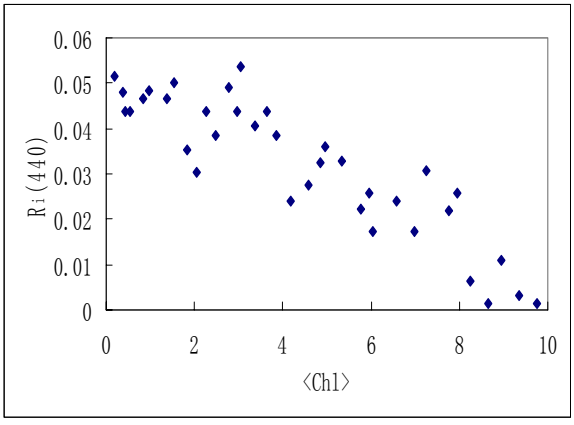

(a)

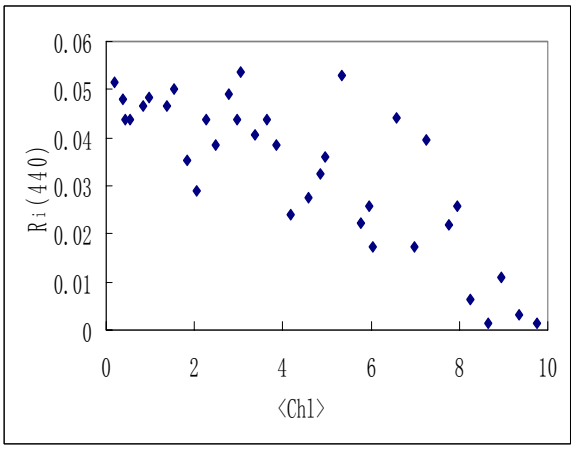

(b)

Figure 5.23; comparison between R_i at 440 nm computed for a stratified ocean with a weighted pigment concentration <*Chl*> (a) both *a* and *b* covary with <*Chl*>;(b) *a* covaries with *Chl(z)* but *b* is independent of z

When both *a* and *b* covary with *Chl(z)*, from Figure 5.23 (a), it can be seen that there are less deviations than when only a covaries with *Chl(z)*, for nearly the whole pigment range. It is similar to the results that were obtained in the case of deeper stratification (z_{max} > 10m) for the same wavelength.

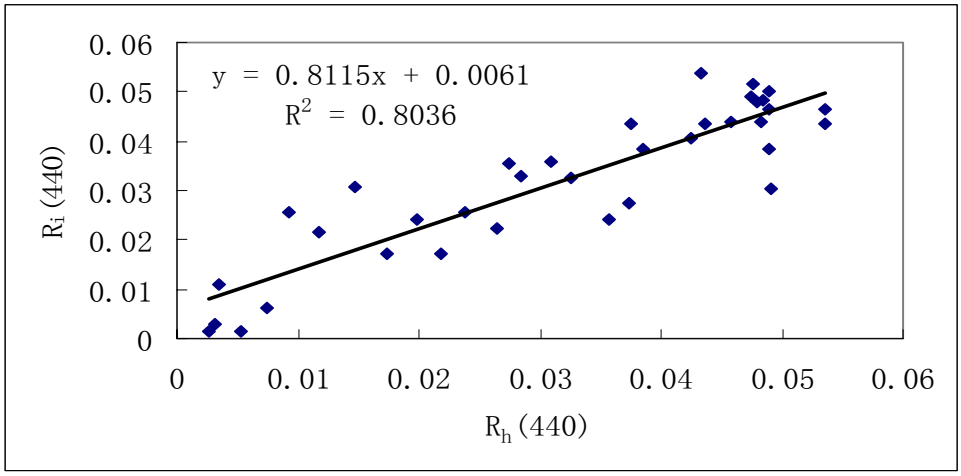

(a)

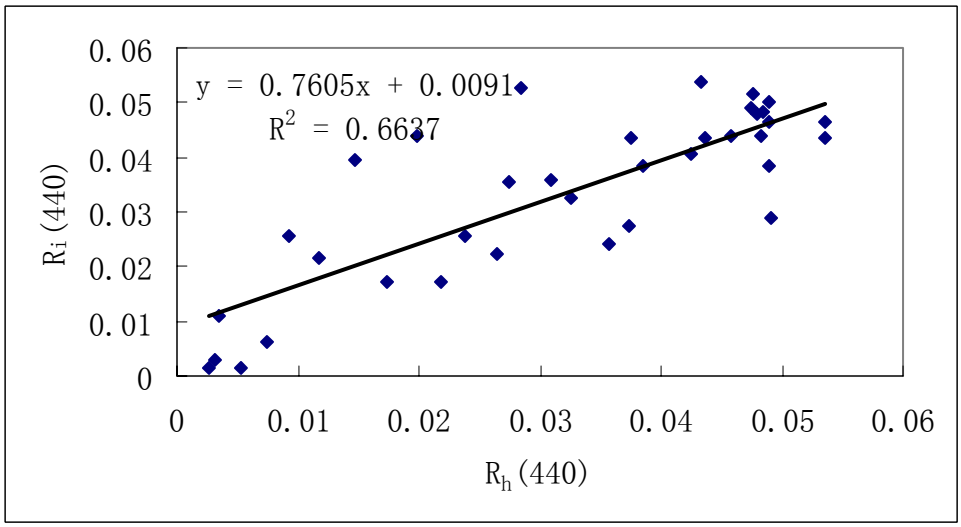

(b)

Figure 5.24(a)-(b); Comparison between *Ri* and R_h at 440 nm computed for a stratified ocean with a weighted pigment concentration <*Chl*> and that of a uniform ocean with *Chl*=<*Chl*>.(a) both *a* and *b* covary with *Chl(z)*;(b) *a* covaries with *Chl(z)* but *b* is independent of z

From Figure 5.24(a) it is seen that at 440nm, R_i agrees well with R_h in the case where *a* and *b* covary with *Chl(z)* but the correlation decreases in the case where only *a* covaries with *Chl(z)*.However in both cases, the correlation is less than for the cases examined with $z_{max} > 10$m

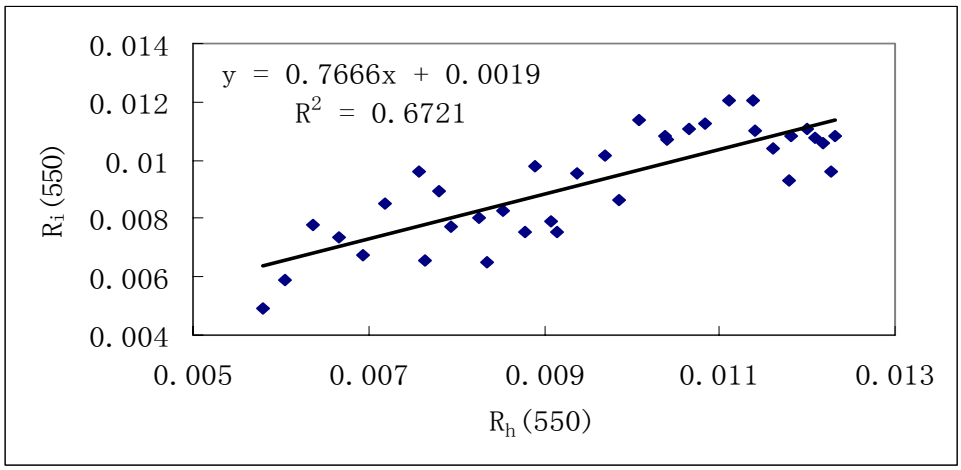

(a)

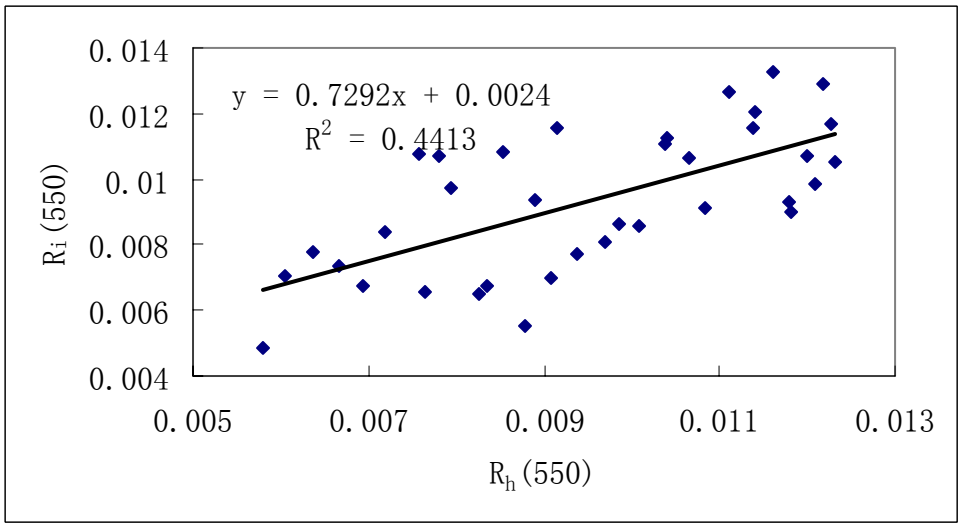

(b)

Figure 5.25; Comparison between R_i and R_h at 550 nm computed for a stratified ocean with a weighted pigment concentration <*Chl*> and that of a uniform ocean with *Chl*=<*Chl*>.(a) both *a* and *b* covary with <*Chl*>;(b) *a* covaries with *Chl(z)* but *b* is independent of z

It was observed that the largest differences between R_i and R_h at 550nm

occurred in situations with this subsurface maxima in *Chl(z)* ,example at z_{max}=2m. For the situation in which b is independent of depth (Figure 5.25b), the low correlation suggests that Gordon and Clark's hypothesis provide little explanation of the variance of *R*. This is understandable. The IOPs in this case depend on two variables, the background chlorophyll concentration Chl_o which determined *b* and *Chl(z)* which determines *a(z)*. Then, because the *Chl(z)* maximum is near the surface, these quantities are essentially independent over the relevant depths and the reflectance depends strongly on them.

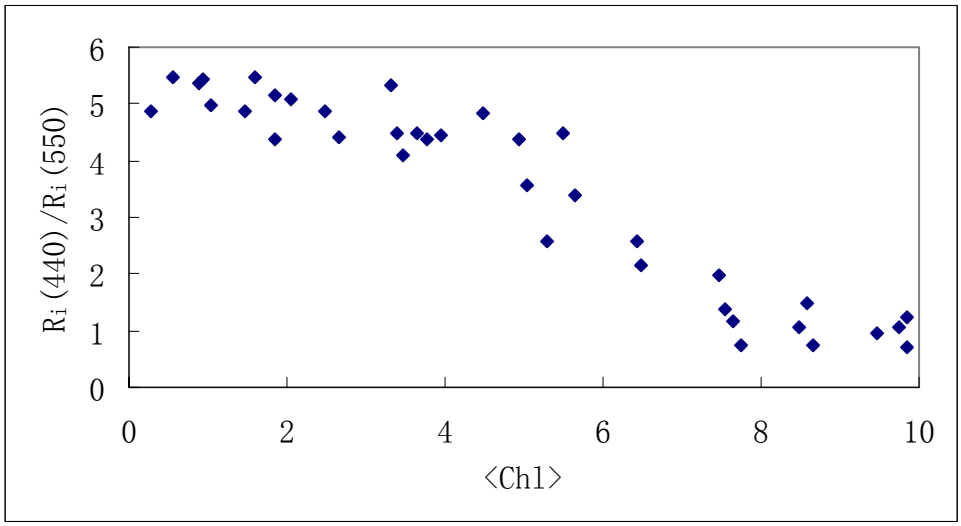

Figure 5.26 Ratio *Ri(440)/Ri(550)* as a function of <*Chl*> evaluated at 440nm for b_p is independent of *Chl(z)*

For the case in which *b* does not covary with depth at 550nm, it can be said that the results obtained look quite similar to the case examined at 440nm, indicating that the reflectance ratio of independent of the chlorophyll profile.

The Gordon and Clark hypothesis regarding the reflectance of a stratified ocean i.e. $R_i[C(Z)]=R_h(<C>)$ has been reviewed here. The results suggest that the hypothesis works well when both *a* and *b* covary with *Chl(z)*.

But when a model of vertical stratification of the IOP's that more closely follow the Kitchen and Zaneveld(1990) is used[a(z) covaries with *Chl(z)* but *b* is independent of *Chl(z)*], more deviations were observed between the value *R* predicted by the hypothesis and the value derived in the simulations for cases of both shallow and deep stratifications.

Chapter 6

In-situ measurements in Singapore coastal waters

6.1 Introduction

This chapter deals with the field data collected during field trips in Singapore coastal waters, in 2004. During these trips, the measurements of the inherent optical properties (backscattering coefficients) and the reflectance were carried out. The measured values of the backscattering coefficients were then used to obtain the reflectance using the Monte Carlo code and this calculated reflectance was then compared to the one obtained in situ.

The depth profiles of water backscattering and absorption coefficients are required as input to the Monte Carlo code in order to compute the water reflectance at the surface. In this study, only the backscattering profiles were available; the absorption coefficients were not measured as the equipment for in-situ measurements of absorption coefficients had not been acquired. Thus, we decided to estimate the absorption coefficient from the reflectance spectra using the QAA inversion method, with the assumption that the absorption coefficient is approximately depth independent. The measured backscattering profile and the QAA derived absorption coefficient are then used in the Monte Carlo code to compute the water reflectance for comparison with the experimentally measured reflectance.

6.2 Sampling Sites and Data Measurement

Field data collection was carried out on the 18th of June and 3rd of

August 2004 in coastal waters around Singapore. The sampling locations are shown in Figures 6.1 and 6.2.

June2004 Sampling location

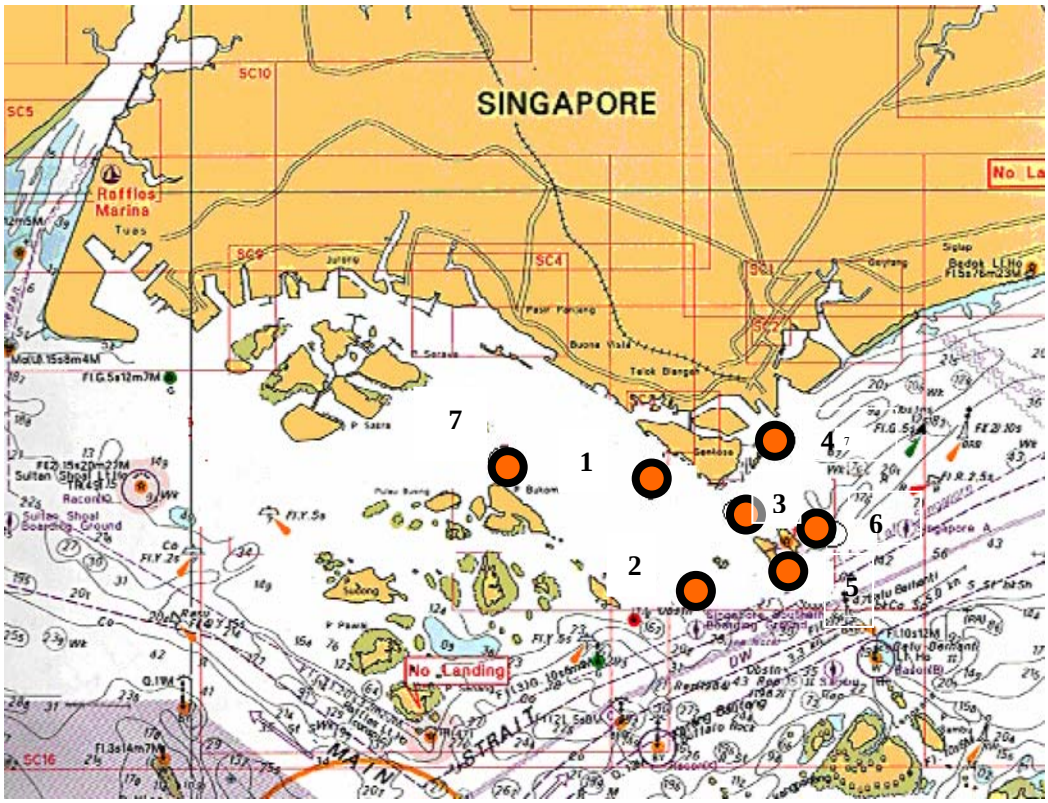

Figure 6.1 showing the 7 locations covered in June 2004, in the southern part of Singapore

August 2004

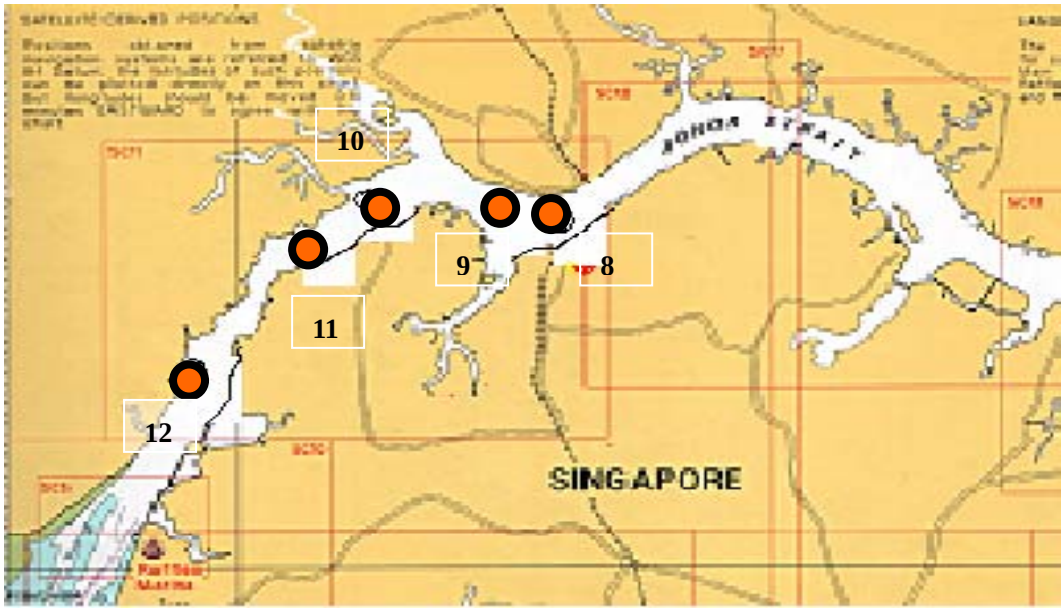

Figure 6.2 showing the 5 locations covered in August 2004, in the Johor Strait

The parameters measured at each location are

1) Water scattering coefficients at 470nm and 700nm, at several depths:1m ,3m , 5m and 7m

2) Remote sensing spectra above water surface

The backscattering coefficients are measured using a submersible backscattering meter (WetLab, model BB2BF) that measures the backscattering coefficient at 470 and 700 nm and the fluorescence of plankton.

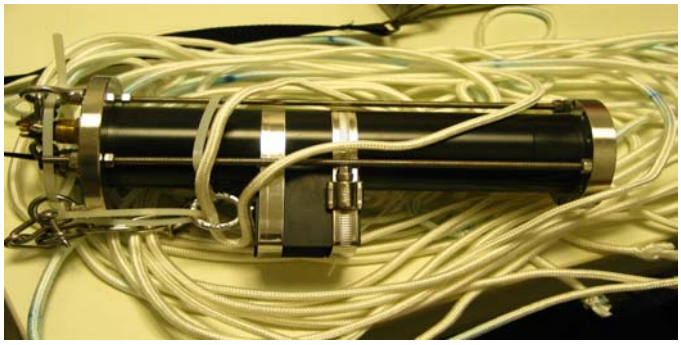

Figure 6.3 Backscattering meter

Figure 6.4 GER 1500

The wavelength dependence of $b_{bp}(\lambda)$ is normally expressed as

$$b_{bp}(\lambda) = X(\frac{\lambda_o}{\lambda})^Y \qquad 6.1$$

where λ_o is a reference wavelength, chosen to be 555nm for this study,

$X=b_{bp}(555)$, the backscattering of particulate matter at 555nm, And Y is the shape factor of the wavelength dependence of backscattering coefficient. If the values of Y and X are known or can be estimated from remote sensing measurements, then b_{bp} at any wavelength can be calculated from this equation. The measured backscattering coefficients at 470 nm and 700nm are used to derive the values of Y and X.

From equation 6.1

$$b_{bp}(470) = X(\frac{555}{470})^{Y}$$
$$b_{bp}(700) = X(\frac{555}{700})^{Y} \qquad 6.2$$

These two equations are solved simultaneously to obtain the values of Y and X by

$$Y = \frac{\ln b_{bp}(470) - \ln b_{bp}(700)}{\ln(\frac{555}{470}) - \ln(\frac{555}{700})}$$

and

$$X = b_{bp}(555) = b_{bp}(470)(\frac{470}{555})^{Y}$$

The total backscattering coefficient was then calculated by

$$b_T(\lambda) = b_{bw}(\lambda) + b_{bp}(\lambda) \qquad 6.3$$

Figures 6.5-6.8 show the values of $b_{bp}(470)$ and $b_{bp}(700)$, Y ,X measured during the boat trips dated June 2004. The data collected during the August 2004 trip are shown in Figures 6.9-6.12.

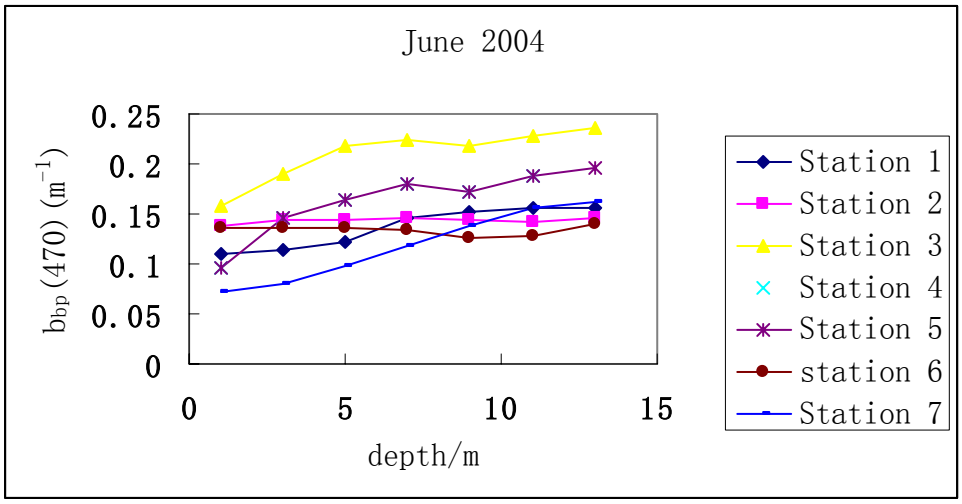

Figure 6.5. Measured b_{bp} values at 470nm versus depth

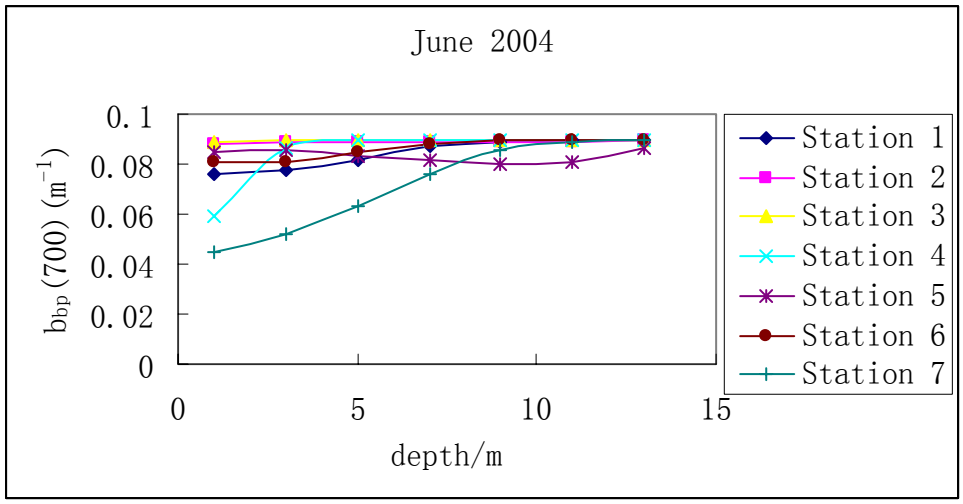

Figure 6.6 Measured b_{bp} values at 700nm versus depth

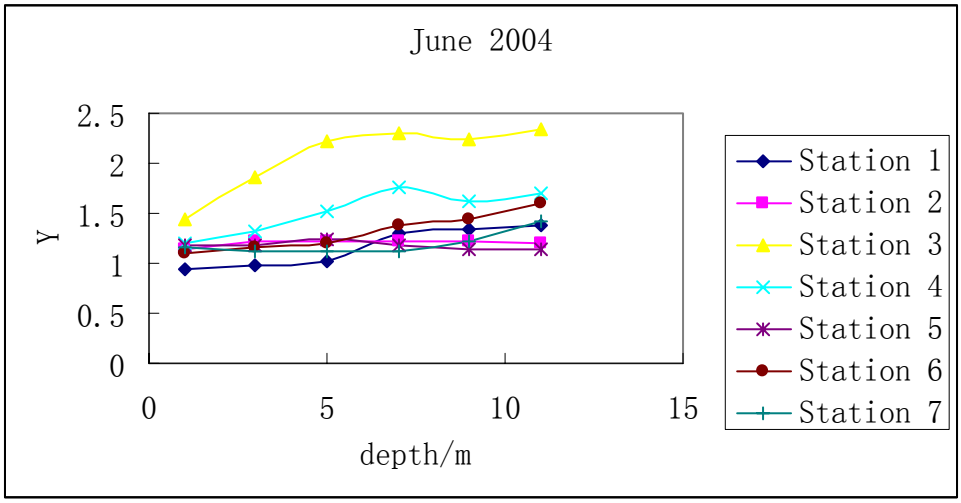

Figure 6.7 Values of Y determined from measurements of b_{bp} at 470 and 400nm, versus depth.

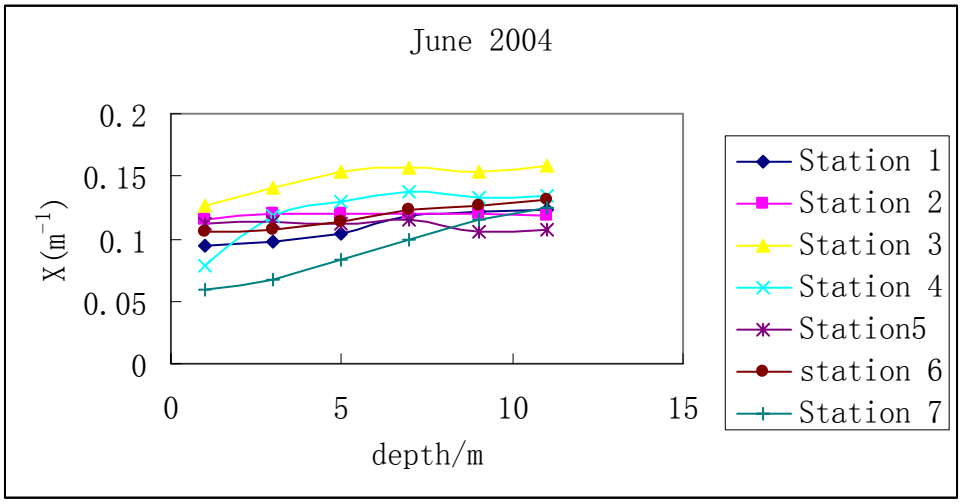

Figure 6.8 Values of X determined from measurements of b_{bp} at 470 and 400nm, versus depth.

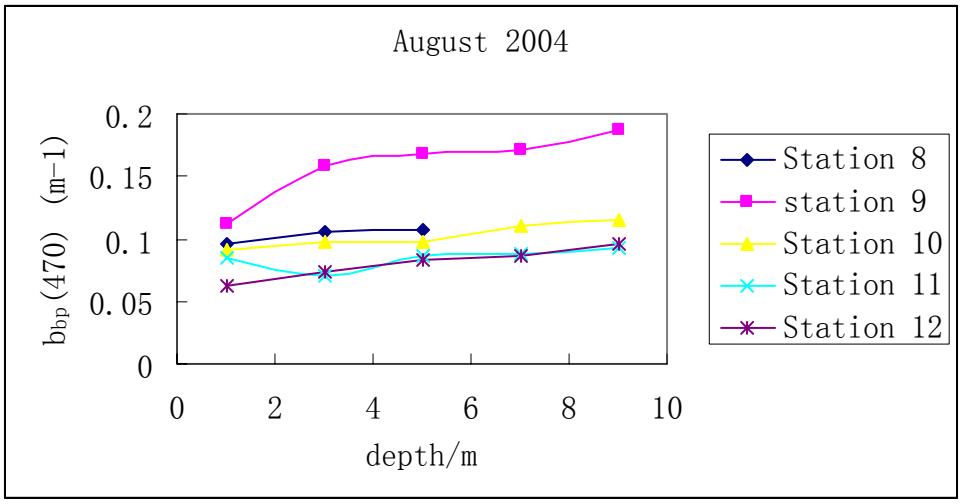

Figure 6.9 Measured b_{bp} values at 470nm versus depth

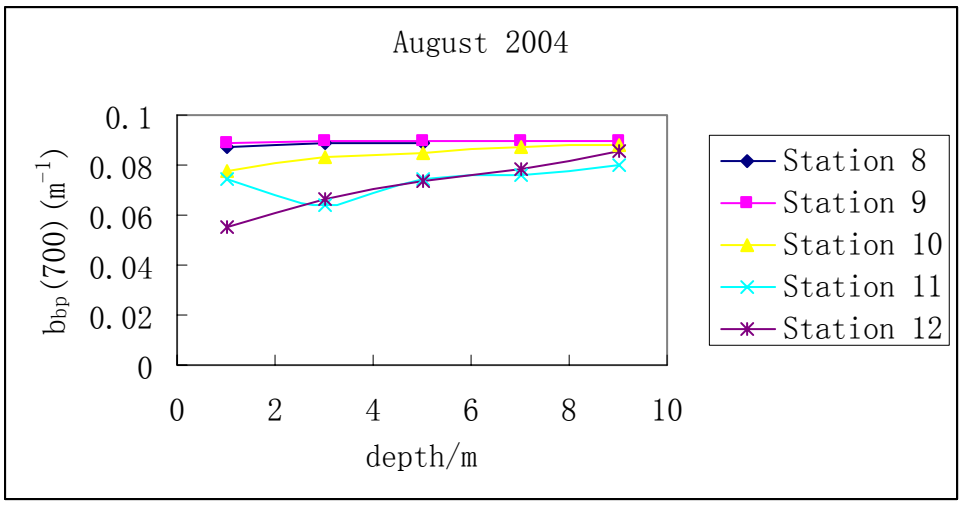

Figure 6.10 Measured b_{bp} values at 700nm versus depth

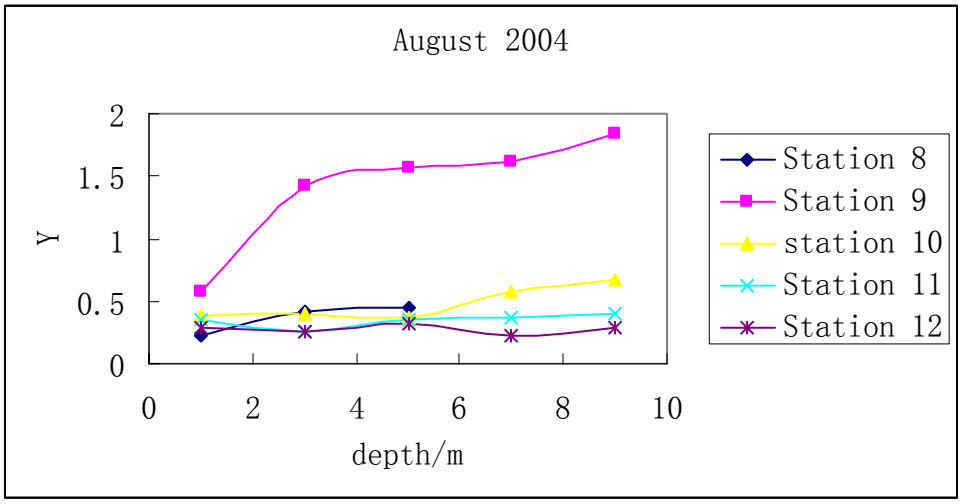

Figure 6.11 Values of *Y* determined from measurements of b_{bp} at 470 and 400nm, versus depth.

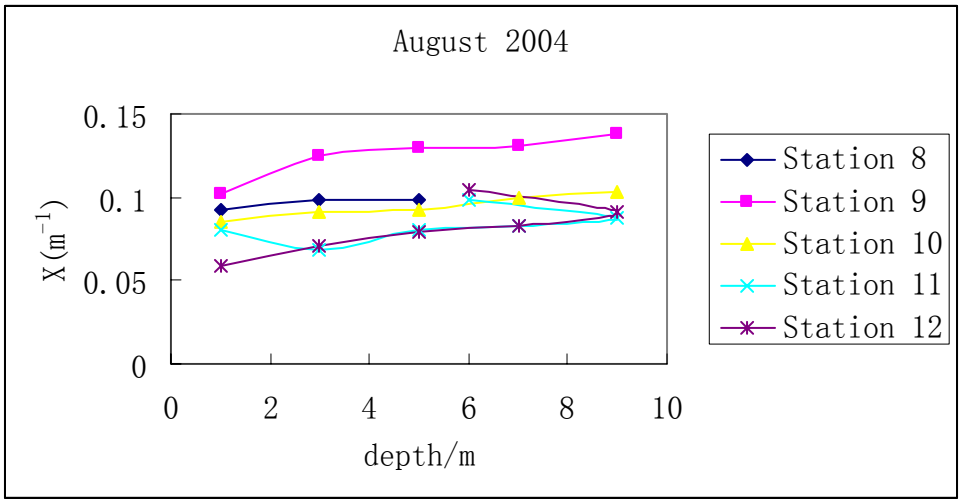

Figure 6.12 Values of *X* determined from measurements of b_{bp} at 470 and 400nm, versus depth.

A portable spectroradiometer (GER 1500) measures the water leaving radiance from 350 nm to 1000 nm. The water reflectance is calculated from the ratio of the water leaving radiance to the downwelling solar irradiance reflected off a calibrated white reference plate. Figure 6.13 shows the reflectance measured at the 12 locations covered.

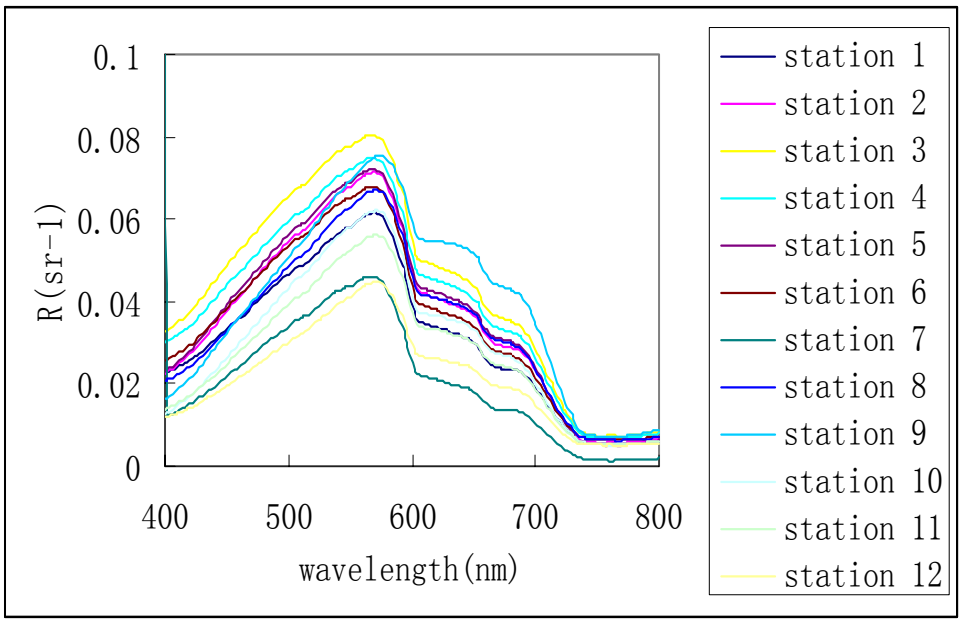

Figure 6.13 In situ reflectance for 12 stations

6.3 Estimating absorption and backscattering coefficients using QAA

The Quasi-Analytical Algorithm (QAA) (Lee et al, 2002) described earlier in Chapter 2 and Appendix B has been found to work quite well in retrieving the absorption coefficient of surface water from measured remote sensing reflectance spectra (Lee and Carder, 2004). In this section, QAA is applied to the reflectance spectra of Singapore waters to retrieve the backscattering and absorption coefficients. The retrieved backscattering coefficients will be compared with the backscattering coefficient measured at several depths below the surface. The retrieved absorption coefficient cannot be compared since there is no in-situ measurement of absorption coefficient values. Instead, the QAA retrieved absorption values are taken as the estimate of the actual values of absorption coefficient in the water and used as inputs to the Monte Carlo code, together with the measured backscattering profiles, to calculate the reflectance spectra. The calculated reflectance spectra are found

to agree well with the measured spectra.

The absorption coefficient $a(\lambda)$ at any point within a natural water body can be described in terms of the additive contribution of its components as

$$a(\lambda)=a_w(\lambda)+a_p(\lambda)+a_g(\lambda) \quad 6.4$$

where $a_w(\lambda)$, $a_p(\lambda)$, $a_g(\lambda)$ are the spectral absorption coefficients of water, particles, and soluble components, respectively. The particle absorption coefficient may be further decomposed as

$$a_p(\lambda) = a_\varphi(\lambda) + a_d(\lambda) \quad 6.5$$

where a_p and a_d are the components due to phytoplankton and detritus respectively.

The quasi-analytical algorithm (QAA) was applied to the above surface remote sensing reflectance R_{rs} that was measured in situ to provide an estimate of the total absorption coefficient, $a(\lambda)$.

This was carried out as follow

1. The measured above surface remote sensing reflectance spectra R_{rs} was converted to below surface spectra r_{rs} using the equation

$$r_{rs} = \frac{R_{rs}}{0.52+1.7R_{rs}} \quad 6.6$$

2. The value of $u = \frac{b_b}{a+b_b}$ are calculated by

$$u(\lambda) = \frac{-g_0 + [(g_0)^2 + 4g_1 r_{rs}(\lambda)]^{\frac{1}{2}}}{2g_1} \quad 6.7$$

using the relation $r_{rs} = g_0 u + g_1 u^2$, and the values of g_o and g_1 are 0.084 and 0.17 respectively.

3. The value of $a(555)$ is obtained via the following steps:

$$\text{(a)}\quad \rho = \ln[\frac{r_{rs}(440)}{r_{rs}(555)}] \qquad 6.8$$

$$\text{(b)}\ a(440)_i = \exp(-2-1.4\rho+0.2\rho^2) \qquad 6.9$$

$$\text{(c)}\ a(555) = 0.0596 + 0.2[a(440)_i - 0.01] \qquad 6.10$$

4. $b_{bp}\ (555)$ is calculated from $r_{rs}(555)$ and $a(555)$ on the basis of

$$\text{(i)}\ b_b = (\frac{ua}{1-u}) \qquad 6.11$$

and

$$\text{(ii)}\ b_{bp}(555) = (\frac{u(555)a(555)}{1-u(555)}) - b_w(555) \qquad 6.12$$

5. this step estimates the shape factor of the wavelength dependence of the particle backscattering coefficient i.e. the value of Y in the following equation,

$$\text{(i)}\quad b_{bp}(\lambda) = b_{bp}(\lambda 0)\frac{\lambda_0}{\lambda} \qquad 6.13$$

$$\text{(ii)}\quad Y = 2.2\{1-1.2[\frac{-0.9r_{rs}(440)}{r_{rs}(555)}]\} \qquad 6.14$$

6. the particle backscattering coefficient at other wavelengths are computed given the value of Y and $b_{bp}\ (555)$

$$\text{(i)}\quad b_{bp}(\lambda) = b_{bp}(555)(\frac{555}{\lambda})^Y \qquad 6.15$$

7.given the values of $u(\lambda)$ and $b_{bp}\ (\lambda)$, $a(\lambda)$ is calculated as follows

$$\text{(i)}\ a(\lambda) = \frac{\{[1-u(\lambda)][b_{bw}(\lambda)+b_{bp}(\lambda)]\}}{u(\lambda)} \qquad 6.16$$

The model described above is then used for the retrieval of the absorption and backscattering coefficients of the surface water in the range of 400-740 nm.

Figures 6.14 and 6.15 show the estimated total absorption coefficients

at 440nm and 555nm for the 12 locations.

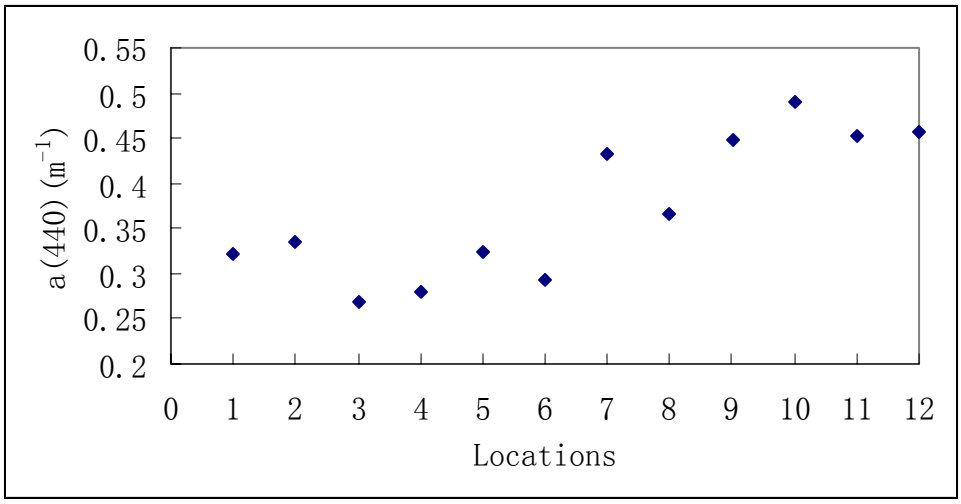

Figure 6.14 Total absorption coefficients at 440nm for 12 locations covered in June and August 2004

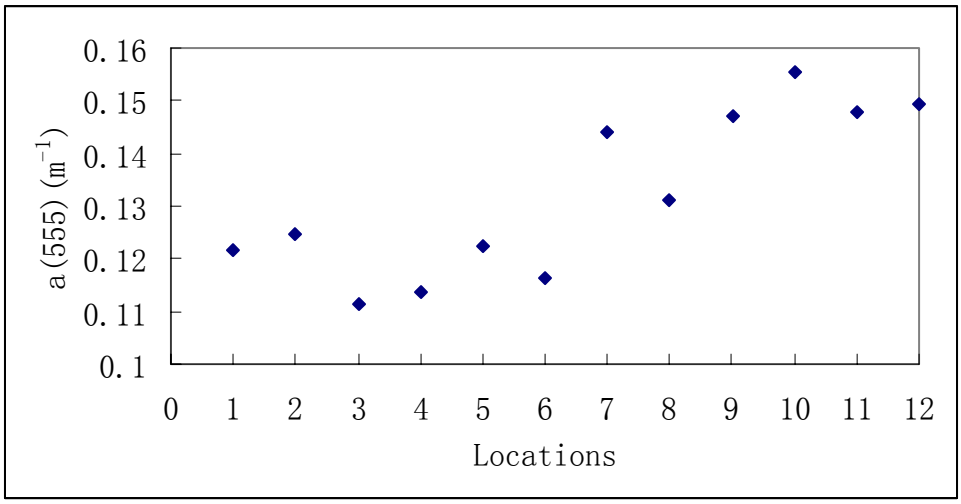

Figure 6.15 Total absorption coefficients at 555nm for 12 locations covered in June and August 2004

6.4 Comparison of measured backscattering values with the QAA derived values

The QAA derived $b_{bp}(555)$ values have been regressed against the in situ measured ones for 1m, 3m, 5m and 7m depth respectively as shown in Figures 6.16(a-d). The QAA retrieved values for the backscattering coefficients at 555nm, $b_{bp}(555)$, were also compared to the average measured

$b_{bp}(555)$ values at 1m, 3m and 5m.

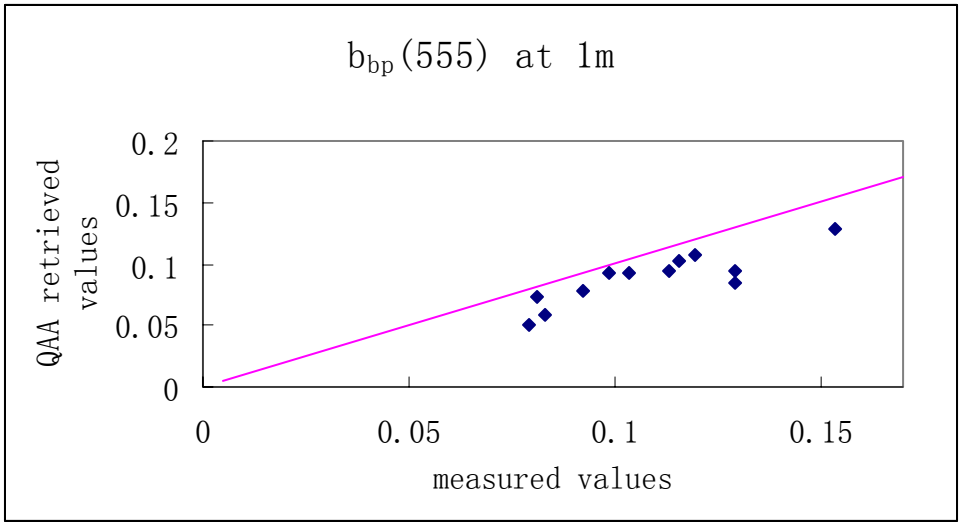

RMSD= 0.05812

Figure 6.16(a) Comparison of measured $b_{bp}(555)$ with QAA retrieved values at depth of 1m

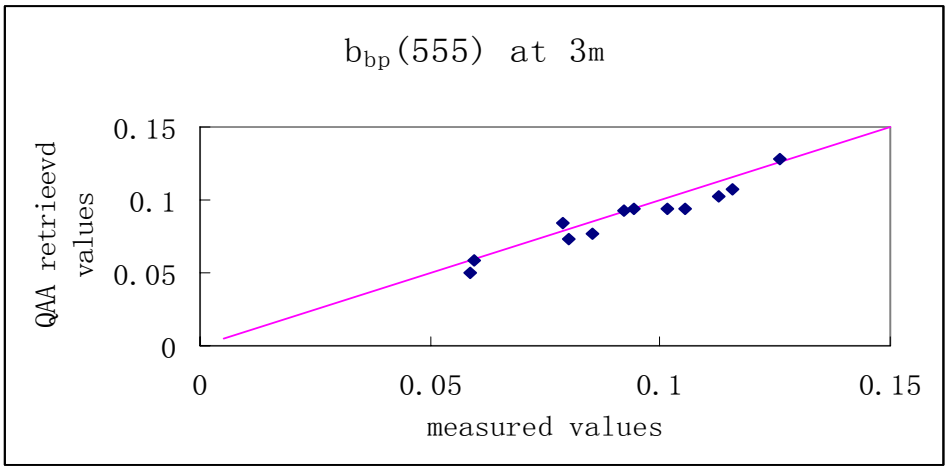

RMSD= 0.01345

Figure 6.16(b) Comparison of measured $b_{bp}(555)$ with QAA retrieved values at depth of 3m

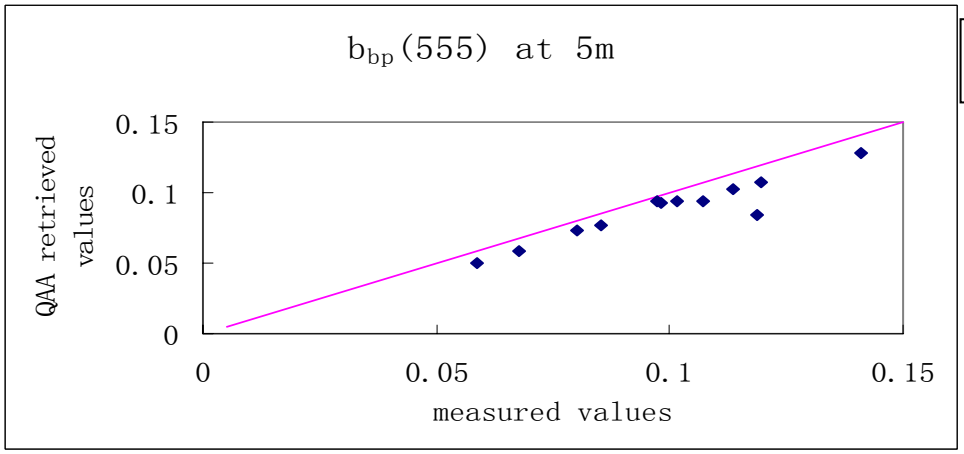

RMSD= 0.023208

Figure 6.16(c) Comparison of measured $b_{bp}(555)$ with QAA retrieved values at depth of 5m

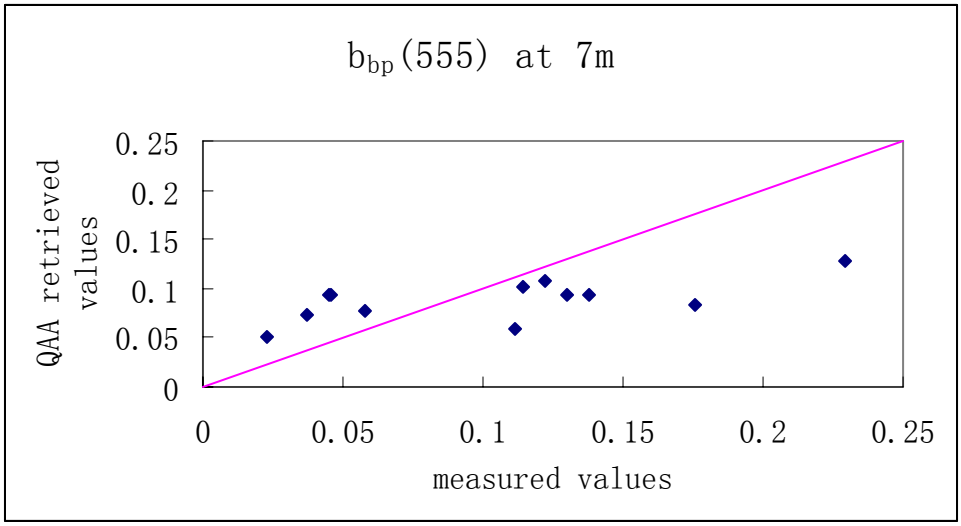

RMSD= 0.051706

Figure 6.16(d) Comparison of measured $b_{bp}(555)$ with QAA retrieved values at depth of 7m

Figure 6.16(a)-(d) Comparison of measured $b_{bp}(555)$ with QAA retrieved values at depths of 1m, 3m, 5m and 7m respectively.

Figures 6.16(a) to (d) presents the retrieved values versus their true values measured at a depth of 1m, 3m, 5m and 7m. The root mean square difference(RMSD) between the QAA retrieved and measured backscattering values is smallest at depths around 3 to 5 m and largest for a depth of 7m. Figure 6.17 shows the QAA values for $b_{bp}(555)$ versus the average values of $b_{bp}(555)$ for the 12 locations. These average values represent the average of the measured $b_{bp}(555)$ values for the depths of 1m, 3m, 5m and 7m. Except for one outlier point, the QAA retrieved backscattering coefficient values agree well with the depth-average values. If the outlier point is ignored, the RMSD is reduced to 0.014.

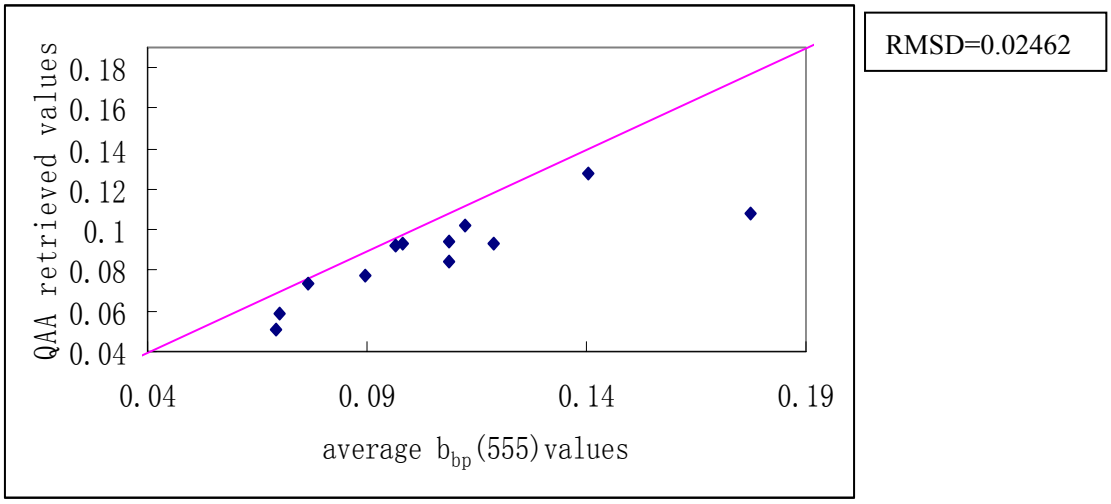

Figure 5.17. QAA retrieved $b_{bp}(555)$ versus the average of the measured $b_{bp}(555)$ values at 1m, 3m and 7m.

However, the field data is limited in number, and covers only a narrow range of natural waters, which is insufficient to completely validate the use of the QAA here (although the QAA was tested with a wide range of simulated data). If the QAA is valid in this context, its retrievals should be at least close to data not only from simulation but also from field measurements. It also needs to be pointed out that when remote sensing reflectance model is applied in the field, because of the actual shape of the of the particle phase function is not known, the differences between the actual g_o and g_1 values (as in Equation 6.7) and values used in calculation might be considerable. This mismatch can contribute to much error to the retrieved values of backscattering coefficients but however there is only very little influence on the absorption coefficients

As is known, several algorithms for the retrieval of the optical constituents' concentration have been developed. It has been seen that these algorithms work well for the open oceans (i.e. case 1 waters) where the water leaving radiance of the open oceans is hardly affected by land run off,

suspended sediments and bottom reflectance. Most often, however, these algorithms fail to yield reasonable estimate of the optical concentration for coastal waters because the environment of such waters is much more complicated. But for a proper retrieval of the optical coefficients, the use of a suitable algorithm is necessary.

6.5 Comparison of Measured Reflectance with Monte-Carlo Simulated Reflectance

For each sampling location, the absorption coefficient estimated using QAA and the measured depth profile of backscattering coefficient are now used as input to the Monte Carlo code to calculate the reflectance. The ocean was assumed to be flat in the simulation and the computations were carried out at every 10nm from 400 to 700nm. The sun was assumed to be at zenith and the surface was assumed to be illuminated by direct sunlight only. The reflectance generated by the Monte Carlo code is then compared with the one that was measured in situ i.e. the above surface remote sensing reflectance. The graphs in Figures 6.18(a-l) show the plots of both Monte Carlo simulated and in situ reflectance versus wavelength.

Location 1

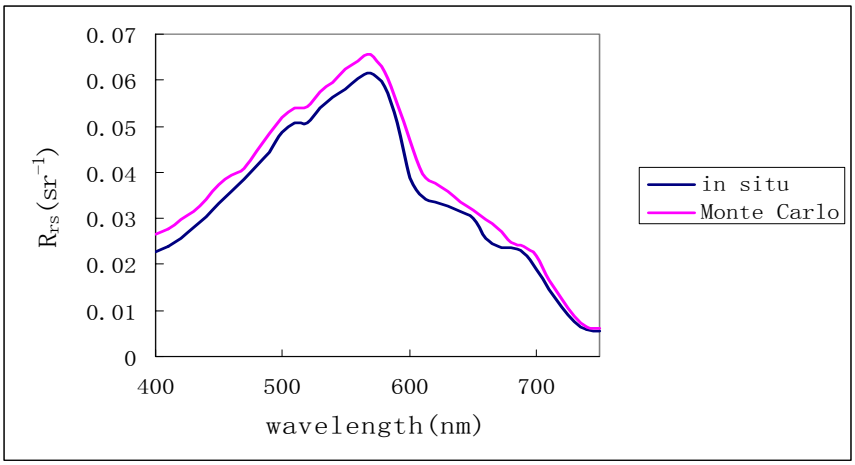

b_{bp} (470)=0.1157m^{-1}
b_{bp} (700)=0.07817 m^{-1}
x=0.09826 m^{-1}
Y=0.984213
RMSD=0.0034478

Figure 6.18(a) Graph showing measured reflectance (in situ) versus the reflectance generated by Monte Carlo code using measured data (Monte Carlo) at Location 1

Location 2

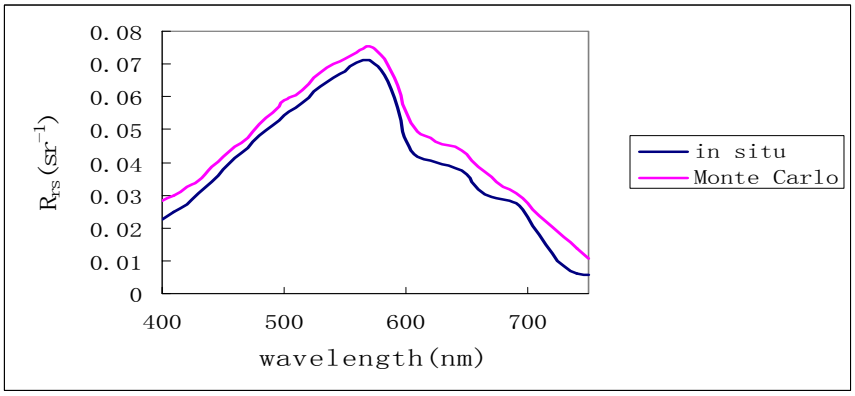

b_{bp} (470)=0.14278 m^{-1}
b_{bp} (700)=0.08856 m^{-1}
x=0.118251 m^{-1}
Y=1.19864
RMSD=0.00536

Figure 6.18(b) Graph showing measured reflectance (in situ) versus the reflectance generated by Monte Carlo code using measured data (Monte Carlo) at location 2

Location 3

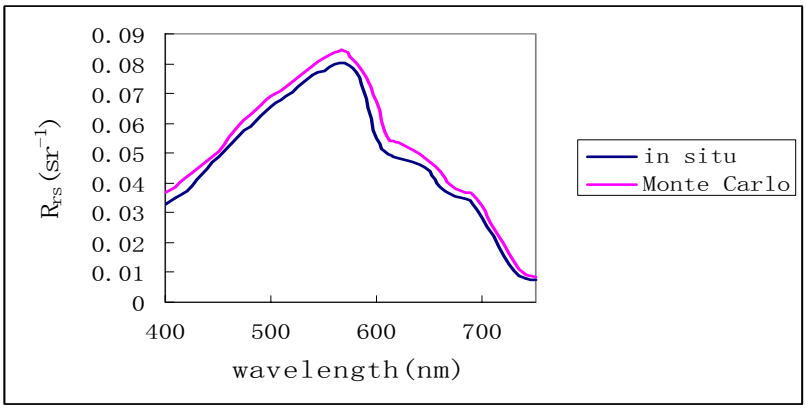

b_{bp} (470)=0.1846 m^{-1}
b_{bp} (700)=0.08955 m^{-1}
x=0.140254 m^{-1}
Y=1.846592
RMSD=0.004197

Figure 6.18(c) Graph showing measured reflectance (in situ) versus the reflectance generated by Monte Carlo code using measured data (Monte Carlo) at location 3

Location 4

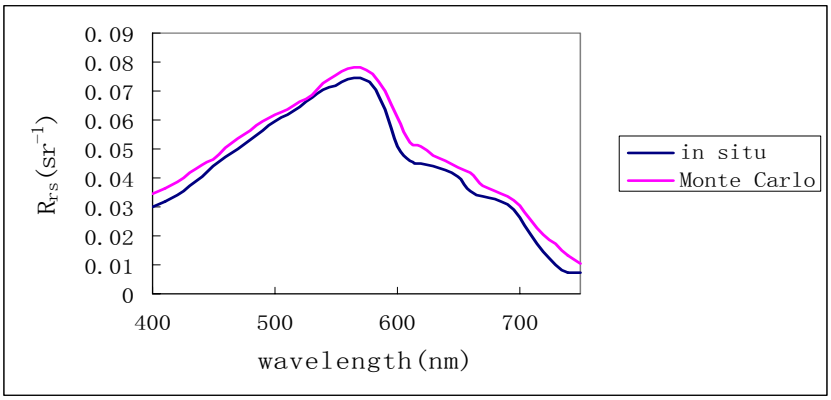

b_{bp} (470)=0.135128 m^{-1}
b_{bp} (700)=0.078328 m^{-1}
x=0.10881 m^{-1}
Y=1.347902
RMSD=0.004401

Figure 6.18(d) Graph showing measured reflectance (in situ) versus the reflectance generated by Monte Carlo code using measured data (Monte Carlo) at location 4

Location 5

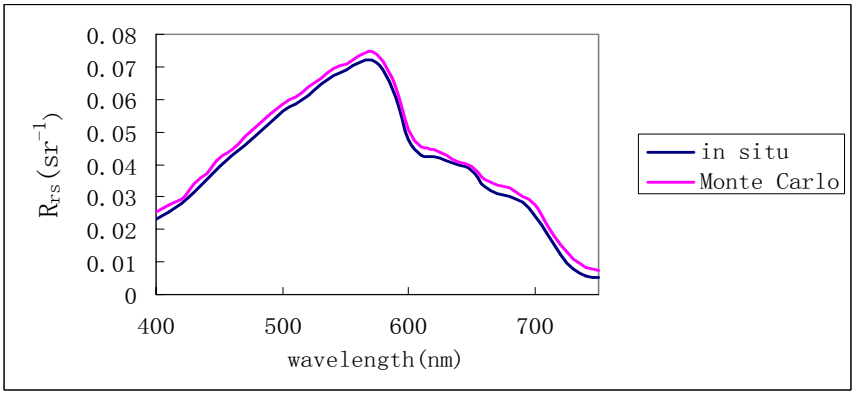

b_{bp} (470)=0.1359 m^{-1}
b_{bp} (700)=0.08429 m^{-1}
x=0.112557 m^{-1}
Y=1.99121
RMSD=0.002369

Figure 6.18(e) Graph showing measured reflectance (in situ) versus the reflectance generated by Monte Carlo code using measured data (Monte Carlo) at location 5

Location 6

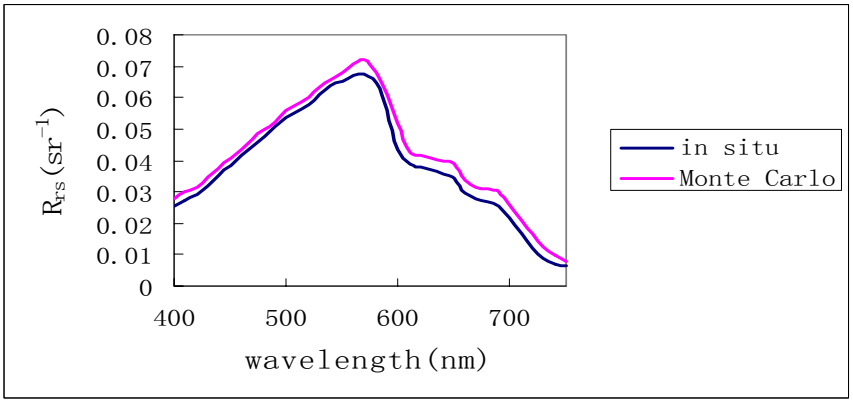

b_{bp} (470)=0.1300 m^{-1}
b_{bp} (700)=0.08234 m^{-1}
x=0.108605 m^{-1}
Y=1.146588
RMSD=0.003478

Figure 6.18(f) Graph showing measured reflectance (in situ) versus the reflectance generated by Monte Carlo code using measured data (Monte Carlo) at location 6

Location 7

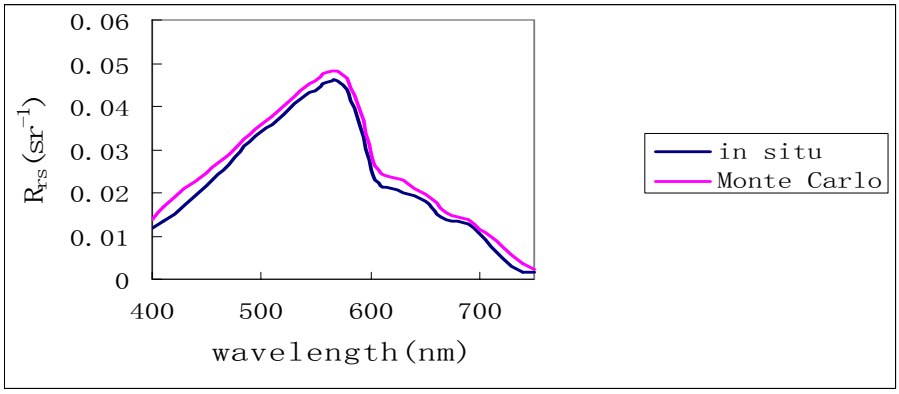

b_{bp} (470)=0.0838 m^{-1}
b_{bp} (700)=0.0534 m^{-1}
x=0.07083 m^{-1}
Y=1.133379
RMSD=0.002409

Figure 6.18(g) Graph showing measured reflectance (in situ) versus the reflectance generated by Monte Carlo code using measured data (Monte Carlo)

Location 8

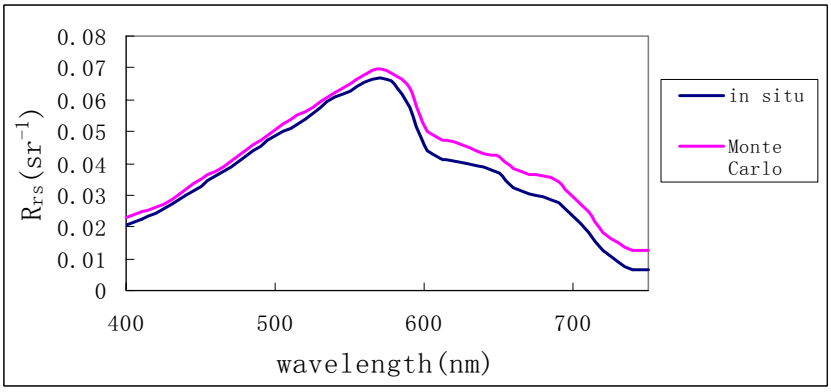

b_{bp} (470)=0.10241 m^{-1}
b_{bp} (700)=0.08848 m^{-1}
x=0.096334 m^{-1}
Y=0.364053
RMSD=0.004217

Figure 6.18(h) Graph showing measured reflectance (in situ) versus the reflectance generated by Monte Carlo code using measured data (Monte Carlo) at location 8

Location 9

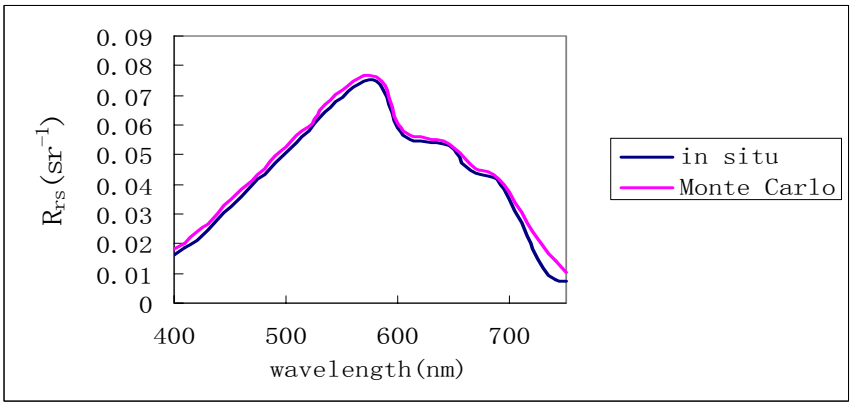

b_{bp} (470)=0.14611 m^{-1}
b_{bp} (700)=0.08960 m^{-1}
x=0.118745 m^{-1}
Y=1.189226
RMSD=0.002671

Figure 6.18(i) Graph showing measured reflectance (in situ) versus the reflectance generated by Monte Carlo code using measured data (Monte Carlo) at location 9

Location 10

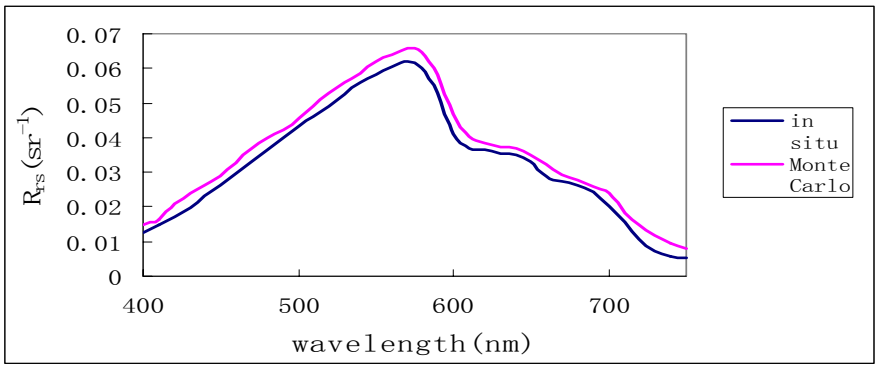

b_{bp} (470)=0.09561 m^{-1}
b_{bp} (700)=0.08186 m^{-1}
x=0.089614 m^{-1}
Y=0.389708
RMSD=0.003232

Figure 6.18(j) Graph showing measured reflectance (in situ) versus the reflectance generated by Monte Carlo code using measured data (Monte Carlo) at location 10

Location 11

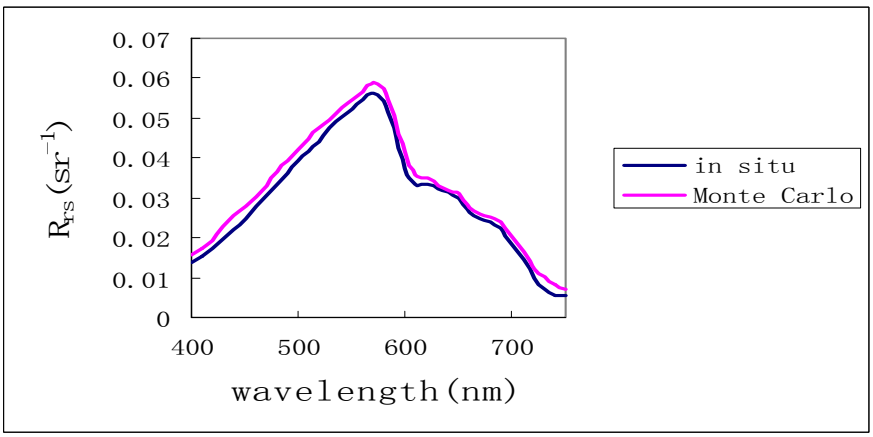

b_{bp} (470)=0.08061 m^{-1}
b_{bp} (700)=0.07086 m^{-1}
x=0.076381 m^{-1}
Y=0.320607
RMSD=0.002457

Figure 6.18(k) Graph showing measured reflectance (in situ) versus the reflectance generated by Monte Carlo code using measured data (Monte Carlo)

Location 12

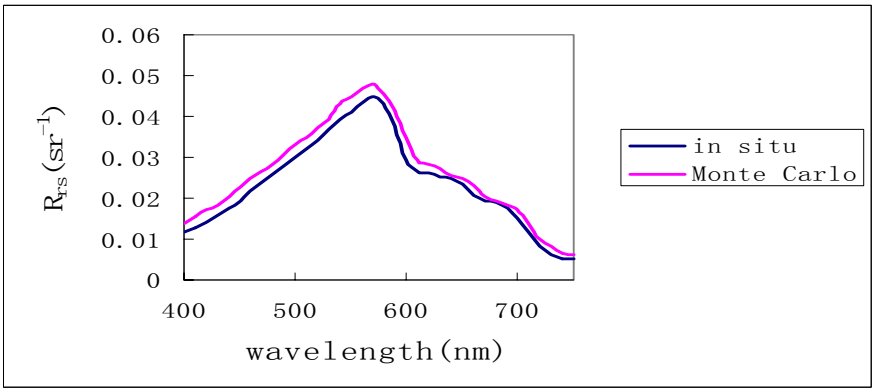

b_{bp} (470)=0.07805 m^{-1}
b_{bp} (700)=0.06503 m^{-1}
x=0.069454 m^{-1}
Y=0.282245
RMSD=0.002639

Figure 6.18(l) Graph showing measured reflectance (in situ) versus the reflectance generated by Monte Carlo code using measured data (Monte Carlo)

Figure 6.18 (a)-(l).Graph showing measured reflectance (in situ) versus the reflectance generated by Monte Carlo code using measured data (Monte Carlo) for the 12 locations covered in June and October 2004

The root mean square difference between the simulated reflectance and the measured reflectance is calculated as follows

$$RMSD = \sqrt{\sum_{i=1}^{N} \frac{1}{N}(R_S - R_M)^2} \qquad 6.17$$

where R_M is the measured reflectance and R_S is the simulated reflectance(by Monte Carlo) and N is the number of wavelengths considered.

Figure 6.19 below shows the RMSD between the simulated and measured reflectance for the 12 locations.

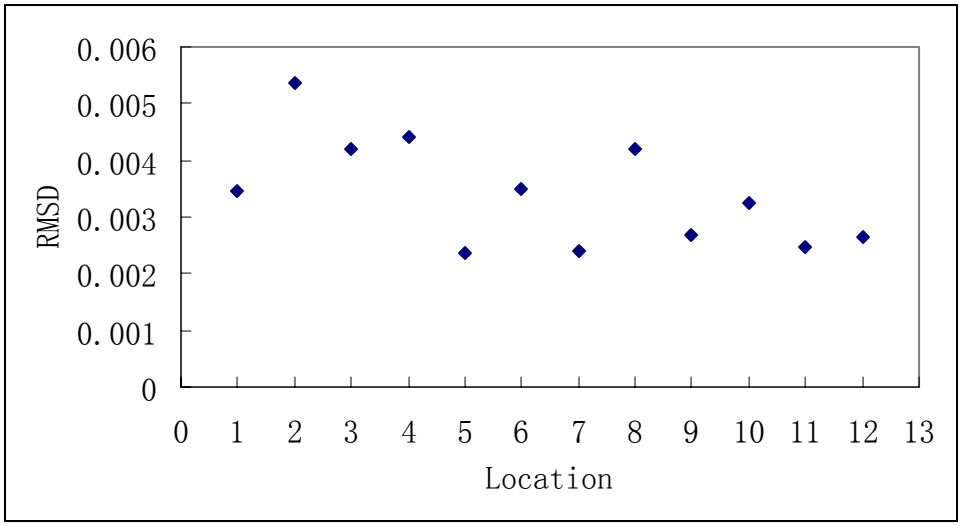

Figure 6.19 the RMSD at the 12 locations

Figures 6.20 (a)-(c) shows the comparison between the measured reflectance values and the ones obtained by the Monte Carlo code at 440nm, 550nm and 640nm. It can be seen the correlation between the two sets of reflectance data is generally high at all the three wavelengths and that the best

correlation is obtained at 550nm (this is the wavelength at which the backscattering coefficient by particles peak). In there graphs, R_{MC} (Y axis) denotes the reflectance value obtained by the Monte Carlo code and R_{IS} (X axis) denotes the in-situ reflectance values measured during the trips.

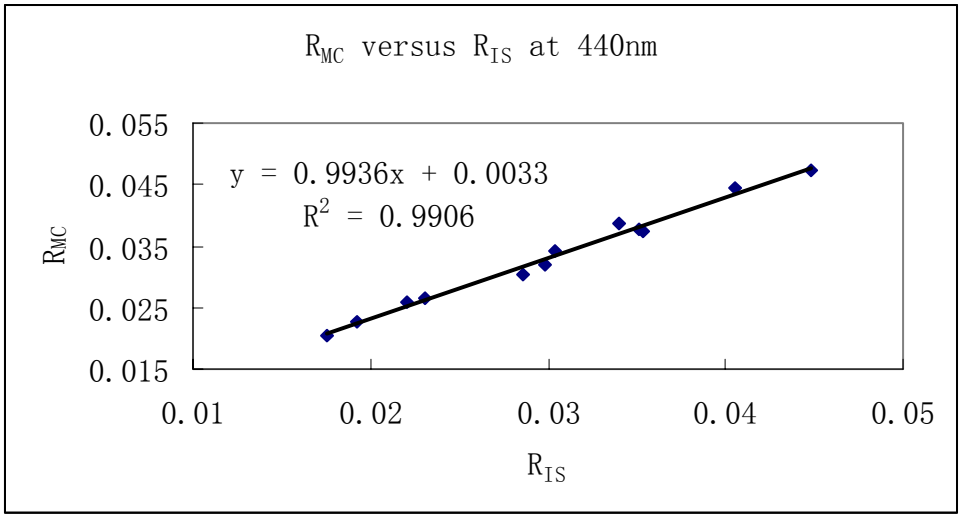

Figure 6.20(a) R_{MC} versus RIS at 440nm

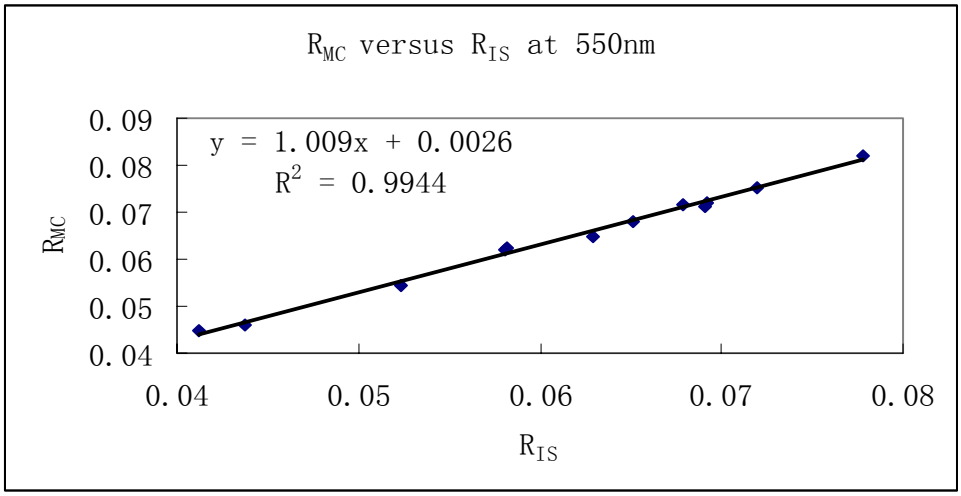

Figure 6.20(b) R_{MC} versus RIS at 550nm

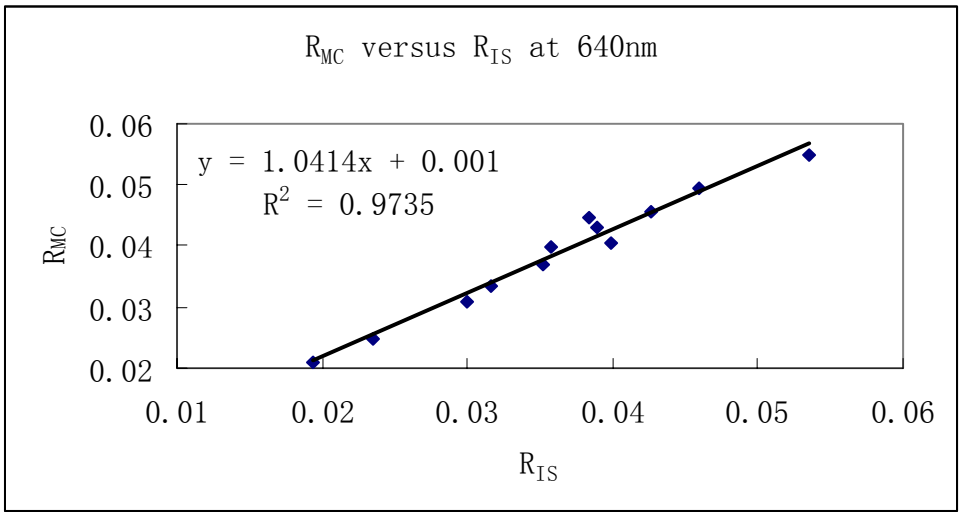

Figure 6.20(c) R_{MC} versus RIS at 640nm

Figure 6.20(a)-(c).The graphs show the reflectance obtained by Monte Carlo (R_{MC})versus the measured reflectance(RIS) at 440nm, 550nm and 640nm

The causes for the difference between the two sets of reflectance can be explained as

1) In both cases, the surface conditions are different. For the in situ case, it cannot be assumed that the surface of the water is constant. Because when the wind speed is greater than zero (as can be observed if field), then the surface of the water would be covered with capillary waves. These would in turn affect the reflecting and refracting of the incident photons. In the current case, the Monte Carlo code developed ignores wind speed, assuming a flat surface.

2) Another important source of uncertainty would be the absorption and backscattering coefficients as input to the Monte Carlo code. As there is no other ways to verify whether the values derived from the QAA do truly represent the existing conditions in the waters examined, they have been assumed to be correct

---

Chapter Seven

Summary and Conclusion

Oceanographic observations have indicated that the optical properties and optically significant constituents of water often show substantial vertical variation in the upper ocean. However, the current algorithms used to retrieve the absorption and scattering coefficients of water from above-surface reflectance unconditionally assume that the water column is vertically homogeneous. This thesis aimed at studying the link between the remote sensing reflectance and the vertical structure of the oceans optical properties,

The tool developed for this purpose is a Monte Carlo code to simulate the penetration of light in sea water. This method was employed as it is conceptually simple and is based on a straightforward mimicry of nature. The computations were not time consuming and the intrinsic error with each run was negligible. It was seen that the code worked well for the ideal case of a homogeneous ocean when comparisons were made with the reflectance results obtained by the Ocean Colour Algorithms working group of the International Ocean Colour Coordinating Group.

The hypothesis that the reflectance of a stratified water column is the same as that of an equivalent homogeneous ocean, with the optical property that is the average of the associated property over the penetration depth, was tested. This hypothesis was seen to be valid for both a two-layer ocean and a continuously stratified ocean, even though the agreement for a two-layer

ocean is better. However, this hypothesis was only tested for the case of open oceans where the concentrations of the optical properties covaried with that of chlorophyll. To be able to determine whether this hypothesis holds for various for different types of stratified water, it should also be tested on Case 2 waters, where the sediment level is higher.

The nonuniform vertical profile of chlorophyll concentration modelled on a Gaussian profile superimposed on a constant background value was then used to describe the continuously stratified water column. A relatively broad range of open ocean conditions characterized by the presence of this subsurface maximum at depths greater than or equal to 20 m was simulated. The reflectance from the stratified water columns (with a Gaussian profile for chlorophyll) was then compared to that of homogeneous water columns (having the same background chlorophyll concentration as the stratified case). It was found that for some vertical structures of *Chl(z)* considered, the reflectance values for the stratified cases differed significantly from those of the homogeneous cases, specially in the case for low surface *Chl* concentrations and shallow pigment maximum.

The multiband quasi analytical algorithm (QAA) was then applied for the retrieval of absorption and backscattering coefficients to both homogeneous and inhomogeneous water columns. For the homogeneous case, it was found that the retrieved values of the optical constituents compared very well with the actual values found in the water column. For the inhomogeneous case (where stratification was included by the use of a Gaussian function), it was observed that there is a good correlation between QAA retrieved values

and the depth weighed average values for the absorption coefficients at 440nm and the backscattering coefficients at 555 nm. The results obtained agreed with the observations made by Andre (1992) who stated that he chlorophyll vertical structure has more influence on remote sensing reflectance when it is shallower in the water column. These results cannot be generalised as they have been applied to only a limited set of data. Therefore the retrieval algorithm should be applied to a larger measured data set describing the behaviour of different types of oceanic conditions.

The Gordon and Clark's hypothesis that the reflectance of a stratified case ocean is identical to that of a hypothetical homogeneous ocean with a phytoplankton pigment concentration (<*Chl*>) that is a depth weighted average of the actual depth varying concentration *Chl(z)* was tested. Two scenarios are used to relate the inherent optical properties to the pigment profile. Firstly the particle absorption and scattering coefficients were made to vary with *Chl(z)*. In the other scenario, the particle absorption coefficient was permitted to covary with *Chl(z)* but the scattering coefficient was made independent of depth (from Kitchen and Zaneveld's theory). It was seen that the case where both the absorption and scattering coefficient covary with pigment concentration showed less error than the case where the scattering coefficient was made independent of the depth varying pigment concentration agreeing with Kitchen and Zaneveld's hypothesis that the scattering coefficient is independent of depth.

On the experimental front, boat trips were taken in June and August 2004 in Singapore waters. The reflectance at visible wavelengths together with

the particle backscattering coefficients at 470 and 700nm were measured. Due to lack of equipment, the absortion coefficient was not retrieved but was instead estimated from the QAA. The estimated absorption coefficients and the measured backscattering coefficients were then used as input to the Monte Carlo code to generate the reflectance values, which were then compared to those obtained during the field measurements. For the whole range (400-750 nm), it was found that the reflectance generated by the code was slightly higher than the in situ one. This difference could be due to the different surface conditions assumed in the simulations and those present during measurements. The QAA was applied to the in situ reflectance for the retrieval of the backscattering coefficients and these values were then compared to those obtained during the field trips. It was seen that the root mean square difference between the measured and QAA retrieved backscattering coefficients was less for the data at depths 3m and 5m and was slightly more for the depth of 1m. The QAA retrieved values of the backscattering coefficient were also compared to the depth-average values, using a constant weighting function, and there is a good agreement in most cases. However, it should be noted that the field data here is quite limited. More experimental work should be carried out to see whether this trend is observed for all locations covered and for different types of waters. It would also be interesting to compare the QAA retrieved values with the values of the optical properties averaged over the penetration depth, using the depth varying weighted function $g(z)$.

The current retrieval algorithms for estimating the concentration of

the optical constituents of sea water are based on the correlation between the measured spectral reflectances and the measured surface concentrations, on the assumption that the water column being studied is homogeneous. This type of correlation does not account for the vertical structure of the inherent optical properties. Hence, this vertical distribution may introduce errors into the algorithm derived surface optical constituents concentrations.

It is difficult to assess to what extent the nonuniformity of the seawater constituents affect the performance of the current retrieval algorithms. These algorithms have been tested on a large amount of field data, collected for various oceanic regions, in different seasons. It is possible that some of these data were collected in the presence of significant effects of nonuniform constituents profile on the ocean reflectance and some were collected in the absence of such effects. One possible but difficult and laborious way to minimise this problem might be based on the development of retrieval algorithms for which the detailed vertical profiles are known or to obtain the retrieval based on continuous profiling instead of discrete water samples.

The concentrations of the sea water constituents derived from remote measurements have only limited value when the profile of these constituents is non uniform. If independent information is available on this vertical profile, an attempt could be made for the retrieval of the entire profile. By combining oceanographic measurements with remote sensing measurements, it is possible to obtain a more complete picture of the ocean .The principal requirement for sea truth data follows directly from this view. From this, the detailed vertical profiles would be known and this could lead to a better understanding of the

influence of inhomogeneity on the measured reflectance above the water surface.

……

Bibliography

……

Andre J.M .1992. Ocean colour remote sensing and the subsurface vertical structure of phytoplankton pigments. Deep-Sea Research. 39:5763-779

Ballestro.D.1999.Remote sensing of vertically structured phytoplankton pigments. Top.Meteor. Oceanog.6(1):14-23

Bricaud, A, A.Morel and L. Prieur.1981. Absorption by dissolved organic matter of the sea(yellow substance) in the UV and visible domains. Limnol.Oceannogr.26(1):43-53

Bricaud, A and A.Morel.1986. Light attenuation and scattering by phytoplanktonic cells:a theoretical modeling. Appl. Opt.25:571-80

Bricaud, A., and D. Stramski, 1990: Spectral absorption coefficients of living phytoplankton and non-algal biogenous matter: A comparison between the Peru upwelling area and the Sargasso Sea. Limnology and Oceanography. **35,** 562-582

Bricaud,A,Babin. M,Morel.A and Claustre.H.1995.Variability in the chlorophyll-specific coefficients of natural phytoplankton: Analysis and parametisation. Journal of Geophysical research.C7:13,321-13,332.

Bricaud, A, Babin.M, Morel.Aand Claustre.H.1998. Variations of light absorption by suspended particles with chlorophyll a concentration in oceanic (case 1) waters: Analysis and implications for bio-optical models. Journal of Geophysical research.:103,31033-31044.

Bukata, RP, J.H. Jerome, K.Y. Kondratyev, and D.V. Pozdynyakov, 1995. Optical Properties and Remote Sensing of Inland and Coastal Waters. CRC Press, New York, 362 pp

Butler, W.L., 1962: Absorption of light by turbid materials. Journal of the Optical Society of America. **52,** 292-299

Carder.K.L, F.R.Chen, Z.P.Lee and S.K.Hawes. 1999. Seminalaytic Moderate Resolution Imaging Spectrometer algorithms for chlorophyll a and absorption with bio optical domains based on nitrate depletion temperatures. Journal of Geophysical Research. 104:5403-5421

Chandrasekhar.S. 1960. Radiative Transfer (Dover ,New York)

Clark D.K.1981. Phytoplankton algorithms for the Nimbus-7 CZCS in Oceanography from Space, J.F.R.Gower,Ed(Plenum, New York),pp227-238

Chavez, F.P., K.R. Buck, R.R. Bidigare, D.M. Karl, D. Hebel, M. Latasa, L. Campbell, and J. Newton, 1995: On the chlorophyll a retention properties of glass-fiber GF/F filters. Limnology and Oceanography. 40**(2),** 428-433
Cullen J.J.1982. The deep chlorophyll maximum: comparing vertical profiled of chlorophyll a. Canadian Journal of fisheries and aquatic sciences.39,791-803

Cullen J.J and R.W Epley.1981. Chlorophyll maximum layers of the Southern California Bight and possible mechanisms of their maintenance. Oceanlogica.Acta,4,23-32

Duntley, S.Q., 1942: The optical properties of diffusing materials. Journal of the Optical Society of America. **32,**61-70

Firestone, E.R., and S.B. Hooker. 1998. SeaWiFS Prelaunch Technical Report Series Final Cumulative Index. NASA Tech. Memo. 1998 – 104566, Vol. 43, S.B. Hooker and E.R. Firestone, Eds., NASA Goddard Space Flight Center, Greenbelt, Maryland, 69 pp.

Frette O, S.R. Erga, J.J.Stamnes and K.Stamnes. 2001. Optical remote sensing of waters with vertical structure. Appl.Opt. 40:1478-1486

Garver S.A and D.A.Siegel. 1997. Inherent optical property inversion of colour spectra and its biogeochemical interpretation.1. Time series from the Sargasso Sea. J.Geophys.Res.102(C8):18607-16625

Gordon H.R and O.B.Brown. 1973. Irradiance reflectivity of a flat ocean as a function of its optical properties. Appl.Opt.12:1549-1551

Gordon H.R and W.R.McCluney. 1975. Estimation of the depth of sunlight penetration in the sea for remote sensing. Appl. Opt. 14:413-416

Gordon .H.R and O.B.Brown. 1975. Diffuse reflection of the ocean: some effects of vertical structure. Appl.Opt.14:2892-2895

Gordon H.R and W.R.McCluney. 1975. Estimation of the depth of sunlight penetration in the sea for remote sensing. Appl. Opt. 14:413-416

Gordon, H.R, O.B.Brown and M.M.Jacobs.1975. Computed relationships between the inherent and apparent optical properties of a flat homogeneous ocean as a function of its optical properties. Appl.Opt.12:1549-51

Gordon.H.R and W.R McCluney. 1975. Estimation o depth of sunlight

penetration in the sea for remote sensing. Appl Opt .14:413-416

Howard R. Gordon, Otis B. Brown, and Michael M. Jacobs.1975. Computed relationship between the inherent and apparent properties of a flat homogeneous ocean. Appl Opt14.417-427

Gordon.H.R and O.B.Brown.1976. Diffuse reflectance of the ocean: some effects of vertical structure. Appl Opt.12:2892-2895

Gordon.H.R.1978.Remote sensing of optical properties in continuously stratified waters. Appl Opt.17:1893-1897

Gordon H.R and D.K.Clark. 1980. Remote sensing optical properties of a stratified ocean: an improved interpretation. Appl Opt. 19:3428-430

Gordon,H.R, R.C.Smith and J.R.V.Zaneveld. 1980. “Introduction to ocean optics” in Ocean Optics VI, S.Q.Duntley, ed, Proc.Spie.208:1-43

Gordon, H.R and A.Morel.1983. Remote assessment of ocean colour for interpretation of satellite visible imagery. A review, R.T. Barbe, C.N.K.Mooers, M.J.Bowman and B.Zeutzschel,edsISpringer-Verlag,New York)

Gordon, H.R, O.B.Brown, R.H.Evans, J.W.Brown, R.C.Smith, K.S.Baker and D.K.Clark. 1988. A semianalytical radiance model of ocean colour. J.Geophys.Res.93:10.909-10,924

Gordon H.R.and G.C Boynton . 1998, A radiance – irradiance inversion algorithm for estimating the absorption and backscattering coefficients of natural waters: vertically stratified water bodies, Appl. Opt., 37, 3886–3896.

Gregg, W.W and K.L Carder.1990. A simple spectral solar irradiance model for cloudless maritime atmospheres. Limnol.Oceanogr.35:1657-675

Haltrin V.I. 1998. Self-consistent approach to the solution of the light transfer problem for irradiances in marine waters with arbitrary turbidity, depth, and surface illumination. I. Case of absorption and elastic scattering.Appl.Opt.37:3773-3784

Hernandez-Aguirre.E, Gaxiola-Castro.G, Najera-Martinez.S, Baumgartner.T, Kahru.M and Mitchell.B.G 2004. phytoplankton absorption, photosynthetic parameters and primary production off Baja California: summer and autumn 1998. Deep-Sea research II 51 799-816

Hoge, F.E and P.E.Lyon. 1996. Satellite retrieval of inherent optical properties by linear matrix inversion of oceanic radiance models: An analysis of model and radiance measurements errors. J. Geophys.Res.101(C7):16,631-16,648

Jerlov, N.G.1979.Marine Optics.Vol.14 of Elsevier Oceanography Series. New York:Elsevier

Jerome, J.H, R.T. Bukata and J.R.Burton.1988. Utilising the components of vector irradiance to estimate the scalar irradiance in natural waters. Appl Opt.27:4012-4018

Kirk J.T.O. 1975. A theoretical analysis of the contribution of algal cells to the attenuation of light within natural waters.II.Spherical cells. New Phytol.75:21-36

Kirk.J.T .1976.Yellow substance (gelbstoff) and its contribution to the attenuation of the photosynthetically active radiation in some inland and coastal south-eastern Australian waters. Aust.J.Mar.Freshwater Res.27:61-71

Kirk,J.T.1981. Monte Carlo procedure for simulating the penetration of light into natural waters .Division of Plant Industry Technical paper .N036

Kirk,J.T.1981. Monte Carlo study of the nature of the underwater light field in and relationship between optical properties of turbid yellow waters. Aust.J.mar.Freshwater.Res.32,517

Kirk, J.T.O .1986. Light and photosynthesis in aquatic ecosystems. Pp.117.Cambridge: Cambridge University

Kishino, M., N. Takahashi, N. Okami, and S. Ichimura, 1985: Estimation of the spectral absorption coefficients of phytoplankton in the sea. Bulletin of Marine Science. **37,** 634-642

Kishino, M., N. Okami, M. Takahashi, and S. Ichimura, 1986: Light utilization efficiency and quantum yield of phytoplankton in a thermally stratified sea. Limnology and Oceanography. **31,** 557-566

Kitchen J.C and J.R Zaneveld. 1990. On the non correlation of the vertical structure of light scattering and chlorophyll a in case 1 waters. J.Geophys.Res. 95C:30,237-20,246

Kullenberg.G .1968. Deep Sea Res. 15, 423

Lalli, C.M and T.R Parsons.1993. Biological Oceanography: An introduction. Pergamon Press, Oxford,301pp

Lee Z., K.L. Carder, Hawes.S.K, R.G.Steward, T.G.Peacock and C.O.Davis. 1994. A model for the hyperspectral remote sensing reflectance. Appl.Opt.33(24):5721-5732

Lee, Z.P, K.L.Carder, C.D Mobley, R.G.Steward and J.S.Parch. 1999. Hyperspectral remote sensing for shallow waters and water properties by

optimization. Appl.Opt. 38:3831-3843

Lee Z.P, K.L. Carder and R. Arnone. 2002. Deriving inherent optical properties from water colour; a multiband quasi-analytical algorithm for optically deep waters. Appl Opt. 41:5755-5772

Lee. ZP and K.L Carder. 2004. Absorption spectrum pf phytoplankton pigments derived from hyperspectral remote sensing reflectance. Remote Sensing of Environment.89 (3):361-368

Lewis.M, J.Cullen and T.Platt.1983.Phytoplnakton and thermal structure in the upper ocean: consequences of nonuniformity in chlorophyll profile. Journal of Geophysical Reasearch.17:1245-11271

Matsumura.S and A.Shiomoto.1993.Vertical distribution of primary productivity function for the estimation of primary productivity using by satellite remote sensing.Bull.Nat.Res. Inst.Far Seas Fish.30:227-270

Mitchell, B.G. 1990: Algorithms for determining the absorption coefficient of aquatic particulates using the quantitative filter technique (QFT).Ocean Optics X. 137-148

Mobley, C.D.1994. Light and Water: radiative transfer in natural waters, Academic Press, New York

Mobley et al.2002, "Phase function effects on oceanic light fields", Applied Optics, Vol.41 No.6, pp 1035-1050.

Mobley, C. D. and Sundman, L. K.2003, “Effect of Optically Shallow Bottoms on Upwelling Radiances: Inhomogeneous and Sloppy Bottoms,” Limn. Ocean. 48, pp. 329-336

Morel,A.1974. Optical properties of pure water and pure sea water. Optical aspects of Oceanography,ed. N.G Jerlov and E.S. Nielsen, 1-24.New York:Academic

Morel ,A and L.Prieur. 1977. Analysis of variations in ocean colour. Limnol Oceanogr. 22:709-22

Morel.A. 1980.In water and remote measurements of ocean colour. Boundary layer Meteorol.18:177

Ocean-colour Algorithm Working Group, International Ocean Colour Coordinating Group. 2003. Models, parameters, and approaches that used to generate wide range of absorption and backscattering spectra (www.ioccg.org)

O’Reilly, J.E., and 24 Coauthors, 2000: SeaWiFS Postlaunch Calibration and

Validation Analyses, Part 3. NASA Tech. Memo. 2000 – 206892, Vol. 11, S.B. Hooker and E.R. Firestone, Eds., NASA Goddard Space Flight Center, 49 pp.

O'Reilly, W.C. and R.T. Guza. 1998. Assimilating coastal wave observations into regional swell predictions. Part I: Inverse methods. J. of Phys. Oceanogr. 28: 679-691.

Parsons, T.R, M.Takahashi and B.Hargrave.1984. Biological Oceanographic processes. 3erd.,Pergamon Press, Oxford, 330pp

Pegau, W.S., and J.R.V. Zaneveld, 1993: Temperature-dependent absorption of water in the red and near infrared portions of the spectrum. Limnology and Oceanography. 38, 188-192

Pelevin V.N.,Rutkovskaya V.A., 1978, A review of photosynthetic radiation in the waters of the Pacific Ocean, Okeanologiya,18 (4), 619–626,(in Russian).

Petzold.T.J.1972. Volume scattering functions for selected ocean waters. Tech Rep.SIO 72-78

Philpot, W. D. (1987*).* Radiative Transfer in Stratified Waters: A Single-Scattering Approximation for Irradiance. Applied Optics 26:4123-4132.

Platt T. S.Sathyendranath , C.M. Caverhill and M.R.Lewis. 1988. Ocean primary production and available light: further algorithms for remote sensing. Deep –Sea Res.35:855-79

Pope, R.M. and E.S. Fry. 1997: Absorption spectrum (380-700 nm) of pure water. II. Integrating cavity measurements. Appl. Opt. **36**: 8710-8723.

Preisendorfer, R.W. 1976. Hydrologic Optics, Volumes 1-6. Department of Commerce, National Oceanic and Atmospheric Administration, Washington, D.C.

Prieur, L. and S. Sathyendranath, 1981. An optical classification of coastal and oceanic waters based on the specific spectral absorption curves of phytoplankton pigments, dissolved organic matter, and other particulate materials. Limnol. Oceanogr., 26(4): 671-689.

Roesler, C.S, M.J. Perry and K.L.Carder.1989.Modeling in situ phytoplankton absorption from total absorption spectra in productive inland marine waters. Limnol.Oceanogr.34:1510-523

Roesler C.S and M.J.Perry. 1995. In situ phytoplankton absorption, fluorescence emission and particulate backscattering spectra determined from reflectance.J.geophys.Res.100:13,279-13,294.

Satheyndranath. S and T.Platt.1988. A three component model of ocean colour and its application to remote sensing in ‘Case 2’ waters.Int.J.Remote Sensing.

Sathyendranath .S and T.Platt. 1989. Remote sensing of ocean chlorophyll: consequence of nonuniform pigment profile. Appl Opt.28.490-495

Satheyndranath .S, G.Gota, V.Stuart, M.Maass and T.Platt.2001. Remotes sensing of phytoplankton pigments; a comparison of empirical and theoretical approaches. Int.J.Remote Sens.22:249-273

SeaWiFS Bio-Optical Algorithm Mini-Workshop (SeaBAM)(1996).Ocean Optics XIII conference.http://seabass.gsfc.nasa.gov/seabam/seabam.html

Shibata, K., 1958: Spectrophotometry of intact biological materials. Absolute and relative measurments of their transmission, reflection and absorption spectra. Journal of Biochemistry. **45,** 599-623

Shifrin, K.S., 1988*:* Physical Optics of Ocean Water. New York, American Institute of Physics, 285

Smith, R.C and K.S.Baker .1981. Optical properties of the clearest natural waters. Applied Optics. 20:177-84

Stramski, D., 1990: Artifacts in measuring absorption spectra of phytoplankton collected on a filter. Limnology and Oceanography. 35, 1,804-1,809

Takuhiko.K and S.Matsumura. 1998. Chlorophyll Biomass off Sanriku, Northwestern Pacific, Estimated by Ocean Colour and Temperature Scanner (OCTS) and a Vertical Distribution Model. Journal of Oceanography.54:509-516

Tassan, S. and G.M. Ferrari, 1995a: An alternative approach to absorption measurements of aquatic particles retained on filters. Limnology and Oceanography. **40,** 1,358-1,368

Thomas.G.E and K.Stamnes.2001. Radiative transfer in the atmosphere and the ocean(Cambridge U.Press, Cambridge,1999)

Waters K.J. 1989. Pigment biomass in the Sargasso Sea during Biowatt 1987 as determined using deep sea monitoring data, M.A.thesis(University of California, Santa Barbara)

Yentsch, C.S., 1957: A non-extractive method for the quantitative estimation of chlorophyll in algal cultures. Nature*.* **179,** 1302-1304

Zaneveld.J.R. 1982.Remotely sensed reflectance and its dependence on vertical structure: a theoretical derivation. Appl. Opt. 21:4146-4150

Web pages and documentation

1. www.ioccg.org
2. www.oceanoptics.com
3. http://oceancolor.gsfc.nasa.gov/DOCS/
4. http://seabass.gsfc.nasa.gov/seabam/seabam.html

Appendix A

Light penetration depth

The penetration depth of the light in the sea is defined for remote sensing purposes as the depth above which 90% of the diffusely reflected irradiance (excluding specular reflectance) originates (Gordon and Mc Cluney(1975). It is demonstrated that for a homogeneous ocean, this is the depth at which the downwelling in-water irradiance falls to 1/e of its value at the surface. Gordon and Mc Cluney(1975)defines a penetration depth that can be directly determined from in water irradiance measurements. This penetration depth is applicable to oceanic sensing in areas in which the water is sufficiently deep that reflection from the bottom does not contribute to the diffuse reflectance observed above the surface.

An approximate theory of the penetration depth can be easily shown using the quasi single scattering approximation to the radiative transfer. The single scattering equations are employed throughout but the beam attenuation coefficient is substituted by c(1-ω_oF), where ω_o is the ratio of the scattering coefficient b to c and F is the fraction of b scattered in the forward direction.

A layer of ocean water of thickness z which is illuminated by collimated irradiance E from the zenith is considered. Then the radiance $I_z(\bar{\mu})$ due to this layer leaving the ocean surface making an angle $\cos^{-1}(\mu')$ with the zenith is given by

$$I_z(\bar{\mu}) = \frac{4E_o T(\mu,\mu')}{n(n+1)^2 1+\mu} p(-\mu)\frac{\omega_o}{1-\omega_o F} \quad \text{x} \quad \text{A1}$$

$$\{1-\exp[\frac{-zc(1-\omega_o F)(1+\mu)}{\mu}]\}$$

where

n=refractive index of water

$T(\mu,\mu')$=Fresnel transmittance from an angle $\cos^{-1}(\mu)$ to $\cos^{-1}(\mu')$

$P(-\mu)$=phase function for scattering through an angle $\cos^{-1}(\mu)$ from the incident beam

$$\mu^2 = 1-n^2(1-\mu'^2)$$

The penetration depth [$z_{90}(\mu')$] for each emerging angle $\cos^{-1}(\mu')$ is defined as the layer thickness from which 90% of the total radiance originates

$$I_{z_{90}}(\mu')/I_{\infty}(\mu') = 0.9$$

$$=1-\exp[-cz_{90}(\mu')(1-\omega_o F)(1+\mu)/\mu] \qquad \text{A2}$$

or

$$z_{90}(\mu')c(1-\omega_0 F) = \frac{2.30\mu}{1+\mu} \qquad \text{A3}$$

But since c(1-ω_oF) is just the quasi single scattering approximation to K(0,-), the attenuation coefficient of the downwelling irradiance just beneath the surface is therefore

$$z_{90}(\mu')K(0,-) = \frac{2.30\mu}{1+\mu} \qquad \text{A4}$$

The above equation shows that $z_{90}(\mu')K(0,-)$ is almost independent of μ' and hence

$$z_{90}(\mu')K(0,-) \cong 1 \qquad \text{A5}$$

The fact that $z_{90}(\mu')$ and μ' are nearly independent suggests that an alternate definition of the penetration depth that is independent of μ'.

This is expressed as

$$\frac{R_{z_{90}}}{R_\infty} = 0.9 \qquad \text{A6}$$

where R_z is the diffuse reflection of the ocean due to a surface layer of thickness z and is given as

$$R_z = 2\pi \int_0^1 N_z(\mu')\mu' d\mu' / E_o \qquad \text{A7}$$

defined for an axissymmetric incident radiance distribution. Therefore the quasi single approximation is

$$z_{90} K(0,-) \cong 1 \qquad \text{A8}$$

During the study of a reflecting bottom on the diffuse reflectance of the ocean, Gordon and Brown have computed R_τ(where τ=cz is the optical depth) using Monte Carlo techniques as a function of τ for three scattering phase functions. $\frac{K(\tau,-)}{c}$ was also computed for the same phase functions and therefore it is possible to compare equation A8 with the results of the exact solutions.

To carry out such a comparison, τ_{90} is first determined by the regression of $\frac{R_\tau}{R_\infty}$ against τ for each phase function and various values of ω_o. Then τ_{90} can be read directly from the curves for each values of ω_o. Hence sinceτ_{90}=cz_{90}

$$\tau_{90}[K(0,-)/c] = z_{90} K(0,-) \qquad \text{A9}$$

is compared to unity. The results showed that equation was satisfied to within $\pm$ 10%, even accounting for the complete effects of multiple scattering as well as skylight in the incident irradiance. This, in other words reinforce the validity of equation A5. Therefore it can be safely concluded that for a homogeneous ocean, the depth above which 90% of the diffusely reflected

radiance originates is $\frac{1}{K(0,-)}$ or more generally the depth at which the downwelling irradiance falls to 1/e or its values at the surface.

Appendix B

Quasi Analytical Algorithm

In this study, a brief description of a quasi analytical algorithm for the retrieval of the absorption and backscattering coefficients from remote sensing of optically deep waters is given. Furthermore, the derived total absorption coefficient is spectrally decomposed into the contributions of phytoplankton pigments and gelbstoff. The algorithm is based on the relationship between r_{rs} and the inherent optical properties of water derived from the radiative transfer equation.

B1 Derivation of total absorption and backscattering coefficients

step	property	formula
0	r_{rs}	$=\frac{R_{rs}}{(0.52+1.7R_{rs})}$
1	$u(\lambda)$	$=\frac{-g_o=[(g_o)^2+4g_1r_{rs}(\lambda)]^{\frac{1}{2}}}{2g_1}$
2	$a(555)$	$=0.0596+0.2[a(440)i-0.01]$ $a(440)i=\exp(-2.0-1.4\rho+0.2\rho^2)$ $\rho=\ln\frac{r_{rs}(440)}{r_{rs}(555)}$
3	$b_{bp}(555)$	$=\frac{u(555)a(555)}{1-u(555)}-b_{bw}(555)$
4	Y	$=2.2\{1\text{-}1.2\exp\text{-}0.9\frac{r_{rs}(440)}{r_{rs}(555)}$
5	$b_{bp}(\lambda)$	$=b_{bp}(555)\frac{555^Y}{\lambda}$
6	$a(\lambda)$	$=\frac{[1-u(\lambda)][b_{bw}(\lambda)+b_{bp}(\lambda)}{u(\lambda)}$

Table B1 Steps of the QAA to derive absorption and backscattering coefficients from remote-sensing reflectance with 555nm as the reference wavelength

Step 0 shows the conversion of above surface remote sensing reflectance spectra R_{rs} to below surface spectra r_{rs} because satellites and many other sensors measure remote sensing reflectance from above the surface. For the R_{rs} to r_{rs} conversion

$$R_{rs}= R_{rs}/(T+\gamma Q R_{rs}) \quad \text{B1}$$

where $T=t_- t_+/\eta^2$ with t_- that radiance transmittance from below to above the surface and t_+ the irradiance transmittance from above to below the surface, and η is the refractive index of water. γ is the water- to air internal reflection coefficient. Q is the ratio of the upwelling irradiance to upwelling radiance evaluated below the surface. For a nadir viewing sensor and the remote sensing domain, Q in general, ranges between 3 and 6. As R_{rs} is small (in the range of 1% at the high end) for most oceanic and coastal waters, the variation of Q values can only slightly affect the conversion between R_{rs} and r_{rs}. As an example, from calculated Hydrolight R_{rs} and r_{rs} values, it is found that T=0.52 and $\gamma Q \approx 1.7$ for optically deep waters and a nadir viewing sensor.

Values of u can be quickly calculated with the equation $u(\lambda) = -g_0 +[(g_0)^2 +4g_1 r_{rs}(\lambda)]^{1/2}/2g_1$ as shown in step 1.

An empirical estimate of a(555) is given by step 2 . The initial estimation of $\Delta a(440)_I$ here is only for the empirical estimation of $\Delta a(555)$ as a(440) is sensitive to the change of water properties. $a(440)_I$ is calculated on the basis of an earlier study but is adapted to bands at 440 and 555nm as in Mueller and Trees. It can be pointed out that a simple empirical algorithm such as this may not accurately estimate $a(440)_I$ for non-case 1 waters; in

turn $\Delta a(555)$ may not be accurate either. However, as $\Delta a(555)$ is small compared with a(555) for most oceanic waters, the errors of $\Delta a(555)$ will have a smaller impact on the accuracy of a(555).

Step 3 calculates $b_{bp}(555)$ from $r_{rs}(555)$ and a(555) on the basis of equation

$$b_b = \frac{ua}{(1-u)}$$

Step 4 gives an estimate of the wavelength dependence (value of Y) of the particle backscattering coefficient. A value for Y is required if the particle backscattering coefficients from one wavelength to another wavelength by equation $b_{bp}(\lambda)=b_{bp}(\lambda_o)(\lambda_o/\lambda)^Y$ need to be calculated. Historically, researches set Y values based on the location of the water sample, such as 0 for coastal waters and 2.0 for open ocean waters. In this context, the empirical algorithm of Lee et al has been used to estimate the Y value and has been adapted for bands 440 and 555nm.

Step 5 computes the particle backscattering coefficients at other wavelengths given the values of Y and $b_{bp}(555)$ by the use of equation $b_{bp}(\lambda)=b_{bp}(\lambda_o)(\lambda_o/\lambda)^Y$

Step 6 completes the calculation for a(λ) given the values of u(λ) (step 1) and b_{bp} (step 5) based on equation $a = \frac{(1-u)b_b}{u}$.

As can be seen from step 1 to step 6, there are two semi analytical expressions and two empirical formulas used for the entire process. Certainly the accuracy of the final calculated a(λ) relies on the accuracy of each individual step. The semi analytical expressions are currently widely accepted and used and can be replaced by better expressions when available.

The empirical formulas used either provides estimates at the reference wavelength [a(555)] or estimates of less important quantities (ex, value of Y).

The order of importance for a property is based on its range of variation and its influence on the final output. Values of r_{rs}, for example, vary widely and have a great influence on the final results, so they are of first order importance. Values of a(555), however, vary over a much narrower range except near shore and have only a small influence on the final results, so a(555) is of second order importance. Although values of Y vary over a range of 0-2.0 or so, they have a relatively small influence on the final results because this value is used in a power law on the ratio of wavelengths for the particle backscattering coefficient. For example, for the expression $(555/440)^{Y}$, a change of Y from 0 to 2.0 merely changes the expression from 1.0 and 1.59. If the true Y value is 1.0 but an estimate of 2.0 is used, this will make the calculated $b_{bp}(440)$ 21% higher than it should be. On the other hand, for the same true Y value of 1.0 but an estimate of 0.0 is used, this will make the calculated $b_{bp}(440)$ 26% lower than it should be. These errors will be transferred to the calculated total absorption coefficient at 440nm, but, as shown, the errors are in a limited range.

The quantities with second order importance, however do affect the end products, and further improvements to the end products can be achieved if the secondary quantities are better estimated with regional and seasonal information, or with improved algorithms.

B2 Decomposition of the total absorption coefficient

For many remote sensing applications, it is desired to know the absorption coefficients for phytoplankton pigment [$a_\varphi(\lambda)$] and gelbstoff [$a_g(\lambda)$] because these properties can be converted to concentrations of chlorophyll or CDOM respectively.

It is indeed more challenging to separate $a_\varphi(\lambda)$ and $a_g(\lambda)$ from the total absorption coefficient as the total absorption is at least a sum of pure water, phytoplankton pigment and gelbstoff. Table B2 extends the calculation for this purpose. As in other semi analytical algorithms, there is no separation of the absorption coefficient of detritus from that of gelbstoff, so the derived $a_g(440)$ here is actually the sum of detritus and gelbstoff absorption coefficients. Lee has developed a simple empirical algorithm for that separation.

Step	Property	formula
7	$\zeta = \frac{a_\phi(410)}{a_\phi(440)}$	$=0.71+\frac{0.06}{0.8+r_{rs}(440)/r_{rs}(555)}$
8	$\xi = \frac{a_g(410)}{a_g(440)}$	$=\exp[S(440-410)]$
9	$a_g(440)$	$=\frac{[a(410)-\xi a(440)}{\xi-\zeta}-\frac{[aw(410)-\zeta a_w(440)}{\xi-\zeta}$
10	$a_\phi(440)$	$=a(440)-a_g(440)-a_w(440)$

Table B2 Steps to decompose the total absorption to phytoplankton and gelbstoff components, with bands at 410 and 440nm

The approach Lee assumed is that a(λ) values at both 410 and 440 nm

are calculated by the steps in Table B1. For the decomposition, two more values must be known; $\zeta = [a_\varphi(410)/a_\varphi(440)$ and $\xi=[a_g(410/a_g\ (440)]$. ζ has been either related to chlorophyll concentration or pigment absorption at a wavelength. As chlorophyll concentration or pigment absorption are still unknowns, the value of ζ cannot be derived by the use of such approaches. Here the value of ζ is estimated in step 7 by the use of the spectral ratio of $r_{rs}(440)/r_{rs}\ (555)$ based on the field data of Lee et al. The value of ξ is calculated in step 8 when we assume a spectral slope of $0.015m^{-1}$. It is to be notes that the values of ζ and ξ may vary based on the nature of waters under study, such as pigment composition, humic versus fulvic acids, and abundance of detritus.

When the values of a(410), a(440), ξ and ζ are known

$$a(410)=a_w(410)+\zeta a_\varphi(440) + \xi a_g(440)$$
$$a(440)=a_w(440) + a_\varphi(440) + a_g(440) \qquad \text{B2}$$

By solving this set of simple algebraic equations, the following is obtained

$$a_g(440) = [a(410) - \zeta a(440)]-[a_w(410) - \zeta a_w(440)]/\xi-\zeta$$
$$a_\varphi(440) = a(440) - a_w(440) - a_g(440) \qquad \text{B3}$$

If values of $a(\lambda)$,$a_g(440)$, and S are known, the $a_\varphi(\lambda)$ spectrum can then be easily calculated

$$a_\varphi(\lambda) = a(\lambda) - a_g(440)\exp(-S(\lambda-440) \qquad \text{B4}$$

Unlike previous approaches, the derivation of $a_\varphi(\lambda)$ here requires no prior knowledge of what kind of phytoplankton pigments might be in the water or of a spectral model for $a\varphi(\lambda)$ at all wavelengths, although there is no need to know $a_\varphi(410)/ a_\varphi(440)$.

Appendix C

Models, parameters, and approaches that used to generate wide range of absorption and backscattering spectra

Ocean Color Algorithm Working Group

IOCCG

June 2003

The Ocean-Colour Algorithms working group used models, parameters, and approaches to generate wide range of absorption and backscattering spectra. This data set contains both inherent optical properties (IOPs) and apparent optical properties (AOPs). IOPs are generated with various available/reasonable optical/bio-optical parameters/models briefly described below.

A four-component model was used to generate IOPs of the bulk water [Bukata et al., 1995; Carder et al., 1991; Doerffer et al., 2002; Fischer and Fell, 1999; Prieur and Sathyendranath, 1981; Roesler et al., 1989],

The absorption $a(\lambda)$ and backscattering coefficients $b_b(\lambda)$ were described as

$$a(\lambda)= a_w(\lambda) + a_{ph}(\lambda) + a_{dm}(\lambda) + a_g(\lambda)$$

$$b_b(\lambda) = b_{bw}(\lambda) + b_{bph}(\lambda) + b_{bdm}(\lambda) \qquad \text{C1}$$

where $a_w(\lambda)$ [Pope and Fry 1997] and $b_{bw}(\lambda)$ [Morel 1974] had been taken from existing records, at a defined temperature and salinity. Phytoplankton concentration, Chl, was used as the free parameter to define different waters and was set in a range of 0.03 – 30.0 µg/l with 20 steps and in total 500 IOP data points were created.

The phytoplankton pigment absorption $a_{ph}(\lambda)$ was expressed as

$$a_{ph}(\lambda)= a_{ph}(440)\, a_{ph}^{+}(\lambda) \quad \text{C2}$$

where $a_{ph}^{*}(\lambda)$ is the $a_{ph}(440)$ normalized spectral shape and

$$a_{ph}(440)=0.05(Chl)^{0.626} \quad \text{C3}$$

$a_{ph}^{+}(\lambda)$ spectrum came from the extensive measurements of Bricaud et al. [Bricaud et al., 1995; Bricaud et al., 1998] and Carder et al. [Carder et al., 1999].

$a_{dm}(\lambda)$ spectrum was modeled as Roesler at al [Roesler et al, 1989] and Bricaud et al [Bricaud et al, 1995]

$$a_{dm}(\lambda)=a_{dm}(440)\exp(-s_{dm}(\lambda-440)) \quad \text{C4}$$

where S_{dm} values are made to vary between 0.07 and 0.015 for each chlorophyll concentration, Chl ,value.

$a_{dm}(440)$, the detritus absorption at the reference wavelength, is randomly determined for each Chl value as

$$a_{dm}(440) =p_1 a_{ph}(440) \quad \text{C5}$$

where p_1 was defined as the ratio of $a_{dm}(440)/a_{ph}(440)$

p_1 was generated from

$$p_1 = 0.1 + \frac{(0.5R_1 a_{ph}(440))}{0.05 + a_{ph}(440)} \quad \text{C6}$$

where R_1 is a random value between 0 and 1. In this way, when $a_{ph}(440)$ values are very small, the $a_{dm}(440)$ values will not be extremely large. Also, since R_1 is a random value, the relationship between $a_{dm}(440)$ and $a_{ph}(440)$ would not be fixed, as observed in field.

The $a_g(\lambda)$ spectrum was modeled from Bricaud et al [Bricaud et al,1981] and is expressed as follows

$$a_g(\lambda) = a_g(440)\exp(-S_g(\lambda-440)) \quad \text{C7}$$

where S_g was randomly varied between 0.01 and 0.02 nm^{-1} for each Chl value.

The gelbstoff absorption at a reference wavelength, $a_g(440)$, was also randomly determined for each Chl value, as

$$a_g(440) = p_2\, a_p(440) \quad \text{C8}$$

where p_2 was generated from the following expression

$$p_2 = 0.3 + (5.7R_2 a_{ph}(440))/(0.02 + a_{ph}(440)) \quad \text{C9}$$

Similarly, R_2 varied randomly between 0 and 1

Following Bukata et al [Bukata et al ,1995], $b_{bph}(\lambda)$ was modeled as

$$b_{bph}(\lambda) = \tilde{b}_{ph}\, b_{ph}(\lambda)$$

$$b_{ph}(\lambda) = c_{ph}(\lambda) - a_{ph}(\lambda) \quad \text{C10}$$

$$c_{ph}(\lambda) = c_{ph}(550)\,(550/\lambda)^{n_1}$$

where the values of $\tilde{b}_{ph}$ depended on the phase function of phytoplankton and in the present case, a 1% bb/b Fourier Forand function had been selected. $C_{ph}(550)$, was obtained from the following expression

$$C_{ph}(550) = p_3(Chl)^{0.57} \quad \text{C11}$$

where p_3 is a random value between 0.06 and 0.6 for a given Chl value

n_1 was obtained from

$$n_1 = -0.4 + (1.6+1.2R_3)/(1 + (Chl)^{0.5}) \quad \text{C12}$$

where R_3 is a random value between 0 and 1 and consequently, n_1 is in the range of 0.1 to 2.0 but varied randomly for each Chl value.

The backscattering term of detritus, minerals was expressed as follows

$$b_{bdm}(\lambda) = \tilde{b}_{dm}\, b_{dm}(\lambda) \quad \text{C13}$$

$b_{dm}(\lambda)=b_{dm}(550)(550/\lambda)n_2$

where the value of $\tilde{b}_{dm}$ depended on the selected phase function and had a value of 0.0813 when the Petzold average phase function was used. As from the previous cases, $b_{dm}(550)$ and n_2 were corrected as follows

$$b_{dm}(550) = p_4 (Chl)^{0.766} \quad \text{C14}$$

with p_4 varying randomly between 0.06 and 0.6 for any Chl value therefore, the values of $b_{dm}(550)$ are not fixed for a given Chl.

n_2 was generated with

$$n_2 = -0.5 + (2.0+1.2R_4)/(1 + (Chl)^{0.5}) \quad \text{C15}$$

where R_4 is another random number between 0 and 1.